EVALUATION OF EARTHQUAKE GROUND MOTIONS

Prepared by

I. M. Idriss, Professor Emeritus
Department of Civil and Environmental Engineering
University of California
Davis, CA 95616-5294
e-mail: *imidriss@aol.com*

and

Ralph J. Archuleta, Professor
Department of Earth Science & Institute for Crustal Studies
University of California
Santa Barbara, CA 93106-1100
e-mail: *ralph@quake.crustal.ucsb.edu*

*<u>**Changes from Draft 6.0 to Draft 6.5**</u>*

Edited several parts of text
Cleaned-up & reorganized reference list
Renamed Appendix B to Appendix B1 and added Appendix B2
Appendix B2 was prepared by Dr. Norman A. Abrahamson & includes two detailed examples of probabilistic seismic hazard evaluations

TABLE OF CONTENTS

APPENDIX D
ATTENUATION RELATIONSHIPS FOR MOTIONS IN EASTERN NORTH AMERICA
(ENA)

APPENDIX E
ATTENUATION RELATIONSHIPS FOR SUBDUCTION EARTHQUAKES

APPENDIX F
EFFECTS OF RUPTURE DIRECTIVITY ON EARTHQUAKE GROUND MOTIONS

APPENDIX G
EFFECTS OF HANGING WALL/FOOT WALL ON EARTHQUAKE GROUND MOTIONS

APPENDIX H
ESTIMATION OF TARGET SPECTRUM AT SPECTRAL DAMPING RATIOS OTHER
THAN 5%

APPENDIX I
ANALYTICAL SIMULATIONS TO GENERATE ACCELEROGRAMS AT A ROCK SITE

APPENDIX J
SELECTION OF ACCELEROGRAMS FOR SEISMIC ANALYSIS PURPOSES

APPENDIX K
INVENTORY OF SELECTED ACCELEROGRAMS

APPENDIX L
USEFUL URLs

LIST OF TABLES

LIST OF FIGURES

EVALUATION OF EARTHQUAKE GROUND MOTIONS

by
I. M. Idriss and Ralph J. Archuleta

1.0 INTRODUCTION

1.1 Introductory Comments

The Division of Dam Safety and Inspections of the Federal Energy Regulatory Commission (FERC) is responsible for the safety of power-generating stations throughout the USA. This responsibility includes concern with the effects of earthquakes at these stations, which typically include dams and appurtenant structures. Accordingly, FERC requested that the writers prepare this document on "Evaluation of Earthquake Ground Motions" that contains the main elements that could be utilized by FERC to establish "Seismic Design Criteria" for all facilities under its jurisdiction.

The purpose of seismic design criteria is to provide guidelines and procedures for obtaining earthquake ground motion parameters for use in evaluating the seismic response of a given structure or facility. Presently, there are three ways by which the earthquake ground motion parameters can be ascertained: use of local building codes; conducting a deterministic seismic hazard evaluation; or conducting a probabilistic seismic hazard evaluation. Obviously, local building codes would not apply to the majority of structures under the jurisdiction of FERC. Both deterministic and probabilistic seismic hazard evaluations are covered in this document.

The earthquake ground motion parameters discussed in this document pertain to a "rock outcrop". Thus, these parameters are intended for use as input to an analytical model that would include the structure under consideration, e.g., a dam-foundation system. Any effects of local site conditions on earthquake ground motions would then be explicitly accounted for in the analyses. Accordingly, the effects of local site conditions on earthquake ground motions, which can be very significant, are not addressed in this document.

To provide the needed basis for estimating earthquake ground motion parameters at a particular "rock outcrop", it is necessary to incorporate the appropriate geologic and seismologic input and to utilize the most relevant available procedures for estimating these parameters. The remaining pages of this document cover these aspects and the attachments include more details regarding specific aspects of the seismic hazard evaluation procedures.

1.2 Organization of the Report

In addition to this introductory section, the report includes six sections and eleven appendices. The appendices are structured so that they can be updated periodically as new developments and publications pertinent to each appendix become available.

2.0 EARTHQUAKE HAZARDS AND CONSEQUENCES

2.1 GENERAL

This section is included in this document merely to highlight why seismic hazards can be very important to facilities under the jurisdiction of FERC. Hazards that may affect such facilities include fault rupture, soil failure, and seiches. Other hazards, such as tsunamis, are not discussed

herein because all of the facilities under FERC's jurisdiction are inland and are unlikely to be affected by tsunamis.

2.2 FAULT RUPTURE

Fault rupture is a hazard that must be dealt with whenever a fault traverses a dam site. The potential for the presence of a fault, or fault traces, at a particular site should be fully investigated to assess the location, orientation, type, sense of movement … etc.

Typical examples of fault rupturing in historic earthquakes are presented in Figs. 2-1 through 2-6. Possible approaches to allowing for the effects of fault rupture on embankment dams are offered, for example, in Sherard et al. (1974) and Allen and Cluff (2000) and other regulatory documents. The exact method that the licensee uses must be documented.
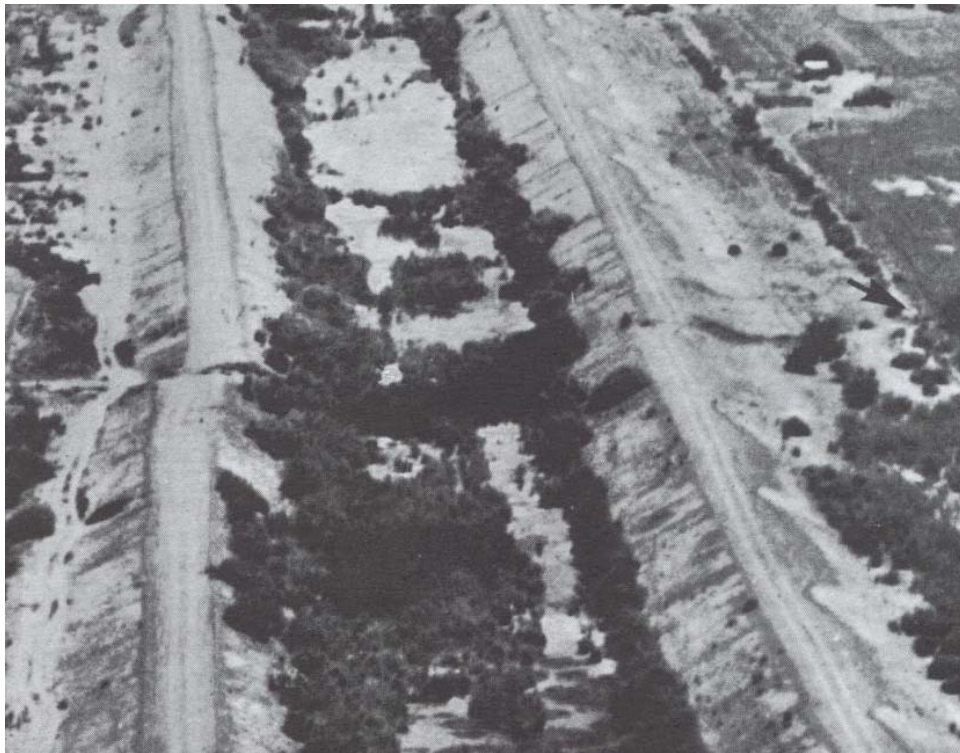
Fig. 2-1 Horizontal (Strike-Slip) fault offset of the Imperial Fault in 1940 across the All-America Canal caused by the 1940 El Centro earthquake

Fig. 2-2 Red Canyon Fault Scarp East of Blarney Stone Ranch Caused by the1959 Montana Earthquake

Fig. 2-3 Fault Rupture of San Fernando Fault in 1971; the late Professor H. Bolton Seed was standing on the Hanging Wall and Lloyd Cluff was standing on the Footwall. (Photograph: Courtesy of Professor Clarence Allen)

Fig. 2-4 View of dam in Taiwan prior to the occurrence of the 1999 Chi-Chi earthquake

Fig. 2-5 View of dam after the 1999 Chi-Chi Earthquake showing damage to portion of dam due to fault rupture
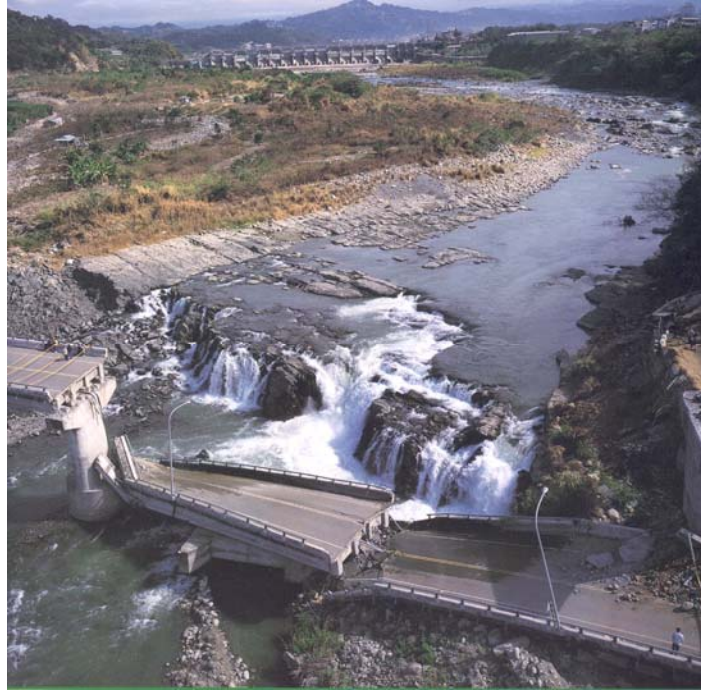
Fig. 2-6 View of fault rupture adjacent to bridge downstream of dam showing formation of falls in river and damage to bridge structure

2.3 SOIL FAILURE

2.3.1 *Foundation and/or Embankment Soils*

Strong earthquake ground motions can induce high pore water pressures and/or high strains in these soils that could have serious consequences, including:

- Settlements, which are mostly abrupt and non-uniform and often lead to longitudinal as well as transverse cracks;

- Loss of bearing support;

- Floatation of buried structures, such as underground tanks or pipes;

- Increased lateral pressures against retaining structures;

- Lateral spreads (limited lateral movements);

- Lateral flows (extensive lateral movements)

Examples of settlements leading to cracks coupled with limited lateral movements are illustrated by the performance of Austrian Dam in California during the 1989 Loma Prieta earthquake as shown in Figs. 2-7 through 2-10.

Fig. 2-7 Aerial view of Austrian Dam (Photograph: Courtesy of David Gutierrez)
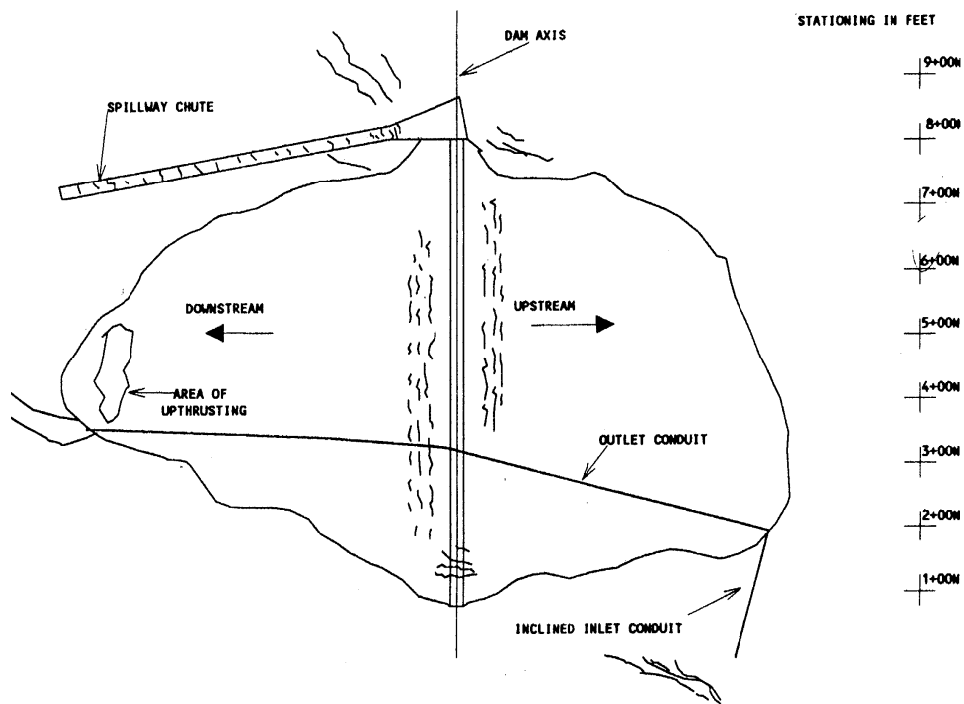
Fig. 2-8 Longitudinal and transverse cracks in Austrian Dam caused by shaking during the 1989
    Loma Prieta earthquake (after Vrymoed, 1991)
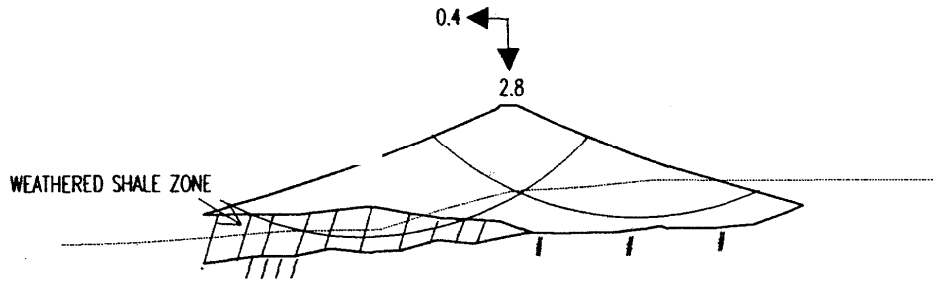
Fig. 2-9 Vertical and horizontal displacements, in feet, of the crest of Austrian Dam at Station 6+00 (after Vrymoed, 1991)
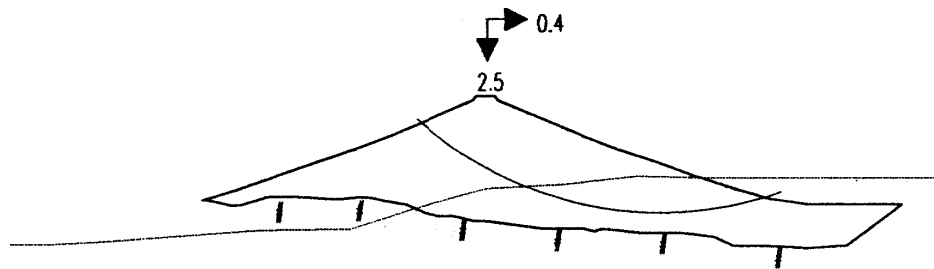
Fig. 2-10 Vertical and horizontal Displacements, in feet, of the crest of Austrian Dam at Station 2+50 (after Vrymoed, 1991)

Among the consequences of increased pore water pressure is the possibility of triggering liquefaction in cohesionless soils, such as sands, silty sands and very low plasticity or non-plastic sandy silt. An example of liquefaction "in progress" is shown in Fig. 2-11 – a view captured during the magnitude 7½ 1978 Miyagi-Ken-Oki earthquake in Japan.

Fig. 2-11 Surface evidence of liquefaction triggered during the 1978 Miyagi-Ken-Oki earthquake in Japan

Examples of lateral spreads (limited lateral movements) and lateral flows (extensive lateral movements) are provided by what happened to the Upper and Lower San Fernando Dams during the 1971 San Fernando earthquake (see Fig. 2-12). Figures 2-13 and 2-14 provide more details of the relatively limited lateral movements (lateral spreads) of the embankment of the Upper San Fernando Dam.

Fig. 2-12 San Fernando Dam Complex shortly after the occurrence of the 1971 San Fernando earthquake

Fig. 2-13 View of Upper San Fernando Dam showing horizontal and vertical deformations and cracks in the upstream face of the dam

Fig. 2-14 Close-up View of Cracks in the Upstream Face of Upper San Fernando Dam

An aerial view of the Lower San Fernando Dam before the occurrence of the 1971 San Fernando earthquake is shown in Fig. 2-15. The devastating effects of the earthquake on this dam are presented in Figs. 2-16 and 2-17. Note that the lateral flows caused by the ground shaking were initiated because of the liquefaction of the soils in the upstream shell of the dam and the resulting loss of strength of these soils.

Fig. 2-15 Aerial view Lower San Fernando Dam before the occurrence of the 1971 San Fernando Earthquake showing the extensive number of residences that would have been affected by a breach of the dam (Photograph: Courtesy of David Gutierrez)

Fig. 2-16 Photograph of the Lower San Fernando Dam taken a few hours after the occurrence of the 1971 San Fernando Earthquake.
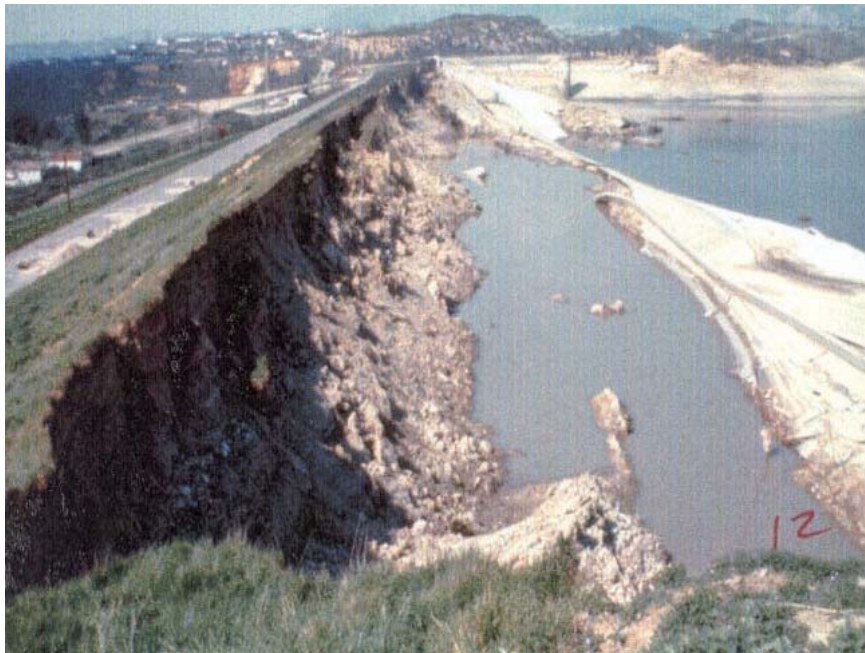
Fig. 2-17 Photograph of the Lower San Fernando Dam taken after partial emptying the reservoir showing the extent of lateral flow of the upstream shell and crest of the dam

2.3.2 *Reservoir Rim*

Landslides along the rim of the reservoir can be triggered by the ground shaking during an earthquake. Such landslides could impact the body of dam negatively, e.g., blocking an intake tower, generating a wave that may overtop the crest … etc. An example of a landslide is the Madison River Slide in the 1959 Montana earthquake shown in Fig. 2-18.

Fig. 2-18 View of the Madison River Slide from earthquake lake side; Slide occurred during the 1959 Montana Earthquake
(Photograph obtained from: http://neic.usgs.gov/neis/eq_depot/usa/1959_08_18_pics.html)

2.4 SEICHES

A seiche is a standing wave in an enclosed or partly enclosed body of water. Seiches are normally caused by earthquake activity, and can affect harbors, bays, lakes, rivers and canals. In the majority of instances, earthquake-induced seiches do not occur close to the source of an earthquake, but some distance away (possibly as far as 100's of kilometers). This is due to the fact that earthquake seismic waves close to the source are richer in high frequencies, while those at greater distances are of lower frequency content which can enhance the rhythmic movement in a body of water. The biggest seiches develop when the period of the ground shaking matches the period of oscillation of the water body.

In 1891, an earthquake near Port Angeles caused an eight-foot seiche in Lake Washington; such a rise in reservoir level could result in overtopping if the free board is not sufficient at the time. The 1964 Alaska earthquake created seiches on 14 inland bodies of water in the state of Washington, including Lake Union where several pleasure craft, houseboats and floats sustained some damage.

Inland areas, though not vulnerable to tsunamis, are vulnerable to seiches caused by earthquakes. Additional vulnerabilities include water storage tanks, and containers of liquid hazardous materials that are also affected by the rhythmic motion.

Seiches create a "sloshing" effect on bodies of water and liquids in containers. This primary effect can cause damage to moored boats, piers and facilities close to the water. Secondary problems, including landslides and floods, are related to accelerated water movements and elevated water levels.

The above description was obtained from the following web site: http://www.pep-c.org/seiche/

3.0 GEOLOGIC AND SEISMOLOGIC CONSIDERATIONS

Earthquake ground motions at a particular site are estimated through a seismic hazard evaluation. The geologic and seismologic inputs needed for completing a seismic hazard evaluation consist of acquiring information regarding the following key elements:

(a) The seismic sources on which future earthquakes are likely to occur;

(b) The size of the possible earthquakes and the frequency with which an earthquake is likely to occur on each source; and

(c) The distance and orientation of each source with respect to the site.

This information is obtained from the following sources of data in the region in which the site is located: (1) The historical seismicity record; (2) the seismographic, or instrumental, record of earthquake activity in the region; and (3) the geologic history, especially within the past few thousand to several hundred thousand years.

3.1 HISTORICAL SEISMICITY

An important first step in a seismic hazard evaluation is the compilation and documentation of the historical seismicity record pertinent to the region in which the site is located. It is essential in assessing this historical seismicity record that local sources of data (e.g., newspaper accounts, manuscripts written about a specific earthquake, etc.) be critically reviewed and that conflicting information be resolved. The historical seismicity record in the USA is relatively brief as it extends only over the past 200 to 400 years. It may be noted, however, that a good deal of the available historical records for many parts of the country have been compiled and can be accessed. It is also important to note that much of the historic seismicity record relies heavily (if not exclusively) on reports of felt ground motions or patterns of damage.

Important as the historical seismicity record is, however, it is not sufficient by itself to estimate the future seismic activity in a region.

3.2 SEISMOGRAPHIC RECORD

The seismographic, or instrumental, record in a region is also an important tool in a seismic hazard evaluation. Instrumental records augment the historical records by providing quantitative data (e.g., size, location, depth, mechanism, and time of occurrence of earthquakes) that are not available from reports of felt ground motions or patterns of damage.

The seismographic record is available only since the year 1900 and, until recently, only from a limited number of stations in selected areas worldwide. Significant increases in the number of stations worldwide have been implemented in the past few years and it is expected that the usefulness of the seismographic record will continue to increase in the coming years.

3.3 GEOLOGIC STUDIES

In many parts of the world, significant earthquake activity can be directly associated with specific faults. A major earthquake typically leaves a distinct geologic record that can be preserved for thousands, and possibly hundreds of thousands, of years.   The faulting associated with an earthquake may displace soil and/or rock strata at shallow depths and may create a fault scarp that remains visible. An example of a fault scarps are shown in Figs. 3-1 and 3-2. Figure 3-1 is an aerial view of the San Andreas Fault, and Fig. 3-2 is the log of the trench across the fault on which the 1968 Borrego Mountain, California, earthquake occurred.

The preserved geologic features along faults can be investigated by geologic and geophysical studies that may include: review of available literature, especially with regard to structural and tectonic history; interpretation of various types of imagery to identify regional structures; reconnaissance of the geology and geomorphology of the region; and the use of trenching, boreholes, age-dating and geophysical techniques.
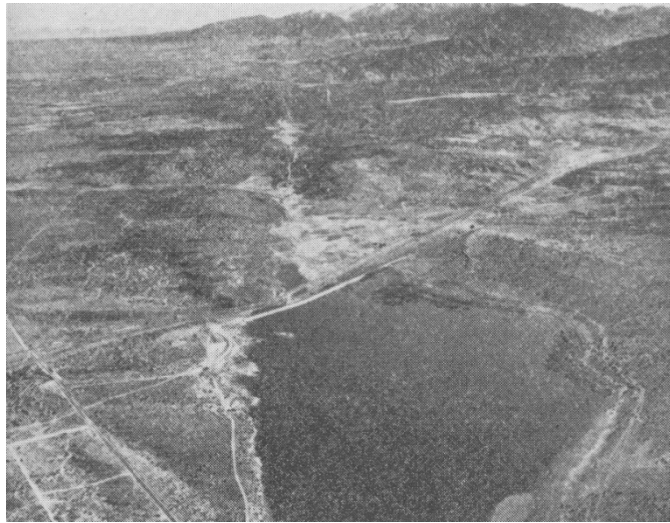
Fig. 3-1 Aerial view of San Andreas Fault near Palmdale Reservoir in Southern California (From Richter, 1958)
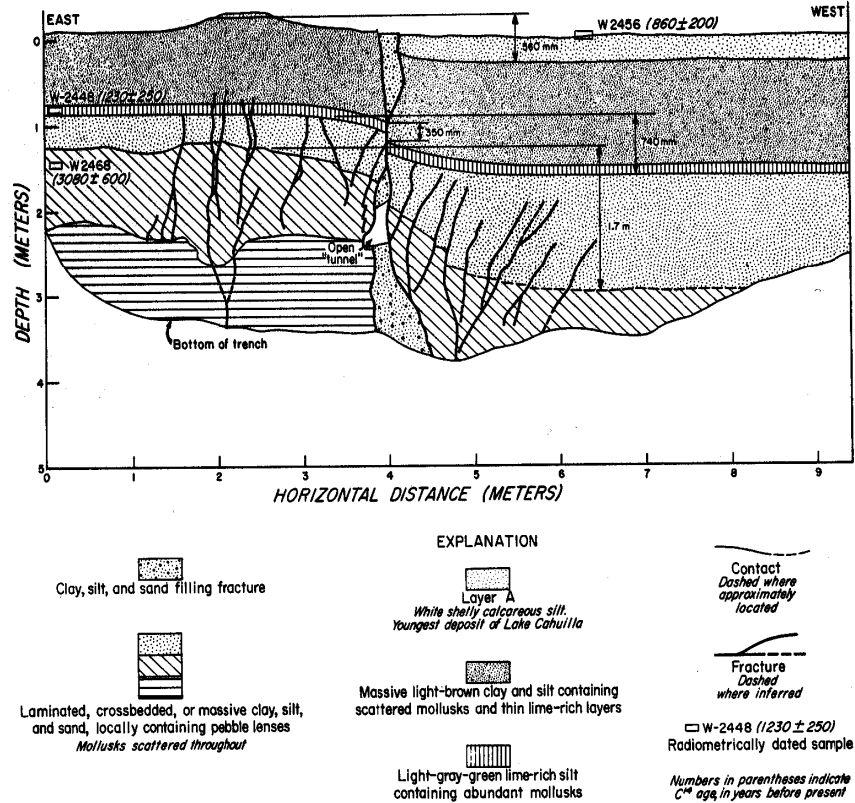
Fig. 3-2 Log of Trench across fault on which the 1968 Borrego Mountain, California, earthquake
occurred (From Clark et al, 1972)

There are various types of faults, as shown in Fig. 3-3. In a thrust (or a reverse) fault, the offset is along an inclined plane and occurs in response to a compressive tectonic strain environment as shown in Fig. 3-3a; examples of major earthquakes on such faults are the 1952 Kern County and the 1971 San Fernando earthquakes in California, and the 1999 Chi-Chi earthquake in Taiwan. The offset on a normal fault is also along an inclined plane, but it occurs in response to extensional strain (Fig. 3-3b); examples are the 1954 Dixie Valley, Nevada, and the 1959 Hebgen Lake, Montana, earthquakes. Offset along a strike slip fault is essentially lateral and occurs along a vertical, or near-vertical, plane as illustrated in Fig. 3-3c; examples are the 1906 San Francisco earthquake in Northern California and the 1992 Landers earthquake in Southern California. The types of faults illustrated in Figs. 3-3a, 3-3b and 3-3c are designated as crustal faults and the illustrations presented in the figure indicate that rupture had extended to the ground surface. Earthquakes have also occurred on crustal faults on which rupture did not extend to the ground surface; these faults are designated as "blind". Examples of earthquakes occurring on "blind" faults are the 1983 Coalinga, the 1987 Whittier-Narrows, and the 1994 Northridge earthquakes in California. The mechanism of each of these earthquakes was a thrust mechanism and the fault involved is designated as a "blind thrust" (Stein and Yeats 1989)

Subduction zones (Fig. 3-3d) occur at the interface between tectonic plates. Examples of earthquakes occurring in subduction zones are the magnitude 9.2 Alaska earthquake in 1964, the magnitude 9.5 Chilean earthquake in 1960, the magnitude 8.1 Michoacan, Mexico, and numerous earthquakes in Japan such the magnitude 8.3 Hokkaido earthquake off the eastern shore of Hokkaido in 2003.

a. Thrust faulting under
horizontal compressive strains

b. Normal faulting resulting
from extensional strains

c. Strike-slip displacement on a
vertical fault plane

d. Under thrust faulting in a
subduction zone
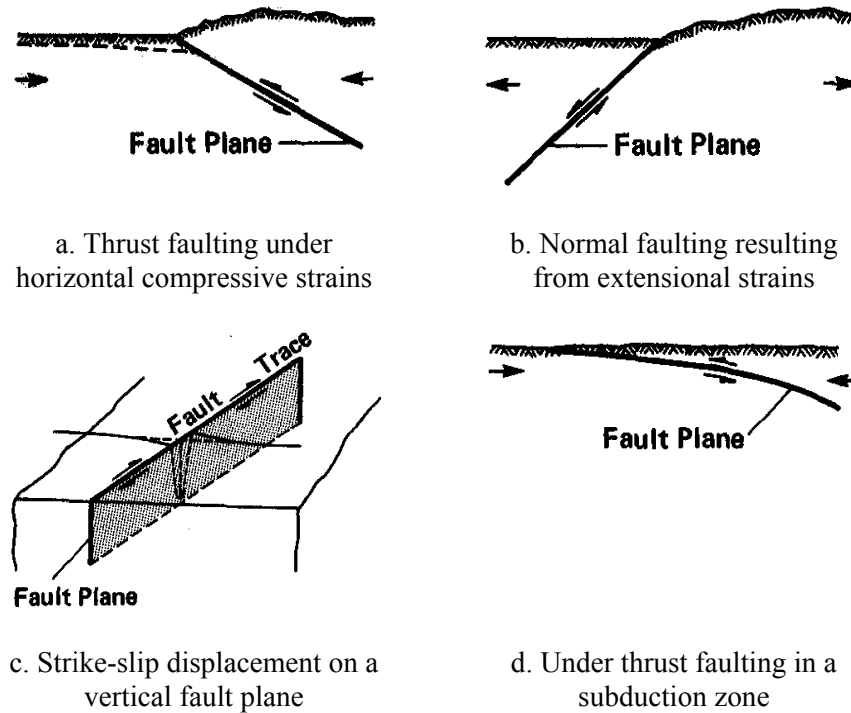
Fig. 3-3 Schematic illustration of four types of faults

Over the years, geologists and seismologists have studied the detailed characteristics of faults, and, until recently, designated each as being a potentially active fault or an inactive fault. This designation is based on recency of fault displacement, which leads to rigid legal definitions of fault activity based on a specified time criterion. Typically, the more critical the facility, the longer is the time criterion specified. For example, the US Nuclear Regulatory Commission considers, for nuclear plants, a fault active if it shows evidence of multiple displacements in the past 500,000 years, or evidence of a single displacement in the past 35,000 years. For dams, the US Bureau of Reclamation specifies 100,000 years, and the US Army Corps of Engineers uses 35,000 years. Faults that have had displacements within these time spans are considered active and those that have not had displacements are considered inactive.

Classifying faults as either "active" or "inactive" does not provide sufficient information about the nature of the fault. Instead, geologists and seismologists have recognized that significant differences exist in the degrees of activity of various faults. These differences are manifested by several key fault parameters, which are briefly described below.

3.3.1 Key Fault Parameters

The key fault parameters that appear most significant include: rate of strain release, or fault slip rate; amount of fault displacement in each event; length (and area) of fault rupture; earthquake size; and earthquake recurrence interval.

3.3.1.1 Slip Rate: The geologic slip rate provides a measure of the average rate of deformation on a fault. The slip rate is estimated by dividing the amount of cumulative displacement, measured from displaced geologic or geomorphic features, by the estimated age of the geological material or feature. The geologic slip rate is an average value over a geologic time period, and reliable to

the extent that strain accumulation and release over this time period has been uniform and responding to the same tectonic stress environment.

Examples of ranges of slip rates of a few selected faults are listed in Table 1.

Table 1 – Examples of Slip Rates

Fault	Slip Rate (mm/year)
Fairweather, Alaska	38 to 74
San Andreas, California	20 to 53
Hayward Fault, Northern California	7 to 11
Wasatch, Utah	0.9 to 1.8
Newport-Inglewood, Southern California	0.1 to 1.2
Atlantic Coast faults	0.0002

The information in Table 1 leads to the following observations: (i) prominent and highly active faults, such as the San Andreas Fault, have a much higher slip rate than minor faults; and (ii) uncertainties exist regarding the slip rate and a range of values needs to be considered in specific application. Observation (ii) pertains to various segments of the fault as well as to a specific segment of the fault.

3.3.1.2 <u>Slip Per Event</u>: The amount of fault displacement for each fault rupture event differs among faults and fault segments and provides another indication of relative differences in degrees of fault activity. The differences in displacement are influenced by the tectonic environment, fault type and geometry, pattern of faulting, and the amount of accumulated strain released.

The amount of slip per event can be directly measured in the field during studies of historical faulting, and is usually reported in terms of a maximum and an average value for the entire fault or for segments of the fault. Displacements for prehistoric rupture events can be estimated for some faults from detailed surface and subsurface seismic geologic investigations (e.g., Sieh, 1978; Swan et al, 1980).

It is often difficult to ascertain what value of maximum or average displacement is most accurate and representative from data available in the literature. Often, reported displacements represent apparent displacement or separation across a fault. For normal faulting events, scarp height has typically been reported as a measurement of the tectonic displacement. The scarp height, however, often exceeds the net tectonic displacement across a fault by as much as two times, due to graben formation and other effects near the fault (Swan et al, 1980). In the case of thrust faults, the reported vertical displacement often is actually the measure of vertical separation, and the net slip on the fault can be underestimated by a significant amount (e.g., Cluff and Cluff, 1984).

Thus, it is very important that the database, from which displacements are determined, be carefully evaluated before selecting the best estimate of maximum or average displacement from data available in the literature.

3.1.3.3 <u>Fault Area</u>: The fault area is critical for both deterministic and probabilistic methods that are used to estimate the earthquake ground motions. The geometry of the fault controls the

distance between the fault and the site and is used in estimating the the magnitude (seismic moment) of the maximum earthquake.

3.3.1.4 <u>Earthquake Size</u>: The earliest measures of earthquake size were based on the maximum intensity and areal extent of perceptible ground shaking (most of the non-instrumental historical seismicity record is expressed in terms of these two observations). Instrumental recordings of ground shaking led to the development of the magnitude scale (Richter, 1935). The magnitude was intended to represent a measure of the energy released by the earthquake, independent of the place of observation.

As stated by Richter (1958): "Magnitude was originally defined as the logarithm of the maximum amplitude on a seismogram written by an instrument of specific standard type at a distance of 100 km. … Tables were constructed empirically to deduce from any given distance to 100 km. … The zero of the scale is fixed arbitrarily to fit the smallest recorded earthquakes." Mathematically, the magnitude, M, is expressed as follows:

$$\textit{Magnitude} \quad \textit{M} = \textit{Log}_{10}\left(\textit{A}\right) - \textit{Log}_{10}\left(\textit{A}_o\right) \tag{1}$$

in which $\textit{A}$ is the recorded trace amplitude for a given earthquake at a given distance as written by the standard type of instrument, and $\textit{A}_o$ is that for a particular earthquake selected as standard. For local earthquakes, $\textit{A}$ and $\textit{A}_o$ are measured in millimeters and the standard instrument is the Wood-Anderson torsion seismograph which has a natural period of 0.8 sec, a damping factor of 0.8 (i.e., 80 percent of critical) and static magnification of 2800. A magnitude determined in this way is designated the local magnitude, $\textit{M}_L$.

For purposes of determining magnitudes for teleseisms, Gutenberg and Richter (1956) devised the surface wave magnitude, $\textit{M}_S$, and the body wave magnitudes, $\textit{m}_b$ and $\textit{m}_B$.

The local magnitude is determined at a period of 0.8 sec, the body wave magnitudes are determined at periods between 1 and 5 sec, and the surface wave magnitude is determined at a period of 20 sec.

In the past 25 or so years, the use of seismic moment has provided a physically more meaningful measure of the size of a faulting event. Seismic moment, with units of force × length (dyne-cm or N-m) is expressed by the equation:

$$\textit{M}_o = \mu \textit{A}_f \textit{D} \tag{2}$$

in which μ is the shear modulus of the material along the fault plane and is typically equal to 3×10^{11} dyne/cm^2 for crustal rocks, $\textit{A}_f$ is the area, in square centimeters, of the fault plane undergoing slip, and $\textit{D}$, in cm, is the average slip over the surface of the fault that had non-zero slip.

Seismic moment provides a basic link between the physical parameters that characterize the faulting and the seismic waves radiated due to rupturing along the fault. Seismic moment is therefore a more useful measure of the size of an earthquake.

Kanamori (1977) and Hanks and Kanamori (1979) introduced a moment-magnitude scale, M, in which magnitude is calculated from seismic moment using the following formula:

$$Log_{10}\left(M_o\right)= 1.5M + 16.05$$

or

$$M = \left(2/3\right)\left[Log_{10}\left(M_o\right)- 16.05\right]$$

[3]

where seismic moment is given in dyne-cm. The moment magnitude is different from other magnitude scales because it is directly related to average slip and ruptured fault area, while the other magnitude scales reflect the amplitude of a particular type of seismic wave. The relationships between moment magnitude and the other magnitude scales, shown in Fig. 3-4, were presented by Heaton et al (1982) based on both empirical and theoretical considerations as well as previous work by others. The following observations can be made from the results shown in Fig. 3-4:

(i). All magnitude scales exhibit a limiting value, or a saturation level, with increasing moment magnitude. Saturation appears to occur when the ruptured fault dimension becomes much larger than the wave length of seismic waves that are used in measuring the magnitude; Moment magnitude does not saturate because it is derived from seismic moment as opposed to an amplitude on a seismogram

(ii). The local magnitude and the short-period body wave magnitude, m_b are essentially equal to moment magnitude up to $M = 6$;

(iii). The long period body-wave magnitude, m_B, is essentially equal to moment magnitude up to $M = 7.5$; and

(iv). The surface wave magnitude, M_S, is essentially equal to moment magnitude in the range of $M = 6$ to 8.
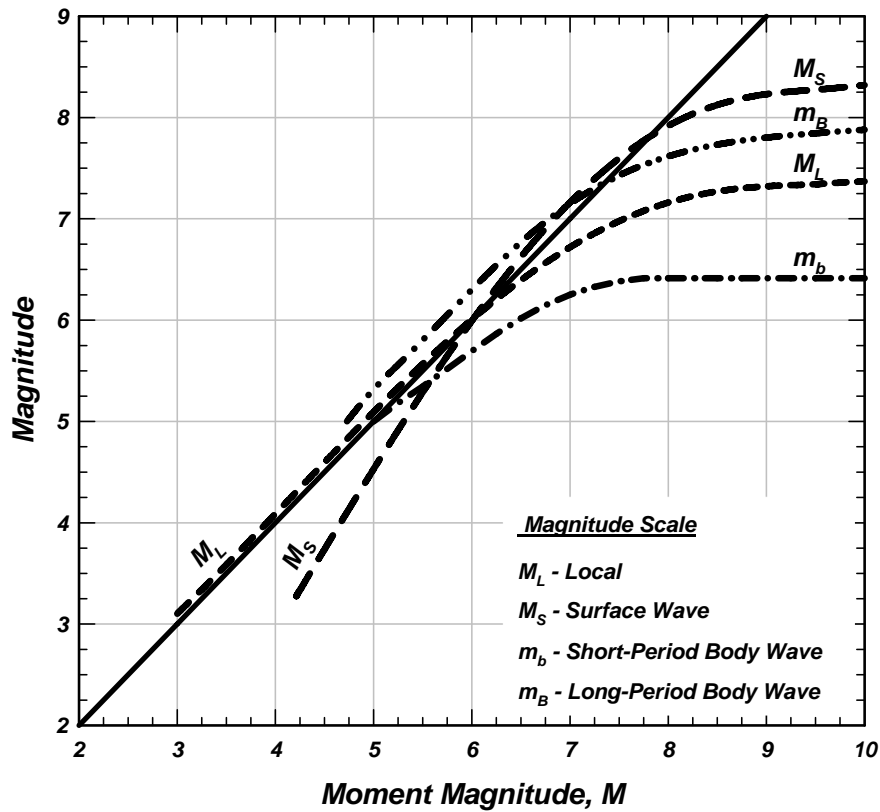
Fig. 3-4 Relation between Moment Magnitude and Various Magnitude Scales (after Heaton et al., 1982)

Typically, the size of an earthquake is reported in terms of local magnitude, surface wave magnitude, or body wave magnitude, or in terms of all these magnitude scales. Based on the observations made from Fig. 3-4, the use of local magnitude for magnitudes smaller than 6, and surface wave magnitude for magnitudes greater than 6 but less than 8 is equivalent to using the moment magnitude. For great earthquakes, such as the 1960 Chilean earthquake (M = 9.5) and the 1964 Alaska earthquake (M = 9.2), however, it is important to use the moment magnitude to express the size of the earthquake. In fact, it is best to use the moment magnitude scale for all events.

It should be noted that the magnitude derived using Eq. [3] is defined as the moment magnitude and given the designation M. This moment magnitude is devised in a way that it is equivalent to M_L for $3 < M_L < 6$. Another, slightly different magnitude is the energy magnitude, M_W, which is given by the following relationship (Kanamori, 1977):

$$Log_{10}(M_o) = 1.5M + 16.1$$

or

$$M_W = (2/3)\left[Log_{10}(M_o) - 16.1\right]$$

[4]

The magnitudes M and M_W are nearly equal, and have been used interchangeably in many applications.

The magnitude scale most often used for central and eastern US earthquakes is m_{bLg}, which was developed by Nuttli (1973a). It is based on measuring the maximum amplitude, in microns, of 1-sec period Lg waves and was devised to be equivalent to m_b. Nuttli initially called this magnitude m_b. To avoid confusion with the true m_b, however, this magnitude is usually referred to as m_{bLg}. It is also called Nuttli magnitude and designated m_N (Atkinson and Boore, 1987); it is referred to as such in the Canadian network.

Boore and Atkinson (1987) derived the following relationship between m_N and moment magnitude M:

$$M = 2.689 - 0.252 m_N + 0.127 \left(m_N\right)^2 \qquad [4]$$

Frankel et al (1996) also derived a relationship between M and m_{bLg}, viz:

$$M = 2.45 - 0.473 m_{bLg} + 0.145 \left(m_{bLg}\right)^2 \qquad [5]$$

Equations [4] and [5] provide nearly identical values of M for the same values of m_{bLg} as illustrated in Fig. 3-5.
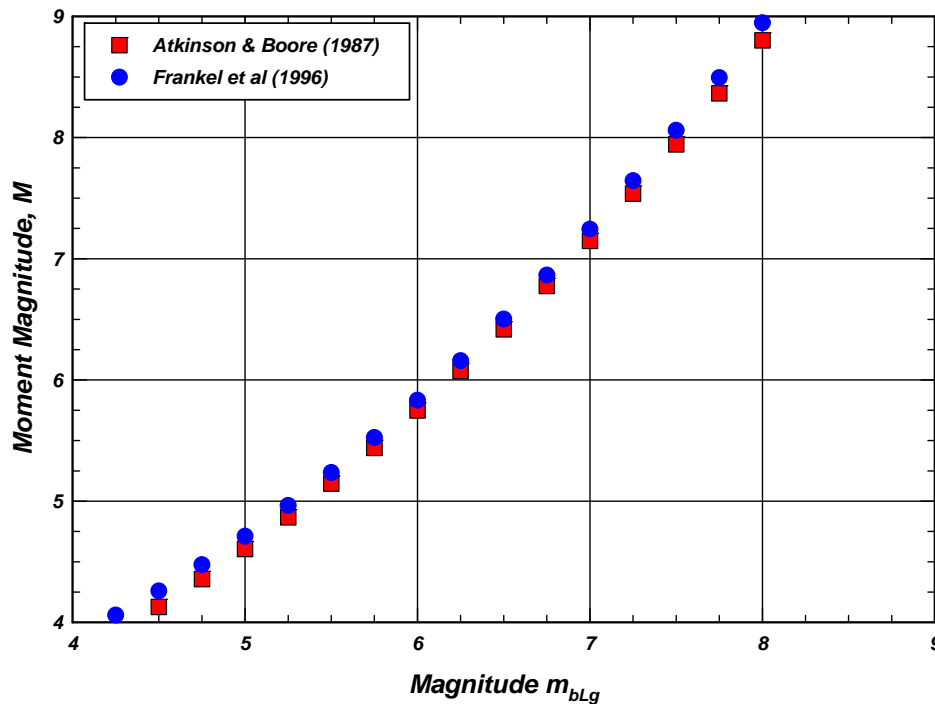
Fig. 3-5 Relationship between M and m_{bLg}

The use of magnitude or seismic moment as a criterion for the comparison of fault activity requires the choice of the magnitude or moment value that is characteristic of the fault. In many instances it is not possible to ascertain whether historical seismic activity is characteristic of the fault through geologic time, unless evidence of the sizes of past earthquakes is available from seismic geology studies of paleoseismicity. As noted earlier, even a long historical seismic record is not enough by itself (Allen, 1975). In a few cases, detailed seismic geology studies have provided data on the sizes of past surface faulting earthquakes (e.g., Sieh, 1978). In general, these data involve measurements of prehistoric rupture length and/or displacement, and a derived magnitude can be estimated probably within one-half magnitude.

3.3.1.3.1 Methods for Estimating Maximum Earthquake Magnitude: There are several available methods for assigning a maximum earthquake magnitude to a given fault (e.g., Wyss, 1979; Slemmons, 1982; Schwartz et al, 1984; Wells and Coppersmith, 1994). These methods are based on empirical correlations between magnitude and some key fault parameter such as: fault rupture length and surface fault displacement measured following surface faulting earthquakes; and fault length and width estimated from studies of aftershock sequences. Data from worldwide earthquakes have been used in regression analyses of magnitude on length, magnitude on displacement, and magnitude on rupture area. In addition, magnitude can be calculated from seismic moment and a relationship between magnitude and slip rate has also been proposed. Each method has some limitations, which may include: non-uniformity in the quality of the empirical data, a somewhat limited data set, and a possible inconsistent grouping of data from different tectonic environments. A number of these methods are summarized in Appendix A.

Geological and seismological studies can define fault length, fault width, amount of displacement per event, and slip rate for potential earthquake sources. These data provide estimates of maximum magnitude on each source. Selection of a maximum magnitude for each source is ultimately a judgment that incorporates understanding of specific fault characteristics, the regional tectonic environment, similarity to other faults in the region, and data on regional seismicity.

Use of a number of magnitude estimation methods can result in more reliable estimates of maximum magnitude than the use of any one single method. In this way, a wide range of fault parameters can be included and the selected maximum magnitude will be the estimate substantiated by the best available data. To evaluate the possible range of maximum magnitude estimates for a source, uncertainties in the fault parameters and in the magnitude relationships need to be identified and evaluated.

3.3.1.4 Recurrence Interval of Significant Earthquakes: Faults having different degrees of activity differ significantly in the average recurrence intervals of significant earthquakes. Comparisons of recurrence provide a useful means of assessing the relative activity of faults, because the recurrence interval provides a direct link between slip rate and earthquake size. Recurrence intervals can be calculated directly from slip-rate, as discussed later in this report, and displacement-per-event data. In some cases, where the record of instrumental seismicity and/or historical seismicity is sufficiently long compared to the average recurrence interval, seismicity data can be incorporated when estimating recurrence. In, many regions of the world, however, the instrumental as well as the historical seismicity record is too brief; some active faults have little or no historical seismicity and the recurrence time between significant earthquakes is longer than the available historical record along the fault of interest.

Plots of frequency of occurrence versus magnitude can be prepared for small to moderate earthquakes and extrapolations to larger magnitudes can provide estimates of the mean rate of occurrence of larger magnitude earthquakes. This technique has limitations, however, because it is based on regional seismicity, and often cannot result in reliable recurrence intervals for specific faults. The impact of such extrapolation on hazard evaluations is discussed in the following section.

3.4 EARTHQUAKE RECURRENCE MODELS

A key element in a seismic hazard evaluation is estimating recurrence intervals for various magnitude earthquakes. A general equation that describes earthquake recurrence may be expressed as follows:

$$N(m) = f(m, t) \tag{6}$$

in which $N(m)$ is the number of earthquakes with magnitude greater than or equal to m, and t is time. The simplest form of Eq. [6] that has been used in most applications is the well known Richter's law of magnitudes (Gutenberg and Richter, 1956; Richter, 1958) which states that the occurrence of earthquakes during a given period of time can be approximated by the relationship:

$$Log_{10}(N(m)) = a - bm \tag{7}$$

in which 10^a is the total number of earthquakes with magnitude greater than zero and b is the slope. This equation assumes spatial and temporal independence of all earthquakes, i.e., it has the properties of a Poisson Model.

For engineering applications, the recurrence is limited to a range of magnitudes between m^o and m^u. The magnitude m^o is the smallest magnitude of concern in the specific application; in most cases m^o can be limited to magnitude 5 because little or no damage has occurred from earthquakes with magnitudes less than 5. The magnitude m^u is the largest magnitude the fault is considered capable of producing; the value of m^u depends on the geologic and seismologic considerations summarized earlier. The cumulative distribution is then given by (…):

$$F_M(m) = P\left(M < m \,/\, \left(m^o \leq m \leq m^u\right)\right)$$
$$= \frac{N(m^o) - N(m)}{N(m^o) - N(m^u)} \tag{8}$$

The probability density function is equal to:

$$f_M(m) = \frac{d}{dm}\left(F_M(m)\right) \tag{9}$$

In Equations [6] through [9], the letters m or M refer to magnitude; the upper case M denotes a random variable, and the lower case m denotes a specific value of magnitude.

When the recurrence relationship is expressed by Richter's law of magnitudes, the following expression is obtained by substituting Eq. [7] into Eq. [8]:

$$N(m) = A^{\circ} \left\{ 1 - \frac{1 - 10^{-b(m - m^{\circ})}}{1 - 10^{-b(m^{u} - m^{\circ})}} \right\}$$

<div align="right">[10]</div>

The parameter A° is the number of events for earthquakes with magnitude greater than or equal to m° (i.e., $Log_{10}(A^{\circ}) = a - bm^{\circ}$).

Development of Eq. [10] requires knowledge of the parameters A°, b, and m^{u}, and a selection of m°. The parameter A° and slope b are based on either the historical seismicity record (including the instrumental record when available) or on geologic data. The slope b, based on regional historical seismicity records, typically ranges from 0.6 to about 1.1. For most faults, the historical seismicity record is relatively short and most of the information is for smaller magnitudes (typically less than 6). Thus, for these smaller magnitude earthquakes, a reasonable fit using Richter's relationship can be obtained and values of A° and b can be calculated.

Discrepancies between earthquake recurrence intervals based on historical seismicity and recurrence intervals based on geologic data are common when applied to a specific fault.

A good example of such a discrepancy is found for the south central segment of the San Andreas fault, whose location is shown in Fig. 3-6. Schwartz and Coppersmith (1984) compiled the historical instrumental seismicity for the period 1900-1980 along this segment of the fault. Using these data, they developed the recurrence curve shown in Fig. 3-7, which is represented by the equation: $Log_{10}(N(m)) = 3.30 - 0.88m$. The instrumental historical seismicity data available for this fault include earthquakes only up to magnitude 6±. Also shown in Fig. 3-7 is a box that represents the estimate of recurrence for the magnitude range of 7.5 to 8 based on geologic data (e.g., Sieh, 1978). As can be noted from the plots in Fig. 3-7, if the line developed from historical seismicity is extrapolated to the magnitude range of 7.5 to 8, the recurrence for such magnitude earthquakes would be underestimated by a factor of about 15 compared to the recurrence estimated from geologic data.
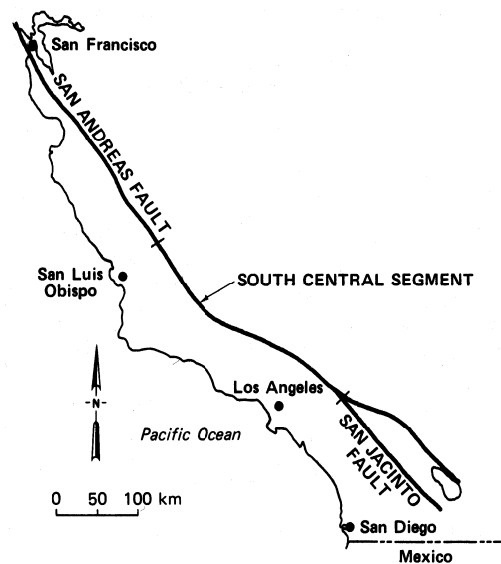
Fig. 3-6 Location of the South Central Segment of the San Andreas Fault
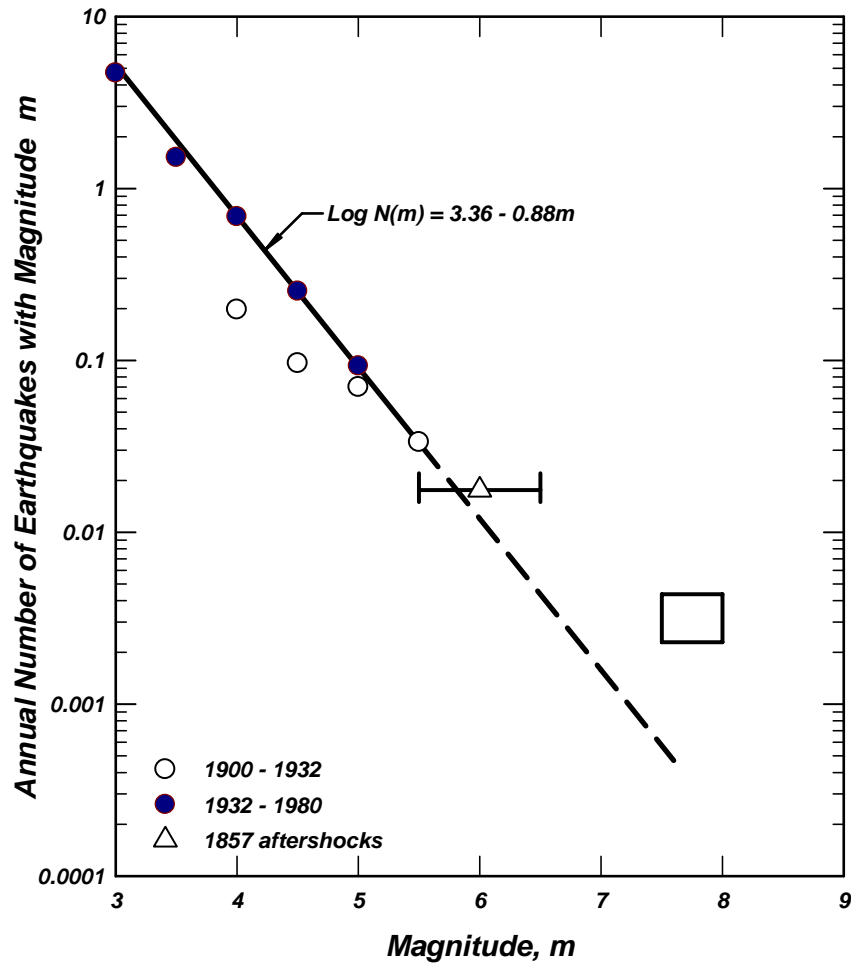
Fig. 3-7 Plot of instrumental seismicity data for the period of 1900 – 1980 along the south Central segment of the San Andreas Fault; the box in the figure represents range of recurrence for M = 7.5 – 8, based on geologic data (from Schwartz and Coppersmith, 1984)

Molnar (1979) developed a procedure to calculate recurrences based on geologic slip rate and seismic moment (Eq. 2). The seismic moment rate $\overset{\bullet}{M}_o^T$, or the rate of energy release along a fault, as estimated by Brune (1968) is given by:

$$\overset{\bullet}{M}_o^T = \mu A_f S \qquad [11]$$

And by Molnar (1979):

$$\overset{\bullet}{M}_o^T = \int_{m^o}^{m^u} n(m) M_o(m) dm \qquad [12]$$

In which S is the average slip rate in cm/year and $n(m) = -dN(m)/dm$. Differentiating Eq. [10], substituting into Eq. [12], integrating and equating the results to Eq. [11] provides the following:

$$A^\circ = \frac{c-b}{b}\;\frac{(1-k)\mu A_f S}{kM_o^u - M_o^\circ}$$

[13]

In which $Log_{10}\left(M_o\right)= 1.5M + 16.05$, M_o^u and M_o° are the seismic moments corresponding to m^u and m°, respectively, and $k = 10^{-b\left(m^u - m^\circ\right)}$.

Equation [13] is also derived on the premise that slip takes place on the fault not only because of the occurrence of m^u, but also during earthquakes with smaller magnitudes, i.e., the strain accumulated along the fault is released through slip due to the occurrence of all magnitude earthquakes. Wesnousky et al (1983) suggest, based on data from Japan, that the accumulated strain on a fault is periodically released in earthquakes of only the maximum magnitude, m^u. Wesnousky et al formulated a recurrence model based on this premise, which they designate as the maximum magnitude recurrence model. The recurrence interval, T^u in years, for the maximum magnitude is the ratio of the seismic moment (Eq. 3) associated with the maximum magnitude divided by the seismic moment rate (Eq. 11); thus:

$$T^u = \left(1.5 Log_{10}\left(m^u\right)+ 16.05\right)\!\big/\mu A_f S$$

[14]

$$N\left(m^u\right)= 1/T^u$$

Earthquakes with magnitude ranging from m° to $\left(m^u - x\right)$, which constitute foreshocks and aftershocks to the maximum earthquake, are assumed to obey Richter's recurrence model with a slope equal to the regional b. The value of x is typically equal to 1 to 1.5. Note that since the occurrence of earthquakes with less than or equal to $\left(m^u - x\right)$ is conditional on the occurrence of m^u, it follows that $N\left(m^u - x\right)= N\left(m^u\right)$.

Another model, which has been used in many applications, is the characteristic earthquake recurrence model (Schwartz and Coppersmith, 1984). This model uses Eq. [7] for the magnitude range m° to an intermediate magnitude, m^i, with a slope based on historical or instrumental seismicity. The recurrence of m^u is evaluated from geologic data using Eq. [14]. The recurrence between the intermediate magnitude and the maximum magnitude using a relation similar to Eq. [7] but having a slope much smaller than the slope used for the magnitude range m° to m^i. The characteristic recurrence model for the South Central Segment of the San Andreas fault is shown in Fig. 3-8.
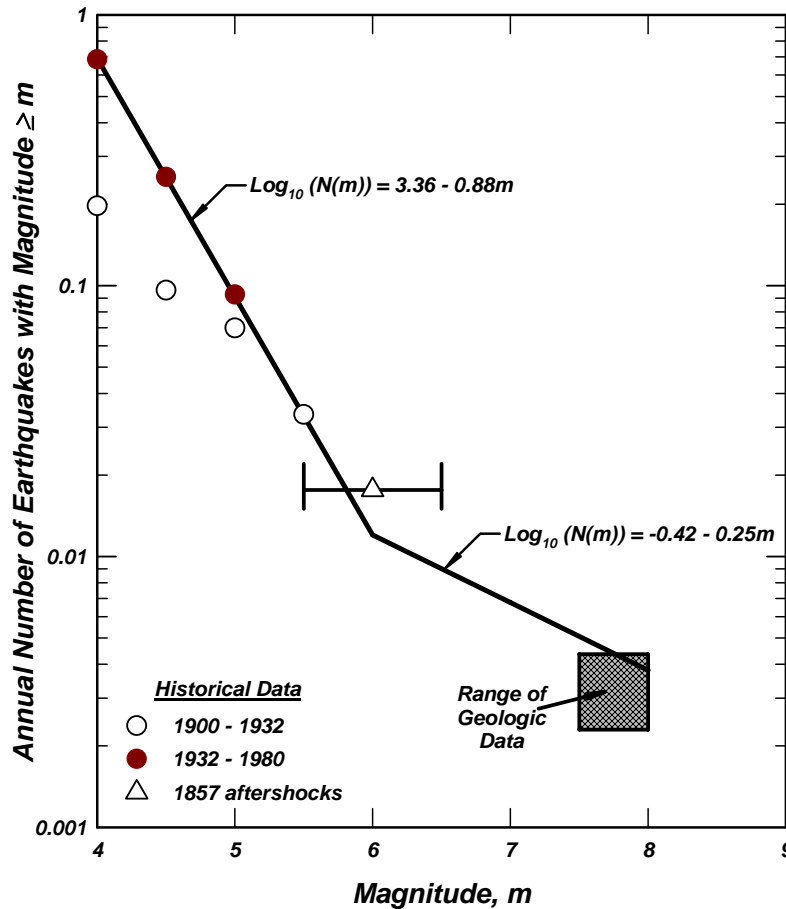
Fig. 3-8 Characteristic earthquake recurrence model for south central segment of San Andreas Fault. This is a plot of the number of earthquakes per year with a magnitude greater than or equal to the magnitude plotted on the abscissa. For example, there is one earthquake every 10 years with a magnitude greater than or equal M 5.

3.5 OTHER SEISMIC SOURCES

The sources described in the previous sections consist of specific faults or fault zones. In many parts of the world there are no known or suspected faults and hence seismic activity in those parts cannot be associated with any specific fault or fault zone. In these cases, earthquakes are considered to occur in a "seismic zone" extending over an area that is typically identified based on felt area and/or instrumental seismicity during past earthquakes. This approach is usually used in Eastern North America (ENA).

Even in geologic settings with a number of known faults, an areal source centered on the site is also considered as a possible seismic source. Often this source is assigned to account for instrumental seismicity that cannot be associated with any known (or suspected) fault. Such a seismic source is usually described as a "random" source. Random seismic sources have been assigned in many parts of Western North America (WNA) such as Washington, Oregon and California.

The distance from the site to such areal seismic sources is usually assigned as a "depth" below the site and typically varies from 5 to 15 km. Data from instrumental seismicity (which would include the depth of each event) are very helpful in assigning this depth.

4.0 ESTIMATION OF EARTHQUAKE GROUND MOTIONS AT A ROCK OUTCROP

4.1 GENERAL

As noted earlier, the intent of this document is to provide guidelines for estimating the earthquake ground motions at a rock outcrop at a particular dam site. Over the years, a variety of procedures have been proposed for making such estimates. These include: empirical procedures using recorded earthquake ground motion data; analytical procedures, and more recently, coupling the results of analytical procedures to augment the recorded data base and then using the combined data base to derive empirically-based relationships. The empirical and the analytical procedures are summarized in the remaining parts of this section of the report and in Appendices A through I.

4.2 EMPIRICAL PROCEDURES

Empirical procedures utilize recorded data to establish relationships relating an earthquake ground motion parameter (e.g., peak acceleration, velocity, displacement, spectral ordinate … etc.) to key variables that influence these parameters. Various relationships have been derived over the years. A number of these relationships are given in Appendices C through G. Some of these relationships utilize only recorded data, and some rely on both recorded data and values calculated using the analytical procedures discussed in Section 4.3 and in Appendix I.

Studies relevant to developing relationships for estimating earthquake ground motion parameters are on-going as more data are recorded and analytical procedures are improved. The results of such studies should be consulted to obtain the latest applicable relationships for a particular application.

4.3 ANALYTICAL PROCEDURES

Different approaches can be used to simulate ground motion from an earthquake source. Some of these approaches are summarized in Appendix I as examples, but not endorsement, of various methods being currently (2005) used. While the approaches can differ, they have in common certain elements and are critical in the evaluation of their applicability. It is also important to note that the synthetic time histories of ground motion are computed for a rock outcrop, i.e., analytical models are computed using linear wave propagation and includes the Earth's free surface.

The basic axiom of an analytical model is that an earthquake represents the release of elastic energy by slip occurring over some fault plane with finite area in the Earth. The earthquake initiates at the hypocenter, the point on the fault where the slip first occurs and from which the first elastic waves are emitted. As the rupture spreads over the fault, other points on the fault will slip and radiate elastic waves. The elastic waves propagate through a complex earth structure that can scatter and attenuate the waves. The final ground motion that is recorded is a convolution of the earthquake source and the path effects. Consequently, both the source and the path must be fully described to understand the ground motion that has been computed.

More details regarding the analytical procedures are provided in Appendix I.

5.0 SEISMIC HAZARD EVALUATION

The purpose of a seismic hazard evaluation is to arrive at earthquake ground motion parameters for use in evaluating the site and facilities at the site during seismic loading conditions. Coupled with the vulnerability of the site and the facilities under various levels of these ground motion parameters, the risk to which the site and the facilities may be subject can be assessed. Alternate designs, modifications, etc. can then be considered for the acceptable level of risk.

As noted earlier, there are three (4 ways if analytical methods are used) ways by which the earthquake ground motion parameters are obtained, namely: use of local building codes; conducting a deterministic seismic hazard evaluation; or conducting a probabilistic seismic hazard evaluation.

Local building codes contain a seismic zone map that includes minimum required seismic design parameters. Typically, local building codes are intended to mitigate collapse of buildings and loss of life, and not necessarily structural or architectural damage. Obviously, local building codes would not apply to the majority of structures under the jurisdiction of FERC.

5.1 DETERMINISTIC SEISMIC HAZARD EVALUATION

In a deterministic evaluation, the current practice consists of the following steps:

(a) A geologic and seismologic evaluation is conducted to define the sources (faults and /or seismic zones) relevant to the site;

(b) The maximum magnitude, m^u, on each source is estimated (Appendix A) and the appropriate distance (see Appendices C through G) to the site is determined;

(c) Recurrence relationships for each source are derived using historical seismicity as well as geologic data and an earthquake with a magnitude $m_2 < m^u$ is selected for each source such that the recurrence $N(m_2)$ for $m \geq m_2$ is the same for all sources; if, for example, $N(m_2)$= 0.005 per year (i.e., a recurrence of 200 years) is used, this earthquake is then designated the "200-year" earthquake;

(d) The needed earthquake ground motion parameters (e.g., accelerations, velocities, spectral ordinates, etc.) are calculated, using one or more attenuation relationship, or an analytical procedure, for the maximum earthquake, m^u, and for m_2 from each source; and

(e) The magnitude and distance producing the largest ground motion parameter for m^u, and for m_2 are then used for analysis and design purposes.

Note that the earthquake having the maximum magnitude (Step b) has often been designated the "maximum credible earthquake" or MCE. For critical structures, usually the MCE is used for selecting the earthquake ground motions. Attenuation relationships such as those summarized in Appendices C through G, are used to obtain the values of these motions. Typically, the median values obtained from these attenuation relationships are used when the seismic source has a relatively low degree of activity (e.g., average slip rate less than 0.1 mm/year). For high slip rate sources, the 84th-percentile values are used.

5.2 PROBABILISTIC SEISMIC HAZARD EVALUATION

5.2.1 General Approach

A probabilistic seismic hazard evaluation (PSHE) involves obtaining, through a formal mathematical process, the level of a ground motion parameter that has a selected probability of being exceeded during a specified time interval. Typically, the annual probability of this level of the ground motion parameter being exceeded, λ, is calculated; the inverse of this annual probability is return period in years. Once this annual probability is obtained, the probability of this level of the ground motion parameter being exceeded over any specified time period can be readily calculated by:

$$P = 1 - exp(-\lambda t)$$
[15]

in which P is the probability of this level of the ground motion parameter being exceeded in t years and λ is the annual probability of being exceeded.

It may be noted that the term return period has occasionally been misused to refer to recurrence interval. Recurrence interval (T in Eq. [14]) pertains to the occurrence of an earthquake on a seismic source having magnitude m or greater, and return period $(1/\lambda)$ is the inverse of the annual probability of exceeding a specific level of a ground motion parameter at a site.

A probabilistic seismic hazard evaluation at a site due to a particular source, n, involves convolving the following three probability functions (e.g., Cornell, 1968; Shah et al, 1975; McGuire, 1976; Der-Kiureghian and Ang, 1977; Kulkarni et al, 1979; Reiter, 1990):

(a) The recurrence rate is used to calculate the probability that an earthquake of a particular magnitude will occur on this source during a specified time interval. This probability function is usually expressed in terms of the mean number of earthquakes, per annum, with magnitude m_i on source n.

(b) The probability that the rupture surface is a specified distance from the site is assessed by considering both fault geometry and the magnitude-rupture length (or area) relationship.

(c) The probability that the ground motions from an earthquake of a certain magnitude occurring at a certain distance will exceed a specified level at the site is based on the selected attenuation relationship, such as those summarized in Appendices C through F.

By combining the three probability functions for each source, the annual probability of exceeding a specified level of ground motion at the site, λ_n is computed. If there are N sources, then the above process is repeated for each source, and the contributions are added to obtain the total seismic hazard at the site, i.e., $\lambda = \sum \lambda_n$ for $n = 1$ to N.

The first probability function (i.e., mean number of earthquakes with magnitude m_i) is obtained from Eq. [9]. Der-Kiureghian and Ang's (1977) probability functions for distance are usually used; similar relationships have also been developed by Chiang et al (1984). Relationships such as those summarized in Appendix A for relating rupture length or rupture area to magnitude are utilized.

Thus, the advantages of using a probabilistic seismic hazard evaluation, over a deterministic approach, include the following:

(i). Contributions from earthquakes with $m = m^o$ to $m = m^u$ on each source are included;

(ii). Contributions from all sources and all distances are included; and

(iii). The results provide the means to select design parameters that can produce comparable degrees of risk at two or more sites; and

(iv). The results are provided for a given time interval.

The disadvantages of a probabilistic seismic hazard evaluation are:

(i). The process is complex;

(ii). The result is an amalgamation from multiple sources and thus are not specific to a "design event" in the same way a deterministic analysis relies on a single event; and

(iii). There is a certain lack of transparency in conducting a probabilistic seismic hazard evaluation.

To account for uncertainty in the various model parameters (e.g., source activity, maximum magnitude, attenuation …), logic trees are used. Logic trees provide a useful tool for both displaying and examining the uncertainties in the model parameters. Each branch of the logic tree leads to a hazard curve. A probability density function can then be constructed using all the calculated hazard curves to obtain the appropriate fractiles, such as the 50-fractile (median or best estimate).

5.2.1.1 Results of a probabilistic seismic hazard evaluation. The results of a probabilistic seismic hazard evaluation include generation of hazard curves, uniform-hazard spectra, contribution by source, magnitude and distance ranges, and magnitude-distance de-aggregation ($\overline{M}$, $\overline{R}$, ε). These results can then be used to select analysis and design parameters, as appropriate. Note that the contributions by magnitude and distance ranges can be multi-modal, in which case the magnitude-distance de-aggregation ($\overline{M}$, $\overline{R}$, ε) process should reflect such a distribution, i.e., resulting in two or more values of ($\overline{M}$, $\overline{R}$, ε).

5.2.2 USGS Web Site

The USGS provides seismic hazard assessments for the U.S. and areas around the world. Values of peak ground acceleration and spectral acceleration for periods of 0.2 and 1 sec are available from the following web site: http://earthquake.usgs.gov/hazmaps/. These values are provided at a specific location (specified by longitude & latitude) for two average return periods – 475 (probability of exceedance 10% in 50 years) and 2475 (probability of exceedance 2% in 50 years) years. The USGS also provides hazard maps for specific regions.

It is important to keep in mind that the values available from this web site are not site specific. Nevertheless, it is valuable to consult this web site for a specific site.

The USGS also maintains a website OpenSHA (http:/www.OpenSHA.org) that can be used for

---

seismic hazard analysis where the user can choose the variables, different empirical relations and perform the calculation to determine the probability of exceedance curve.

6.0 GUIDELINES

These guidelines are provided in this document for FERC to establish the requirements for a seismic hazard evaluation at a particular site. The seismic design criteria for that site are then to be based on the results of such an evaluation.

6.1 REQUIRED GEOLOGIC STUDIES

The geologic studies required for a seismic hazard evaluation include the following:

- Identify the faults in the region that may affect the dam site. Ascertain style of faulting, degree of activity of each significant fault, maximum magnitude, recurrence relationship … etc.

- Identify any seismic zones (including random sources) pertinent to the site. Ascertain the extent of each zone, the maximum magnitude that can occur within each zone, and the recurrence relationship pertinent to each zone.

- Having identified the seismic zones the applicant must produce maps that clearly show the geometry of the faults for the expected events and geometry between the faults and the site.

- Produce tables that identify the magnitude of events, the geometry of the faults and closest distance to each fault, closest distance to the projection of each fault onto the earth's surface, and the distance(s) used for empirical studies.

- Special studies are required if a fault traverses or is suspected to traverse the dam or a critical appurtenant structure.

6.2 REQUIRED SEISMOLOGIC STUDIES

The seismologic studies required for a seismic hazard evaluation include the following:

- Collect the historical as well as the instrumental records of seismic activity in the region. The USGS (through the ANSS) maintains seismicity catalogs for all located events in regions of the USA. Lacking instrumental records, the historical records, which are generally based on intensity for felt events near the site, can also be used.
- It is important to determine, if possible, the maximum and minimum depths of events in the region. This information is available in seismicity catalogs. For historical seismicity, it is reasonable to assume that the historical events had a similar depth range.
- The probable style of faulting expected for the largest events that will be used to determine the ground motion can best be based on the instrumental records. In addition, the style of faulting should be consistent with the overall active tectonics. In some areas of the US, however, it may not be possible to determine the probable style of faulting.
- If a probabilistic study is to be used, it will be necessary to determine the rate of occurrence of earthquakes for a particular magnitude, generally based on Gutenberg-

Richter statistics (plots of number of earthquakes versus magnitude, see Figure 3.8 as an example).

6.3 DETERMINISTIC DEVELOPMENT OF EARTHQUAKE GROUND MOTIONS

A deterministic evaluation should always be conducted for the site to obtain the target spectrum for each source (identified in the geologic/seismologic studies) significant to the site. As noted in Section 5.1, the 84th percentile values are to be used for faults with high degree of fault activity, and the median values for those with a relatively low degree of fault activity (estimated slip rate less than 0.1 mm/year). The latest available attenuation relationships for estimating spectral ordinates at a rock site are to be used for this purpose. Several attenuation relationships should be considered.

6.4 PROBABILISTIC DEVELOPMENT OF EARTHQUAKE GROUND MOTIONS

If sufficient information, or if a logic tree can be reasonably constructed, for the seismic sources that can affect the site, then a probabilistic seismic hazard analysis (PSHA) may be completed for the site. It is essential that the seismologic as well as the geologic data pertinent to each source be utilized in establishing the appropriate recurrence relationship for each source, and that a number of attenuation relationships be used.

Values obtained from the USGS web site (http://earthquake.usgs.gov/hazmaps/) for both the 475 (10% in 50 years) and for 2475 (2% in 50 years) return periods should be obtained for comparison purposes. Analysis and design should be based on site-specific results; the USGS web site values are used only for comparison.

6.5 MINIMUM REQUIRED PARAMETERS FOR CONTROLLING EVENT(S)

The following ground motion parameters should be provided for each controlling event:

- Geometry and location of the fault, magnitude of the earthquake and closest distance to site. Because there are many definitions of distances from the fault to the site, the choice of the single distance that is selected must be clearly explained and must be consistent with the attenuation relationship used. There should be a map that shows the relationship between the fault(s) of the controlling event(s) and the site.

- Target peak acceleration and spectral ordinates for motions generated by this event at a rock outcrop at the site.

- If accelerograms are to be used, either recorded accelerograms or spectrum-compatible accelerograms can be used. A minimum of 3 recorded accelerograms should be selected; preference should be given to accelerograms recorded during earthquakes having comparable magnitude and at distances comparable to the magnitude and distance of the controlling event. The site conditions of the recording station should be "rock" to the extent possible (i.e., if there are no relevant recording at rock site, then other site conditions can be considered; in no case, however, should accelerograms recorded at soft soil sites be used). The "seed" motion selected for use in constructing a spectrum-compatible accelerogram should follow these criteria as well.

The following plots should be provided for each recorded accelerogram to be used directly in the analysis, seed accelerogram, and spectrum-compatible accelerogram:

- Acceleration spectrum (pseudo-absolute acceleration versus period) together with the Target spectrum;

- Time series of acceleration, velocity and displacement;

- Husid plot to assess duration (based on 5% to 95% of Arias intensity); and

- Fourier amplitude versus frequency (log-log scale).

Sample plots are shown in Figs. 6-1 through 6-4 (***Figures to be included in a later draft***).

6.6 SELECTION OF APPLICABLE ACCELEROGRAMS

(TBC)

7.0 REVIEW PROCESS

This section is to be completed based on final discussions with ICODS (maybe by reference to a new or existing directive).

8.0 ACKNOWLEDGMENTS

(TBC)

9.0 REFERENCES

1.   Abrahamson, N. A. and Shedlock, K. M. (1997) "Overview", Seismological Research Letters, Vol. 68, No. 1, January / February, pp 9-23.

2.   Abrahamson, N. A. and Somerville, P. G. (1996) "Effects of the Hanging Wall and Footwall on Ground Motions during the Northridge Earthquake", Bulletin of the Seismological Society of America, Vol. 86, No. 1, January, pp 93-99.

3.   Abrahamson, N. A. and W. J. Silva (1997) "Empirical Response Spectral Attenuation Relations for Shallow Crustal Earthquakes", Seismological Research Letters, Seismological Society of America, Vol. 68, No. 1, January 1997, pp 94-127.

4.   Abrahamson, N. A. and W. J. Silva (2007). Abrahamson-Silva NGA Empirical Ground Motion Model for the Average Horizontal Component of PGA, PGV, and Spectral Acceleration for periods from 0.01-10.0 seconds, Report to the Pacific Earthquake Engineering Research Center, Berkeley, CA.

5.   Abrahamson, N., P. Somerville, and C. Cornell (1990). Uncertainty in numerical strong motion predictions, in *Proc. Of the Fourth U.S. National Conference on Earthquake Engineering*, Vol. 1, 407-416.

6.   Adams, J. and Halchuk, S. (2003). Fourth generation seismic hazard maps of Canada: Values for over 650 Canadian localities intended for the 2005 National Building Code of Canada. Geological Survey of Canada, Open File 4459, 155 pp.

7.   Aki, K. (1966) "Generation and Propagation of *G* waves from the Niigata Earthquake of June 16, l964. Part II. Estimation of Seismic Moment, Released Energy and Stress-Strain Drop from the *G*-wave Spectrum", Bulletin of the Earthquake Research Institute, Tokyo University, Vol. 44, pp 73-88.

8.   Aki, K. (1967) "Scaling Law of Seismic Spectrum", Journal of Geophysical Research, Vol. 72, pp 1217-1231.

9.   Aki, K. and P. Richards (1980). *Quantitative Seismology Theory and Methods*, W. H. Freeman and Company, San Francisco.

10.   Allen, C. R. (1986) "Seismological and Paleo-Seismological Techniques of Research in Active Tectonics", Active Tectonics, National Academy Press, Washington, D.C., pp 148-154.

11.   Anderson, J. G., and Hough, S. E. (1984) "A Model for the Shape of the Fourier Amplitude Spectrum of Acceleration at High Frequencies", Bulletin of the Seismological Society of America, Vol. 74, pp 1969-1993.

12.   Andrews, D. (1980). A stochastic fault model, I. Static case, *J. Geophys. Res.* **85**, 3867-3877.

13.   Arabasz, W. J., and Robinson, R. (1976) "Micro-Seismicity and Geologic Structure in the Northern South Island, New Zealand", New Zealand Journal of Geology and Geophysics, Vol. 19, pp 561-601.

14.   Archuleta, R. J. (1984) "A Faulting Model for the Imperial Valley Earthquake", Journal of Geophysical Research, Vol. 89, pp 4559-4585.

15.   Archuleta, R. J., and Hartzell, S. H. (1981) "Effects of Fault Finiteness on Near-Source Ground Motion", Bulletin of the Seismological Society of America, Vol. 71, pp 939-957.

16.   Archuleta, R., P. Liu, J. Steidl, F. Bonilla, D. Lavallée, and F. Heuze (2003). Finite-fault site-specific acceleration time histories that include nonlinear soil response, *Phys. Earth Planet. Int.,* **137**, 153-181.

17.   Atkinson, G. M. and Boore, D. M. (1997) "Stochastic Point-Source Modeling of Ground Motions in the Cascadia Region", Seismological Research Letters, Vol. 68, pp 24-40.

18.   Atkinson, G. M, and B. M. Boore (2003). Empirical ground motion relations for subduction zone earthquakes and their applications to Cascadia and other regions, Bull. Seism. Soc. Am., 1703.

19.   Atkinson, G. M. and D. M. Boore (1998). Evaluation of models for earthquake source spectra in eastern North America, *Bull. Seism. Soc. Am.*, **88**, 917-934.

20.   Atkinson, G. M. and P. G. Somerville (1994). Calibration of time history simulation methods, *Bull. Seism. Soc. Am.*, **84**, 400-414.

21.   Atkinson, G. M., and Boore, D. M. (1987) "On the m_n, M Relation for Eastern North American Earthquakes", Seismological Research Letters, Vol. 58, pp 119-124.

22.   Baker, J. and C. A. Cornell (2006). Spectral shape, epsilon and record selection, Earth. Eng. Struct. Dyn., 35, 1077-1095.

23.   Benioff, H. (1955) "Mechanism and Strain Characteristics of the White Wolf Fault as Indicated by the Aftershock Sequence; Earthquakes in Kern County, California during 1955", California Division of Mines Bulletin 171, pp 199-202.

24.   Benjamin, J. R. and Associates (1988) "A Criterion for Determining Exceedance of the Operating Basis Earthquake", EPRI Report NP-5930, Electrical Power Research Institute, Palo Alto, California.

25.   Bernreuter, D. L., Savy, J. B., Mensing, R. W. and Chen, J. C. (1989) "Seismic Hazard Characterization of 69 Nuclear Power Plant Sites East of the Rocky Mountains", U. S. Nuclear Regulatory Commission, NUREG/CR-5250.

26.   Boatwright, J. (1988). Stochastic simulation of high-frequency ground motions based on seismological models of the radiated spectra, *Bull. Seism. Soc. Am.*, **78**, 489-508.

27.   Bolt, B. A. (1969) "Duration of Strong Motions", Proceedings of the 4th World Conference on Earthquake Engineering, Santiago, Chile, pp 1304-1315.

28.   Boore, D. M. (1983) "Stochastic Simulation of High-Frequency Ground Motions Based on Seismological Models of the Radiated Spectra", Bulletin of the Seismological Society of America, Vol. 73, pp 1865-1894.

29. Boore, D. M. (1983). Stochastic simulation of high-frequency ground motions based on seismological models of radiated spectra, *Bull. Seism. Soc. Am.*, **73**, 1865-1894.

30. Boore, D. M (2006).   Point source stochastic model software, available at: http://quake.wr.usgs.gov/~boore/software+online.htm

31. Boore, D. M., and Atkinson, G. M. (1987) "Stochastic Prediction of Ground Motion and Spectral Response Parameters at Hard-Rock Sties in Eastern North America", Bulletin of the Seismological Society of America, Vol. 77, pp 440-467.

32. Boore, B. M and G. M. Atkinson (2006). Boore-Atkinson provisional NGA empirical ground motion model for the average horizontal component of PGA, PG and Sa at spectral periods of 0.05, 0.1, 0.2, 0.3, 0.5, 1, 2, 3, 4, and 5 seconds, Report to the Pacific Earthquake Engineering Research Center, Berkeley, CA.

33. Brune, J. N. (1970) "Tectonic Stress and the Spectra of Seismic Shear Waves from Earthquakes", Journal of Geophysical Research, Vol. 75, pp 4997-5009. <u>***Note***</u>: Errata included in Journal of Geophysical Research, Vol. 76, pp 5002, 1971.

34. Brune, J.N. (1970). Tectonic stress and the spectra of seismic shear waves from earthquakes, *J. Geophys. Res*., **76**, 5002.

35. Campbell, K. W. (1997) "Empirical Near-Source Attenuation Relationships for Horizontal and Vertical Components of Peak Ground Acceleration, Peak Ground Velocity, and Pseudo-Absolute Acceleration Response Spectra", Seismological Research Letters, Vol. 68, No. 1, January / February, pp 154-179.

36. Campbell, K. W. and Y. Bozorgnia (2006). Campbell-Bozorgnia NGA Empirical Ground Motion Model for the Average Horizontal Component of PGA, PGV, PGD and Sa at Selected periods Ranging from 0.01-10.0 Seconds, (version 1.0), Report to the Pacific Earthquake Engineering Research Center, Berkeley, CA.

37. Chiou, B. S-J and R. R. Youngs (2006). Chiou and Youngs PEER-NGA Empirical Ground Motion Model for the Average Horizontal Component of Peak Acceleration and Pseudo-Spectral Acceleration for Spectral Periods of .01 to 10 Seconds, Report to the Pacific Earthquake Engineering Research Center, Berkeley, CA.

38. Cohee, B. P., P. G. Somerville and N. A. Abrahamson (1991). Simulated ground motions for hypothesized $M_W = 8$ subduction earthquakes in Washington and Oregon, *Bull. Seism. Soc. Am.*, **81**, 28-56.

39. Coppersmith, K. J. (1991) "Seismic Source Characterization for Engineering Seismic Hazard Analysis", Proceedings of the Fourth International Seismic Zonation Conference, Vol. 1, pp 160.

40. Cornell, C. A. (1968) "Engineering Seismic Risk Analysis", Bulletin of the Seismological Society of America, Vol. 58, pp 1583-1606.

41. Cornell, C.A., and VanMarke, E. H. (1969), "The Major Influences on Seismic Risk", Proceedings of the Third World Conference on Earthquake Engineering, Santiago Chile, Vol. A-l, pp 69-93.

42.   Dan, K., T. Watanabe, T. Tanaka, and R. Sato (1990). Stability of earthquake ground motion synthesized by using different small-event records as empirical Green's functions, *Bull. Seism. Soc. Am.*, **80**, 1433-1455.

43.   Day, S. M. (2001). Tests of 3D elastodynamic codes, Final Report, PEER, Lifelines Task 1A01, (http://peer.berkeley.edu/lifelines/LL-CEC/notes/topic1.html).

44.   Day, S. M. (2005). 3D ground motion simulation in basins, Final Report, PEER, Lifelines Task 1A03, (http://peer.berkeley.edu/lifelines/LL-CEC/notes/topic1.html).

45.   Day, S.M. (1982). Three-dimensional simulation of spontaneous rupture: the effect of nonuniform prestress, *Bull. Seism. Soc. Am.*, **72**, 1881-1902.

46.   dePolo, C. M., and Slemmons, D. B. (1990) "Estimation of Earthquake Size for Seismic Hazards", *in* Krinitsky, E. L., and Slemmons, D. B., eds., Reviews in Engineering Geology, Vol. VIII, Neotectonics in Earthquake Evaluation, Geological Society of America, Boulder, CO, pp 1-28.

47.   Der Kiureghian, A. and H. S. Ang, (1975) "A line source model for seismic risk analysis", Technical Report, Structural Research Series No. 419, Dept. of Civil Engineering, University of Illinois, Urbana, IL.

48.   Dobry, R., Idriss, I. M.., and Ng, E. (1978) "Duration Characteristics of Horizontal Components of Strong-Motion Earthquake Records", Bulletin of the Seismological Society of America, Vol. 68, No. 5, pp 1487-1520.

49.   Earthquake Engineering Research Institute (EERI) Committee on Seismic Risk (1989) "The Basics of Seismic Risk Analysis", Earthquake Spectra, Vol. 5, pp 675-702.

50.   Electric Power Research Institute (EPRI) (1986) "Seismic hazard methodology for the central and eastern United States", Technical Report NP-4726A: EPRI, Palo Alto, California, Revised 1988, 10 volumes.

51.   Frankel, A. (1995). Simulation strong ground motions of large earthquake using recordings of small earthquakes: the Loma Prieta mainshock as a test case, *Bull. Seism. Soc. Am.*, **85**, 1144-1160.

52.   Frankel, A., Mueller, C., Barnhard, T., Perkins, D., Leyendecker, E. V., Dickman, N., Hanson, S., and Hopper, M. (1996) "National Seismic-Hazard Maps", Documentation, U. S. Geological Survey, Open-File Report 96-532.

53.   Gardner, J. K., and Knopoff, L. (1974) "Is the Sequence of Earthquakes in Southern California with Aftershocks Removed, Poissonian?" Bulletin of the Seismological Society of America, Vol. 64, pp 1363-1367.

54.   Graves, R. W. (1996). Simulating seismic wave propagation in 3-D elastic media using staggered grid finite differences, *Bull. Seism. Soc. Am.*, **86**, 1091-1106.

55.   Guatteri, M., P. Mai, G. Beroza, and J. Boatwright (2003). Strong ground-motion prediction from stochastic-dynamic source models, *Bull. Seism. Soc. Am.*, **93**, 301-313.

56. Gutenberg, B., and Richter, C. R. (1944) "Seismicity of the Earth and Associated Phenomena", Princeton University Press, Princeton, New Jersey.

57. Hall, J. F., Heaton, T. H., Walling, M. W., and Wald, D. J. (1995) "Near-Source Ground Motions and its Effects on Flexible Buildings", Earthquake Spectra, Vol. 11, pp 569-605.

58. Hanks, T. C. (1982) "f_{max}", Bulletin of the Seismological Society of America, Vol. 72, pp 1867-1879.

59. Hanks, T. C. and H. Kanamori (1979). A moment magnitude scale, *J. Geophys. Res.* **84**, 2348-2350

60. Hanks, T. C., and Kanamori, H. (1979) "A Moment Magnitude Scale", Journal of Geophysical Research, Vol. 84, pp 2348-2350.

61. Hanks, T. C., and McGuire, R. K. (1981) "The Character of High Frequency Strong Ground Motion", Bulletin of the Seismological Society of America, Vol. 71, pp 2071-2095.

62. Hartzell, S. (1978). Earthquake aftershocks as Green's functions, *Geophysics Res. Lett.*, **5,** 1-4.

63. Hartzell, S., A. Leeds, A. Frankel, R. Williams, J. Odum, W. Stephenson and W. Silva (2002). Simulation of broadband ground motion including nonlinear soil effects for a magnitude 6.5 earthquake on the Seattle fault, Seattle, Washington, *Bull. Seism. Soc. Am.*, **92**, 831-853.

64. Hartzell, S., S. Harmsen, A. Frankel, and S. Larsen (1999). Calculation of broadband time histories of ground motion: Comparison of methods and validation using strong-ground motion from the 1994 Northridge, California, earthquake, *Bull. Seism. Soc. Am.*, **89**, 1484-1504.

65. Herrero, A. and P. Bernard (1994). A kinematic self-similar rupture process for earthquake, *Bull. Seism. Soc. Am.*, **84**, 1216-1228.

66. Hutchings, L. (1994). Kinematic earthquake models and synthesized ground motion using empirical Green's functions, *Bull. Seism. Soc. Am.*, **84**, 1028-1050.

67. Idriss, I. M. (1995) "An Overview of Earthquake Ground Motions Pertinent to Seismic Zonation", Proceedings, Fifth International Conference on Seismic Zonation, Nice, France, October 1995, Vol. III, pp

68. Idriss, I. M. (1985) "Evaluating Seismic Risk in Engineering Practice", Proceedings, 11th International Conference on Soil Mechanics and Foundation Engineering, San Francisco, 12-16 August 1985, Vol. 1, pp 255 – 320.

69. Idriss, I. M. (1993) "Procedures for Selecting Earthquake Ground Motions at Rock Sites", Report No. NIST GCR 93-625, Report to National Institute of Standards & Technology, Gaithersburg, Maryland, Center for Geotechnical Modeling, Department of Civil & Environmental Engineering University of California at Davis.

70. Idriss, I. M. (2007). Empirical model for estimating the average horizontal values of pseudo-absolute spectral accelerations generated by crustal earthquakes, Vol 1, Sites with V_{S30} =450 to 900 m/s, Report to the Pacific Earthquake Engineering Research Center, Berkeley, CA.

71. Irikura, K. (1983). Semi-empirical estimation of ground motions during large earthquake, *Bull. Disaster Prev. Res. Inst., Kyoto Univ.*, **33**, 63-104.

72. Irikura, K. (2002). Recipe for estimating ground motions from active fault earthquakes, in *Seismotectonics in Convergent Plate Boundary*, Eds. Y. Fujinawa and A. Yoshida, Terra Scientific Publishing Co., Tokyo, 45-55.

73. Irikura, K. and K. Kamae (1994). Estimation of strong ground motion in broad-frequency band based on a seismic source scaling model and an empirical Green's function technique, *Annali. Di Geofisica,* **37**, 1721-1743.

74. Jarpe, S. P., and Kasameyer, P. K. (1996). Validation of a procedure for calculating broadband strong-motion time-histories with empirical Green's functions, *Bull. Seism. Soc. Am.*, **86**, 1116-1129.

75. Johnston, A. C., Coppersmith, K. J., Kanter, L. R., and Cornell, C. A. (19xx) "The Earthquakes of Stable Continental Regions", Volume 1 of "Assessment of Large Earthquake Potential", Electric Power Research Institute (EPRI), TR-102261.

76. Joyner, W. and D. Boore (1986). On simulating large earthquakes by Green's-function addition of smaller earthquakes, in *Earthquake Source Mechanics*, American Geophysical Union, Washington, D.C., 269-274.

77. Joyner, W. B., and Boore, D. M. (1981) "Peak Acceleration and Velocity from Strong-Motion Records Including Records from the 1979 Imperial Valley, California, Earthquake", Bulletin of the Seismological Society of America, Vol. 71, pp 2011-2038.

78. Kamae, K., K. Irikura and A. Pitarka (1998). A technique for simulating strong ground motion using hybrid Green's function, *Bull. Seism. Soc. Am.*, **88**, 357-367.

79. Kanamori, H. (1977) "The Energy Release in Great Earthquakes", Journal of Geophysical Research, Vol. 82, pp 2981-2987.

80. Lavallée, D. and R. Archuleta (2003). Stochastic modeling of slip spatial complexities for the 1979 Imperial Valley, California, earthquake, *Geophys. Res. Lett.*, **30**, 1245.

81. Lilhanand, K., and Tseng, W. S. (1988) "Development and Application of Realistic Earthquake Time Histories Compatible with Multiple-Damping Design Spectra", Proceedings of the Ninth World Conference on Earthquake Engineering, Tokyo-Kyoto, Japan.

82. Ma, S., P. Liu and R. J. Archuleta (2004). Hybrid modeling of elastic P-SV wave motion: a combined finite-element and staggered-grid finite-difference approach, *Bull. Seism. Soc. Am.*, **94**, 1557-1563.

83. Mai, P. M. and G. C. Beroza (2002). A spatial random field model to characterize complexity in earthquake slip, *J. Geophys. Res*. **107**, 1-21.

84. Mai, P. M. and G. C. Beroza (2003). A hybrid method for calculating near-source, broadband seismograms: application to strong motion prediction, *Phys. Earth and Planet. Int.,* **137**, 183-199.

85. Midorikawa, S. (1993) "Preliminary Analysis for Attenuation of Peak Ground Velocity on Stiff Sites", Proceedings, International Workshop on Strong Motion Data, Vol. 2, Dec. 13-17, 1993, Menlo Park, California, Port and Harbor Research Institute, Japan, U. S. Geological Survey, Menlo Park, Ca.

86. Miyake, H., T. Iwata and K. Irikura (2003). Source characterization for broadband ground-motion simulation: kinematic heterogeneous source model and strong motion generation area, *Bull. Seism. Soc. Am*., **93**, 2531-2545.

87. Moczo, P., J. Kristek and Bystricky (2001). Efficiency and optimization of the 3-D finite-difference modeling of seismic ground motion, *J. Comp. Acoustics*, **9**, 539-609.

88. National Research Council (1988) "Probabilistic seismic hazard analysis", National Academy Press, Washington, DC.

89. Nuttli, O. W. (1973) "Seismic Wave Attenuation and Magnitude Relations for Eastern North America", Journal of Geophysical Research, Vol. 78, pp 876-885.

90. O'Connell, D., U. Jeffrey, and L. Block (2001). Source characterization and ground-motion modeling of the 1892 Vacaville-Winters earthquake sequence, California, *Bull. Seism. Soc. Am*., **91**, 1471-1497.

91. Oglesby, D. D. and S. M. Day (2002) Stochastic faulting stress: Implications for fault dynamics and ground motion, *Bull. Seism. Soc. Am*. **92**, 3006-3021.

92. Olsen, K. B. and R. J. Archuleta (1996). Three-dimensional simulation of earthquakes on the Los Angeles fault system, *Bull. Seism. Soc. Am.,* **86**, 575-596.

93. Olsen, K. B., R. J. Archuleta and J. R. Matarese (1995). Three-dimensional simulation of a Magnitude 7.75 earthquake on the San Andreas Fault, *Science*, **270**, 1628-1632.

94. Olson, A. H., J. A. Orcutt, and G. A. Frazier (1984). The discrete wave number finite element method of synthetic seismograms, *Geophys. R. Astr. Soc.*, **77**, 421-460.

95. Ordaz, M., J. Arboleda, and S. Singh (1995). A scheme of random summation of an empirical Green's function to estimate ground motions from future large earthquakes, *Bull. Seism. Soc. Am*., **85**, 1635-1647.

96. Pacific Gas and Electric (2001). Appendix A to Section 2.5, Humboldt Bay ISFSI Site Safety Analysis Report, January 8, 2001.

97. Pacific Gas and Electric (2002). Humboldt Bay ISFSI Project, Technical Report, TR-HBIP-2002-01.

98.   Reiter, L. (1990) *Earthquake Hazard Analysis* Columbia University Press, New York.

99.   Richter, C. F. (1935) "An Instrumental Earthquake Magnitude Scale", Bulletin of the Seismological Society of America, Vol. 25, pp 1-32.

100.   Sadigh, K, C-Y. Chang, J. A. Egan, F. Makdisi, and R. R. Youngs, (1997) "Attenuation Relationships for Shallow Crustal Earthquakes Based on California Strong Motion Data", Seismological Research Letters, Seismological Society of America, Vol. 68, No. 1, January 1997, pp 180-189.

101.   Schneider, J. F. (1993) "Guidelines for Determining Design Basis Ground Motions, Volume 1: Method and guidelines for Estimating Earthquake Ground Motion In Eastern North America", Electric Power Research Institute, Palo Alto, California.

102.   Scholz, C. H. (1990) *The Mechanics of Earthquakes and Faulting* Cambridge University Press, Cambridge, 439 pp

103.   Schwartz, D. P. (1988) "Geology and Seismic Hazards – moving into the l990s", Proceedings, Earthquake Engineering and Soil Dynamics II, Recent Advances in Ground Motion Evaluation, American Society of Civil Engineers, Geotechnical Special Publication 20, pp 1-42.

104.   Schwartz, D. P., and Coppersmith, K. J. (1984) "Fault Behavior and Characteristic Earthquakes from the Wasatch and San Andreas faults", Journal of Geophysical Research, Vol. 89, pp 5681 - 5698.

105.   Seed, H. B., Ugas, C., and Lysmer, J., 1976, Site dependent spectra for earthquake-resistant design: Bulletin of the Seismological Society of America, Vol. 66, no. I, pp 221-244.

106.   Senior Seismic Hazard Analysis Committee (SSHAC), 1995, Recommendations for Probabilistic Seismic Hazard Analysis: Guidance on Uncertainty and Use of Experts, Lawrence Livermore National Laboratory Publication UCRL-ID-122160: U.S. Nuclear Regulatory Commission publication NUREG/CR-6372.

107.   Sibson, R.

108.   Silva, W. J., and Lee, K., 1987, WES RASCAL code for synthesizing earthquake ground motions Report 24, in State-of-the Art for Assessing Earthquake Hazards in the United States: U.S.: U.S. Army Corps of Engineers, Waterways Experiment Station, Miscellaneous Papers S-73-1, Vicksburg, Mississippi.

109.   Singh, S. K., and Havskov, J., 1980, On moment-magnitude scale: Bulletin of the Seismological Society of America, Vol. 70, pp 379-383.

110.   Somerville, P. G., Smith, N. F., Graves, R. W. and Abrahamson, N. A., 1997, Modification of empirical strong ground motion attenuation relations to include the amplitude and duration effects of rupture directivity: Seismological Research Letters, Vol. 68, pp 199-222.

111.   SRL, 1997. Seismological Research Letters, Vol. 68.

112. Stepp, J.C., 1972, Analysis of the completeness of the earthquake hazard sample in the Puget Sound area and its effect on statistical estimates of earthquake hazard: Proceedings of International Conference on Microzonation for Safer Construction, Research, and Application 2, Seattle, Washington, pp 897-909.

113. Talwani, P., 1990, Neotectonics in the southeastern United States with emphasis on the Charleston, South Carolina, area; *in* Krinitzsky, E. L., and Slemmons, D. B., Neotectonics in earthquake evaluation: Geological Society of America Reviews in Engineering Geology, Vol. 8, pp 111-129.

114. Toro, G. R., Abrahamson, N., and Schneider, J. F., 1997, Model of strong ground motions from earthquakes in central and eastern North America: best estimates and uncertainties: Seismological Research Letters, Vol. 68, pp 58-73.

115. Trifunac, M. D. and Brady, A. G., 1975, On the correlation of seismic intensity with peaks of recorded strong motion, Bulletin of the Seismological Society of America, Vol. 65, pp 139-162.

116. U.S. Army Corps of Engineers, 1995, Response spectra and seismic analysis for hydraulic structures: Engineering Circular EC 1110-2-6050.

117. Uhrhammer, R. A., 1986, Characteristics of northern and central California seismicity (abs.): Earthquake Notes, Vol. 57, n. 1, pp 21.

118. Wells, D. L., and Coppersmith, K. J., 1994, New empirical relationships among magnitude, rupture length, rupture width, rupture area and surface displacement: Bulletin of the Seismological Society of America, Vol. 84, pp 974-1002.

119. Wesnousky, S. G., 1994, The Gutenberg-Richter or characteristic earthquake distribution, which is it?: Bulletin of the Seismological Society of America, Vol. 84, pp 1940-1959, and 1996, Reply to Yan Kagan's comment: Bulletin of the Seismological Society of America, Vol. 86, pp 286-291.

120. Wesnousky, S., Scholz, C. H., Shinazaki, K., and Matsuda, T., 1983, Earthquake frequency distribution and mechanics of faulting: Journal of Geophysical Research, Vol. 88, pp 9331-9340.

121. Wyss, M. (1979) "Estimating Maximum Expectable Magnitude of Earthquakes from Fault Dimensions," Geology, Vol. 7, No. 7, pp 336-340.

122. Youngs, R. R. and Coppersmith, K. (1985) "Implications of fault slip rates and earthquake recurrence models to probabilistic seismic hazard estimates", Bulletin of the Seismological Society of America, Vol. 75, pp 939-964.

123. Youngs, R. R., S. J. Chiou, W. L. Silva, and J. R. Humphrey (1997) "Strong Ground Motion Attenuation Relationships for Subduction Zone Earthquakes Based on Empirical Data and Numerical Modeling", Seismological Research Letters, Seismological Society of America, Vol. 68, No. 1, January 1997, pp 64-73.

124. Youngs, R.R., and Coppersmith, K. J., 1985a, Development of a fault-specific recurrence model, Earthquake Notes (abs.) Vol. 56, no. 1, pp 16.

125. Youngs, R.R., Coppersmith, K. J., Taylor, C. L., Power, M.S., DiSilvestro, L. A., Angell, M. M., Hall, N. T., Wesling, J. R., and Mualchin, L., 1993a, A comprehensive seismic hazard model for the San Francisco Bay Region, Proceedings of the Second Conference on Earthquake Hazards in the Eastern San Francisco Bay Area, March 25-29, 1992: California Division of Mines and Geology.

126. Youngs, R.R., Swan, F. H., and Power, M.S., 1988, Use of detailed geologic data in regional probabilistic seismic hazard analysis -- an example from the Wasatch Front, Utah, in Earthquake Engineering and Soil Dynamics 11 -- Recent Advances in Ground Motion Evaluation: American Society of Civil Engineers Geotechnical Special Publication 20, pp 156-172.

127. Youngs, R.R., Swan, F. H., Power, M.S., Schwartz, D. P., and Green, R. K., 1987, Probabilistic analysis of earthquake ground shaking hazard along the Wasatch front, Utah, in Assessment of Regional Earthquake Hazards and Risk Along the Wasatch Front, Utah, U.S.: U.S. Geological Survey Open-File Report 87-585, Vol. II, pp M-1-110.

APPENDIX A
METHODS FOR ESTIMATING EARTHQUAKE MAGNITUDE

The magnitude of an earthquake has been related to surface rupture length, subsurface rupture length, rupture area, and to maximum as well as to average surface displacement. Wells and Coppersmith (1994) published the most recent compilation of available measurements of surface rupture length, rupture area, and surface displacement, and magnitude. They derived the following expressions relating magnitude to surface rupture length, rupture area, and surface displacement:

$$M = 5.08 + 1.16 Log_{10}(SRL) \qquad \text{[A-1]}$$

$$M = 4.38 + 1.49 Log_{10}(RLD) \qquad \text{[A-2]}$$

$$M = 4.07 + 0.98 Log_{10}(RA) \qquad \text{[A-3]}$$

$$M = 6.69 + 0.74 Log_{10}(MD) \qquad \text{[A-4]}$$

$$M = 6.93 + 0.82 Log_{10}(AD) \qquad \text{[A-5]}$$

In which **M** is moment magnitude, **SRL** is surface rupture length in km, **RLD** is subsurface rupture length in km, **RA** is rupture area km^2, **MD** is maximum surface displacement in m, and **AD** is average surface displacement in m.

These expressions were derived by Wells and Coppersmith using measurements for crustal earthquakes generated by strike slip, reverse and normal faults, and suggested that these expressions are appropriate for most applications.

It is noteworthy that the expression relating magnitude to rupture area (Eq. A-3) has the least dispersion. It is also noteworthy that Wyss (1979) also derived an expression relating moment magnitude to rupture area using both crustal earthquakes as well as subduction events. The equation derived by Wyss is:

$$M = 4.15 + Log_{10}(RA) \qquad \text{[A-6]}$$

Values of **M** obtained using Eq. A-3 are presented in Fig. A-1 together with those calculated using Eq. A-6. The value of moment magnitude calculated using the equation by Wyss is about 0.1 larger than that calculated using the equation by Wells & Coppersmith for small rupture areas (10s of km^2), and about 0.15 for very large rupture areas (1000s of km^2).
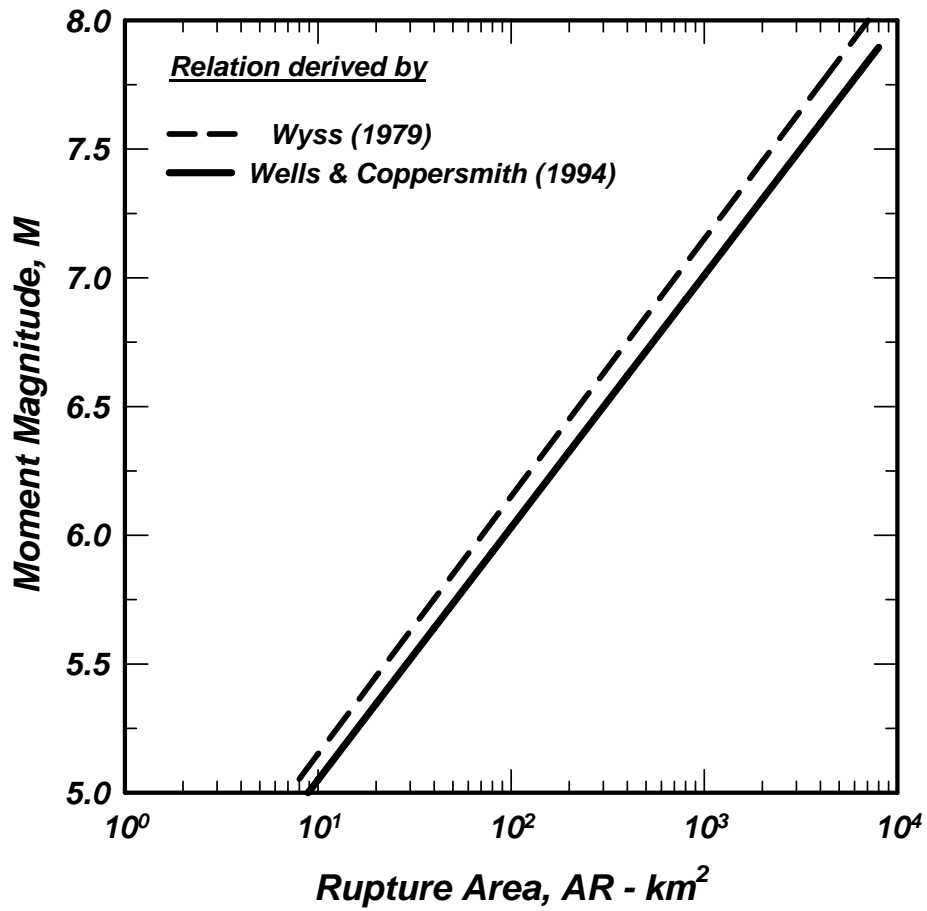
Fig. A-1 Comparison of Values of Moment Magnitude Calculated using Equations Derived by Wyss (1979) and by Wells & Coppersmith (1994)

APPENDIX B1
PROBABILISTIC SEISMIC HAZARD ANALYSIS

A probabilistic seismic hazard analysis (PSHA) is conducted for a site to obtain the probability of exceeding a given level of a ground motion parameter (e.g., acceleration, velocity, spectral acceleration … etc). Typically, the annual probability of being exceeded is calculated; the inverse of this annual probability is defined as return period.

Three probability functions are calculated and combined to obtain the annual probability of exceeding a given ground motion parameter, S . These probability functions are:

$v_n(m_i)$: mean number of earthquakes (per annum) of magnitude m_i occurring on source n.

$p_{R_n/m_i}(r_j)$: given an earthquake of magnitude m_i occurring on source n, the probability that the distance to the source is r_j.

$G_{S/m_i,r_j}(z)$: probability that S exceeds z given an earthquake of magnitude m_i occurring on source n at a distance r_j.

The mean number (per annum) λ_n on source n is then given by:

$$\lambda_n = \sum_i \sum_j v_n(m_i) p_{R_n/m_i}(r_j) G_{S/m_i,r_j}(z)$$

If there are N sources, then the annual probability of exceeding the value of z is given by:

$$\lambda(z) = \sum_{\ell=1}^{N} \lambda_\ell(z)$$

and the average return period is given by $1/\lambda(z)$.

APPENDIX B2
EXAMPLES – PROBABILISTIC SEISMIC HAZARD ANALYSIS

B2.1 INTRODUCTION

This appendix describes the types of results that should be included in a probabilistic seismic hazard analysis (PSHA) and in the development of time histories for possible dynamic analyses. The standard equations for conducting the PSHA and time history development are summarized in Appendix B1. The emphasis in this appendix is on the results of a PSHA and on the presentation of these results. The details for developing realistic scenario earthquake spectra are described since this is not part of a standard PSHA practice. The focus of this appendix is on the presentation and characterization of the hazard results, and not on the source and ground motion characterizations. Two sites, one in a high activity region (San Francisco Bay Area) and one in a moderate activity region (Pacific Northwest), are used as examples.

B2.2 SOURCE CHARACTERIZATION

The source characterization should include a description of the key sources and a map of faults and source zones and the historical seismicity. There should also be a table that clearly shows the fault and source zone parameters used in the PSHA, including alternatives models and parameter values with their associated weights.

Maximum Magnitude
Inconsistent use of terminology is a cause of confusion in many PSHA reports. In listing the fault and source zone parameters, the term "maximum magnitude" is often used for both the true maximum magnitude and for the mean magnitude from full rupture of a fault.

For source zones, the maximum magnitude is the largest magnitude that can occur in the source zone. If an exponential distribution is used for the magnitudes (e.g. Gutenberg-Richter model), then the maximum magnitude is the magnitude at which the exponential distribution is truncated. For faults, the dimension of the fault (length or area) is typically used to estimate the mean magnitude for full rupture of the fault. This mean magnitude is better described as the "mean characteristic magnitude" and not as the maximum magnitude because the PSHA will typically consider a range of ranges about this mean magnitude to account for the variability of the magnitude for a given rupture dimension. For example, the widely used Youngs and Coppersmith (1985) model for the magnitude distribution has the characteristic part of the model centered on the mean characteristic magnitude and the maximum magnitude is 0.25 units larger.

B2.3 ATTENUATION RELATIONSHIPS

In most cases, the attenuation relationships are selected from existing models for the appropriate tectonic regime (shallow crustal earthquakes in active tectonic regions, shallow crustal earthquakes in stable continental regions, or subduction zone earthquakes). Alternative models that are considered applicable should be used to capture the epistemic uncertainty in the ground motion models. The PSHA report needs to describe the weights used for each alternative model.

In some cases, new ground motion models are derived for a specific project using either empirical data or numerical simulations. The most commonly used numerical simulation procedure is the point source stochastic model (Boore, 2006). If new project-specific ground motion models are derived, then a description of the development of the new model should be included.

B2.4 HAZARD RESULTS

The basic result of a PSHA is the hazard curve which shows the probability of exceeding a ground motion for a range of ground motion values. As a minimum, the hazard should be shown for a least two spectral periods: one short period, such as PGA, and one long period, such as T=2 sec. The selection of the spectral periods should consider the period of the structure.

The mean hazard curves should be plotted to show the hazard curve from each source and the total hazard curve to provide insight into which sources are most important. The mean hazard curves should also be shown in terms of the total hazard using each attenuation relation separately to show the impact of the different ground motion models. Finally, the fractiles of the hazard should be plotted to show the range of hazard that arises due to the uncertainty in the characterization of the sources and ground motion.

B2.5 DEAGGREGATION

The hazard curve gives the combined effect of all magnitudes and distances on the probability of exceeding a given ground motion level. Since all of the sources, magnitudes, and distances are mixed together, it is difficult to get an intuitive understanding of what is controlling the hazard from the hazard curve by itself. To provide insight into what events are the most important for the hazard at a given ground motion level, the hazard curve is broken down into its contributions from different earthquake scenarios. This process is called deaggregation.

In a hazard calculation, there is a large number of scenarios considered (e.g. thousands or millions of scenarios). To reduce this large number of scenarios to a manageable number, similar scenarios are grouped together. A key issue is what constitutes "similar" scenarios. Typically, little thought has been given to the grouping of the scenarios. Most hazard studies use equal spacing in magnitude space and distance space. This may not be appropriate for a specific project. The selection of the grouping of scenarios should be defined by the engineers conducting the analysis of the structure.

In a deaggregation, the fractional contribution of different scenario groups to the total hazard is computed. The most common form of deaggregation is a two-dimensional deaggregation in magnitude and distance bins. The dominant scenario can be characterized by an average of the deaggregation. Two types of averages are considered: the mean and the mode.

The mean magnitude and mean distance are the weighted averages with the weights given by the deaggregation. The mean has advantages in that it is defined unambiguously and is simple to compute. The disadvantage is that it may give a value that does not correspond to a realistic scenario

The mode is the most likely value. It is given by the scenario group that has the largest deaggregation value. The mode has the advantage it will always correspond to a realistic source. The disadvantage is that the mode depends on the grouping of the scenarios, so it is not robust.

It is useful to plot both the deaggreagation by M-R bin and the mean M, R, and epsilon.

B2.6 UNIFORM HAZARD SPECTRA

A common method for developing design spectra based on the probabilistic approach is uniform hazard spectra. A uniform hazard spectrum (UHS) is developed by first computing the hazard at

a suite of spectral periods using response spectral attenuation relations. That is, the hazard is computed independently for each spectral period. For a selected return period, the ground motion for each spectral period is measured from the hazard curves. These ground motions are then plotted at their respective spectral periods to form the uniform hazard spectrum.

The term "uniform hazard spectrum" is used because there is an equal probability of exceeding the ground motion at any period. Since the hazard is computed independently for each spectral period, in general, a uniform hazard spectrum does not represent the spectrum of any single earthquake. It is common to find that the short period (T<0.2 sec) ground motions are controlled by nearby moderate magnitude earthquakes, whereas, the long period (T>1 sec) ground motions are controlled by distant large magnitude earthquakes.

The "mixing" of earthquakes in the UHS is often cited as a disadvantage of PSHA. There is nothing in the PSHA method that requires using a UHS. A suite of realistic scenario earthquake spectra can be developed as described below. The reason for using a UHS rather than using multiple spectra for the individual scenarios is to reduce the number of engineering analyses required. A deterministic analysis has the same issue. If one deterministic scenario leads to the largest spectral values for long spectral periods and a different deterministic scenario leads to the largest spectral values for short spectral periods, a single design spectrum that envelopes the two deterministic spectra could be developed. If such an envelope is used, then the deterministic design spectrum also does not represent a single earthquake.

The choice of using a UHS rather than multiple spectra for the different scenarios is the decision of the engineering analyst, not the hazard analyst. The engineering analyst should determine if it is worth the additional analysis costs to avoid exciting a broad period range in a single evaluation. The hazard report should include the UHS as well as the scenario spectra described below.

B2.7 SPECTRA FOR SCENARIO EARTHQUAKES

In addition to the UHS, realistic spectra for scenario earthquakes should be developed. Two different procedures for developing scenario earthquake spectra are described below. Both methods start with the identification of the controlling earthquake scenarios (magnitude, distance) from the deaggregation plots. As noted above, the controlling earthquakes will change as a function of the spectral period.

Median Spectral Shape
The most common procedure used for developing scenario earthquake spectra given the results of a PSHA is to use the median spectral shape (Sa/PGA) for the earthquake scenario from the deaggregation and then scale the median spectral shape so that it matches the UHS at the specified return period and spectral period. This process is repeated for a suite of spectral periods (e.g. T=0.2 sec, T=1 sec, T=2.0 sec). The envelope of the resulting scenario spectra become equal to the UHS if a full range of spectral periods of the scenarios is included. This avoids the problem of mixing different earthquake scenarios that control the short and long period parts of the UHS.

A short-coming of the median spectral shape method is that it assumes that the variability of the ground motion is fully correlated over all spectral periods. For example, if the UHS at a specified spectral period and return period corresponds to the median plus 1 sigma ground motion for the scenario (epsilon =1), then by scaling the median spectral shape, we are using the median plus 1 sigma ground motion at each period. Spectra from real earthquakes will have peaks and troughs

so we don't expect that the spectrum at all periods will be at the median plus 1 sigma level. This short-coming is addressed in the second method.

Expected Spectral Shape

In this method, the expected spectral shape for the scenario earthquake is computed. In this case, the expected spectral shape depends not only on the scenario earthquake, but also on the epsilon value required to scale the scenario spectrum to the UHS. Again, consider a case in which the UHS is one standard deviation above the median spectral acceleration from the scenario earthquake for a period of 2 sec. At other spectral periods, the chance that the ground motion will also be at the 1 sigma level decreases as the spectral period moves further from 2 sec.

To compute the expected spectral shape, we need to consider the correlation of the variability of the ground motion at different spectral periods. (This is the correlation of the variability of the ground motion, not the correlation of the median values). In the past, this correlation has not been commonly included as part of the ground motion model, but the correlation tends to be only weakly dependent on the data set. That is, special studies that have developed this correlation can be applied to a range of ground motion models.

Below, the equations for implementing this progress are given. First, we need to compute the number of standard deviations, $\varepsilon_U(T_o, T_{RP})$, needed to scale the median scenario spectral value to the UHS at a spectral period, T_o, and for a return period, T_{RP}. This is given by

$$\varepsilon_U(T_o, T_{RP}) = \frac{\ln\left(UHS(T_o, T_{RP})\right) - \ln\left(\hat{S}a(M, R, T_o)\right)}{\sigma(T_o, M)}$$

where $\hat{S}a(M, R, T_o)$ and $\sigma(T_o, M)$ are the median and standard deviation of the ground motion for the scenario earthquake from the attenuation relations.

The expected epsilon at other spectral periods is given by

$$\hat{\varepsilon}(T) = c\, \varepsilon_U(T_o, T_{RP})$$

where c is the square root of the correlation coefficient of the residuals at period T and T_o. An example of the values of coefficient c computed from the PEER strong motion data for M>6.5 for rock sites are listed in Table B2-1 for reference periods of 0.2, 1.0, and 2.0.

The expected spectrum for the scenario earthquake is then given by

$$Sa(T) = \hat{S}a(M, R, T_o) \exp\left(\hat{\varepsilon}(T_o, T_{RP})\sigma(T_o, M)\right)$$

This expected spectrum for the scenario earthquake is called the "conditional mean spectrum" by Baker and Cornell (2006).

Table B2-1. Example of the Slope of the Relation between
Epsilons for the Expected Spectral Shape

Period (Sec)	T_o=0.2	T_o=1.0	T_o=2.0
0.0	0.91	0.68	0.43
0.075	0.91	0.54	0.31
0.1	0.91	0.50	0.27
0.2	1.00	0.48	0.26
0.3	0.93	0.63	0.39
0.4	0.84	0.71	0.45
0.5	0.71	0.77	0.52
0.75	0.62	0.92	0.66
1.0	0.45	1.00	0.76
1.5	0.37	0.87	0.85
2.0	0.26	0.81	1.00
3.0	0.24	0.77	0.94

B2.8 TIME HISTORIES

Time histories are developed using the spectral matching approach for the Pacific Northwest example and using the scaling approach for the northern California example. The basis for selecting the reference time histories should be described. One draw-back of using the expected scenario spectra is that additional time histories will be required. If the project will be using the average response of 7 time histories, then 7 time histories are needed for each scenario spectrum. The average response is computed for each scenario and then the larger response from the two scenario is used.

If the scaling procedure is used, then time history report should list the scale factors and include the following plots:

Acceleration, velocity, and displacement seismograms for the scaled time histories,

Fourier amplitude spectra for the scaled time histories,

Comparison of the spectra of the scaled time histories with the design spectrum.

If the spectral matching procedure is used, then there are additional plots that are needed to check that the modified time history is still appropriate (e.g. check that the spectral matching has not lead to an unrealistic ground motion). The acceleration, velocity, and displacement seismograms of the modified ground motion should have the same gross non-stationary characteristics as the reference motion. For spectral matching, the time history report should include the following plots:

Acceleration, velocity, and displacement seismograms for the reference and modified time histories,

Fourier amplitude spectra for the reference and modified time histories,

Comparison of Husid plots (normalized arias intensity) for the reference and modified time histories,

Comparison of the spectra of the reference and modified time histories with the scenario earthquake spectrum.

B2.9 EXAMPLES OF PROBABILISTIC SEISMIC HAZARD ANALYSIS

B2.9.1 *Pacific Northwest Example*

A site located in northwestern Washington is used as an example. In this example, a return period of 2000 years is used. This return period is just for this example and does not imply this is this an accepted return period for dams. The selection of the return period for design ground motions for dams has not been resolved.

Source Characterization
For this example, a simplified source characterization is used. Five sources are considered: the Cascadia interface, the Juan de Fuca intra-slab, the Seattle fault, the Hood Canal fault, and a background zone. The location of the site with respect to the faults and source zones is shown in Figure B2-1. The parameters used for the sources are given in Tables B2-2a and B2-2b. These are based on the source models used by PG&E (2001, 2002), Adams and Halchuk (2003), and the USGS as part of the national hazard maps. The objective of these examples is on the presentation of the hazard results, so a detailed description of the source models is not included here. In a complete hazard study, such detailed source descriptions should be included.

Ground Motion Models
In the Pacific Northwest, both crustal and subduction earthquakes need to be considered. These two tectonic classes of earthquakes require separate ground motion models. For the crustal sources, the five NGA models recently developed as part of the PEER/Lifelines program are used. These new ground motion models include Abrahamson and Silva (2007), Boore and Atkinson (2006), Campbell and Bozorgnia (2006), Chiou and Youngs (2006), and Idriss (2007). For the Idriss model, the rock site class is used. For the other four models, a V_{S30} of 600 m/s is used. These five models are given equal weight.

For the subduction earthquakes, two models are used: Youngs et al (1997) and Atkinson and Boore (2003). For the Youngs et al model, the rock relation is used. For the Atkinson and Boore model, NEHRP site class C is used. The two models are given equal weight.

Table B2-2a. Source parameters for fault sources

	Mean Characteristic Magnitude	Recurrence Interval (yrs) of Characteristic Eqk	Slip-Rates (mm/yr)	Style-of-Faulting
Cascadia	8.2 (0.105) 8.4 (0.22) 8.5 (0.075) 8.6 (0.07) 8.7 (0.205) 8.8 (0.074) 8.9 (0.175) 9.1 (0.075)	230 (0.05) 300 (0.15) 340 (0.05) 370 (0.15) 500 (0.45) 660 (0.15)		Interface
Seattle Fault	6.9 (0.2) 7.1 (0.6) 7.3 (0.2)	5000 (0.5)	0.7 (0.25) 1.1 (0.25)	Reverse
Hood Canal fault	7.0 (1.0)		0.1 (1.0)	Strike-slip

Table B2-2b. Source parameters for areal source zones

Source	b	N(M>5)	b,N wt	M_{max}	Top (km)	Bottom (km)	Style-of-Faulting
Juan de Fuca Plate Onshore Deep	1.119 0.899 0.678	0.0007 0.0035 0.0159	(0.16) (0.68) (0.16)	6.7 (0.3) 7.1 (0.6) 7.3 (0.1)	40	80	Intra-slab
Puget Sound Deep	0.547 0.491 0.430	0.0650 0.0985 0.1770	(0.16) (0.68) (0.16)	6.9 (0.3) 7.1 (0.6) 7.3 (0.1)	50	90	Intra-slab
Cascades Mtns Background	0.92 0.87 0.83	0.0019 0.0028 0.0039	(0.16) (0.68) (0.16)	6.5 (0.5) 7.0 (0.5)	0	15	Reverse

Hazard Results
The basic hazard results are shown in Figures B2-2a and B2-2b for PGA and T=2 sec, respectively. These figures also show how each source contributes to the hazard. For PGA (Figure B2-2a), the deep earthquakes in the Juan de Fuca plate slab have the largest contribution to the hazard. The Cascadia source has about one-half of the contribution of the Juan de Fuca source. For long spectral periods (e.g. T=2 sec), the Cascadia source dominates the hazard at long return periods, but the Juan de Fuca source is still dominant at short return periods (less than 200 years).

The sensitivity of the hazard to the attenuation relations is shown in Figure B2-3a and B2-3b for PGA and T=2 sec, respectively. Since there are two classes of attenuation relations (subduction and crustal), the sensitivity is shown in terms of each class. In the top frame of each figure, the

sensitivity to the subduction attenuation relation is shown. In the lower frame, the sensitivity to the crustal attenuation relation is shown. For both PGA and T=2 sec, the hazard has a strong dependence on the subduction attenuation relation, but not on the crustal attenuation relation.

The epistemic uncertainty in the hazard is shown in Figures B2-4a and B2-4b for PGA and T=2 sec, respectively. The mean hazard is the weighted average of the hazard (y-axis) computed for each combination of alternative models. The fractiles represent the range of the hazard for the alternative models. In this case, the range of the fractiles is dominated by the epistemic uncertainty in the subduction attenuation relations. A range of a factor of 10 from the 5th to the 95th fractile is common in regions with large uncertainty in the ground motion model.

The UHS for return periods of 500, 1000, 2000, and 5000 years is shown in Figure B2-5a. This figure also compares the Cascadia (M=9, R=55 km) ground motions (median and 84th percentile) for the MCE as used in deterministic analyses. In this example, the deterministic spectra are shown separately for the two subduction attenuation relations used since these two model have significant differences. The deterministic spectra from the two subduction models are similar at long periods for which the Cascadia source dominates the hazard.

Figure B2-5b compares the UHS to the Juan de Fuca (M=7.5, R=40 km) ground motions for the MCE. For this scenario, the two subduction models are similar at short periods, but the Atkinson & Boore model leads to much larger ground motions at long periods.

The deaggregation for a return period of 2000 years is shown in Figures B2-6a and B2-6b for PGA and T=2 sec, respectively. Figure B2-6a shows that for PGA, the mode of the deaggregation is M=7.0-7.5 at distances of 50-80 km. Figure B2-6b shows that for T=2 sec, the mode of the deaggregation is M=8.5-9.0 at distances of 50-60 km.

In addition to the mode, the deaggregation can be characterized by the mean magnitude, distance, and epsilon. These mean values are shown in Figure B2-7 as a function of return period for PGA and T=2 sec. This figure shows that the mean magnitude for PGA increases as the return period increases from 100 to 500 years, but for longer return periods, the mean magnitude does not increase. For return periods greater than 500 years, the mean distance continues to decrease and the mean epsilon increases. In contrast to the PGA, For T=2 sec, the mean magnitude continues to increase as the return period increases from 100 to 10,000 years.

Expected Spectra for Scenario Earthquakes
From the deaggregation, the following scenario earthquakes were selected:

Source	M	Distance (km)	T_o (sec)
Juan de Fuca	7.3	50 km	0.2
Cascadia	8.8	55 km	2.0

The expected spectra are developed for these of these events. First, the median and standard deviation for the two scenarios listed above are computed using the two subduction ground motion models. The average of the median and the standard deviation for the two scenario earthquakes are listed in Tables B2-4a and B2-4b.

Next, the number of standard deviations needed to scale the median Sa to the UHS is determined. This value, ε_U, is shown in Table B2-3. The expected epsilon values at the other spectral periods are then computed (fifth column in Tables B2-4a and B2-4b) and the spectrum is then computed (sixth column in Tables B2-5a, and B2-5b).

The expected spectra for the scenarios are compared to the UHS in Figure B2-8. This figure shows that the expected spectrum falls below the UHS at periods away from the reference period. A suite of these expected spectra will be enveloped by the UHS. The expected spectra are realistic ground motions for a future earthquake. To limit the number of scenarios considered, these expected spectra will need to be broadened so that they cover the UHS with a small number of scenarios. To limit the number of scenarios considered, these expected spectra can be broadened so that they cover the UHS with a small number of scenarios. As an example, the two expected scenarios are broadened into two design spectra in Figure B2-9. The engineer conducting the analysis of the structure needs to determine to what degree it is worth broadening the expected spectra to reduce the number of scenarios considered.

Table B2-3. Computation of the epsilon needed to match the UHS

Period (sec)	UHS 2000 Yr (g)	Median Sa(g)	σ	ε_U
0.2	0.946	0.439	0.682	1.126
2.0	0.210	0.096	0.766	1.021

Table B2-4a. Development for the expected spectrum for
T=0.2 sec and a return period of 2000 years

Period (Sec)	c (T_o=0.2)	Median Sa(g)	σ	$\hat{\varepsilon}$	Expected Spectrum (g)
0.00	0.91	0.192	0.625	1.024	0.364
0.075	0.91	0.269	0.648	1.024	0.522
0.10	0.91	0.314	0.671	1.024	0.624
0.20	1.00	0.439	0.682	1.126	0.947
0.30	0.93	0.419	0.691	1.047	0.864
0.40	0.84	0.400	0.694	0.946	0.771
0.50	0.71	0.389	0.706	0.799	0.683
0.75	0.62	0.286	0.720	0.698	0.472
1.00	0.45	0.218	0.751	0.507	0.319
1.50	0.37	0.147	0.770	0.417	0.202
2.00	0.26	0.107	0.801	0.293	0.135
3.00	0.24	0.050	0.874	0.270	0.063

Table B2-4b. Development for the expected spectrum for
T=2.0 sec and a return period of 2000 years

Period (Sec)	c (T$_o$=2.0)	Median Sa(g)	σ	$\hat{\varepsilon}$	Expected Spectrum (g)
0.00	0.43	0.144	0.590	0.439	0.186
0.075	0.31	0.211	0.611	0.317	0.256
0.10	0.27	0.237	0.636	0.276	0.282
0.20	0.26	0.320	0.647	0.266	0.380
0.30	0.39	0.321	0.650	0.399	0.416
0.40	0.45	0.361	0.659	0.460	0.488
0.50	0.52	0.346	0.676	0.531	0.495
0.75	0.66	0.248	0.696	0.674	0.396
1.00	0.76	0.188	0.716	0.777	0.327
1.50	0.85	0.130	0.742	0.869	0.248
2.00	1.00	0.096	0.766	1.022	0.211
3.00	0.94	0.037	0.839	0.961	0.082
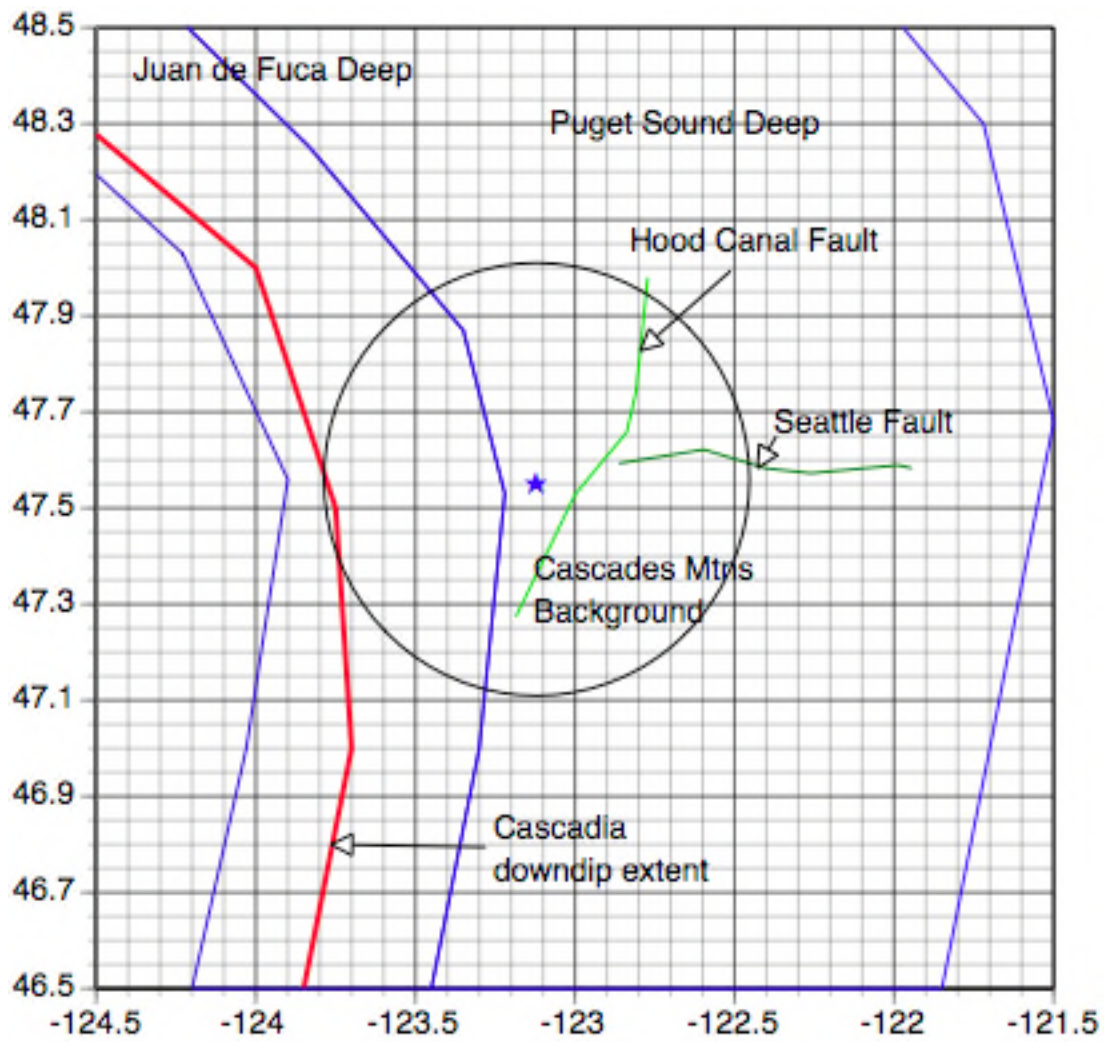
Figure B2-1. Faults and sources considered in the example.
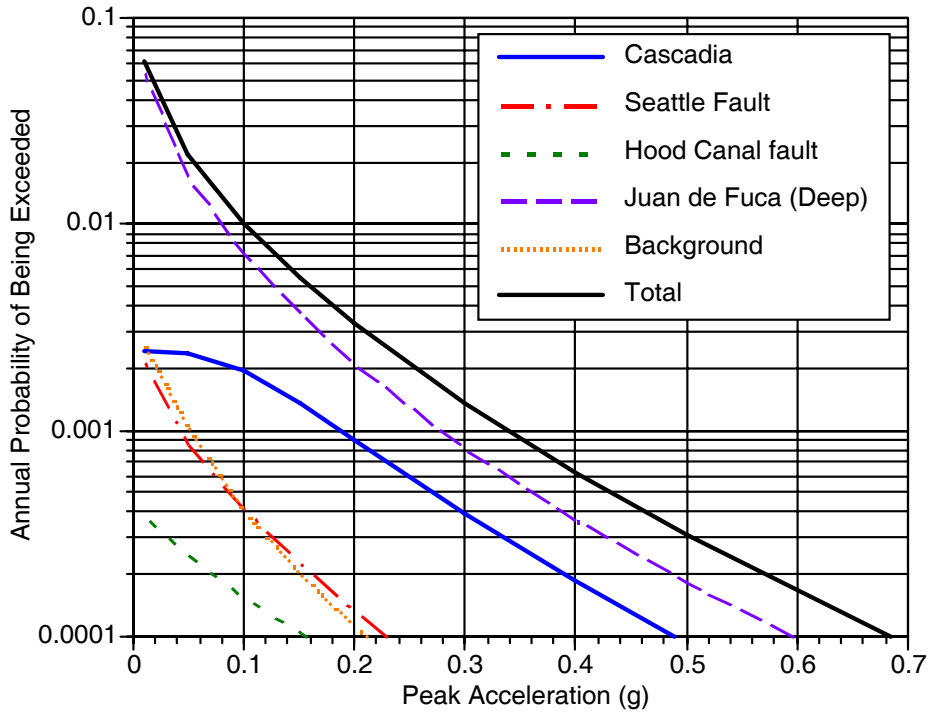
Figure 2a. Contribution to the PGA hazard by source.
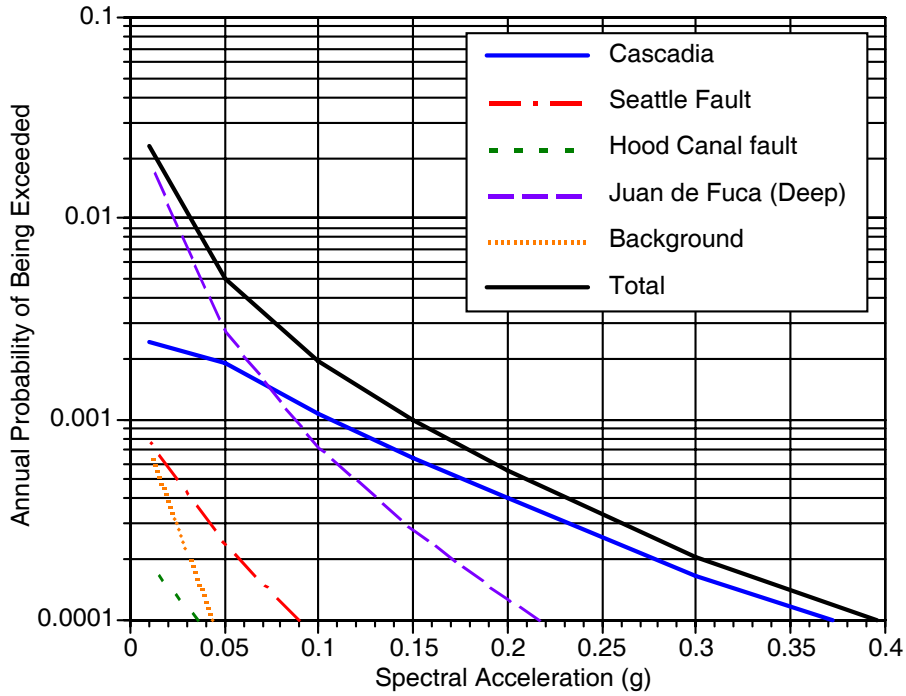
Figure B2-2b. Contribution to the T=2 sec hazard by source
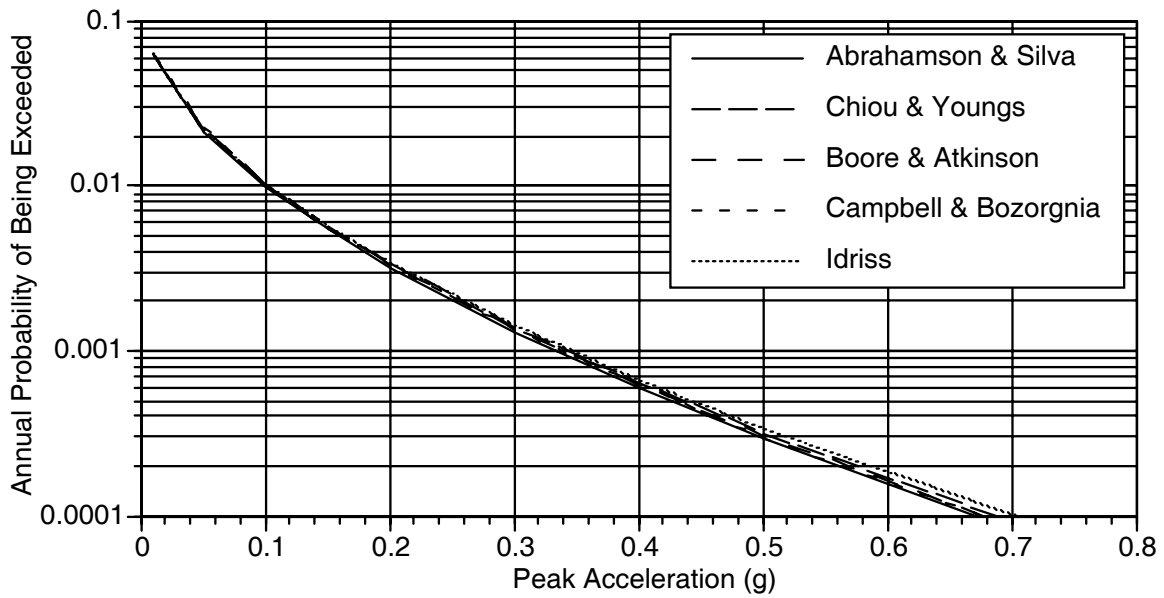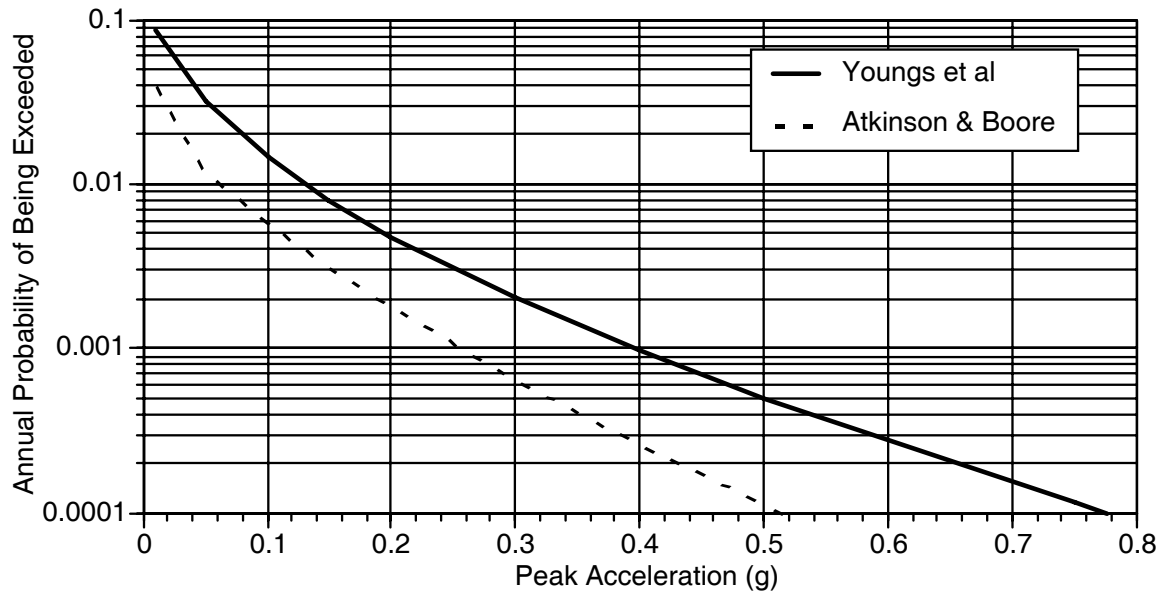
Figure B2-3a. Sensitivity of PGA hazard to attenuation relation.
Top frame: subduction models. Bottom frame: crustal models.
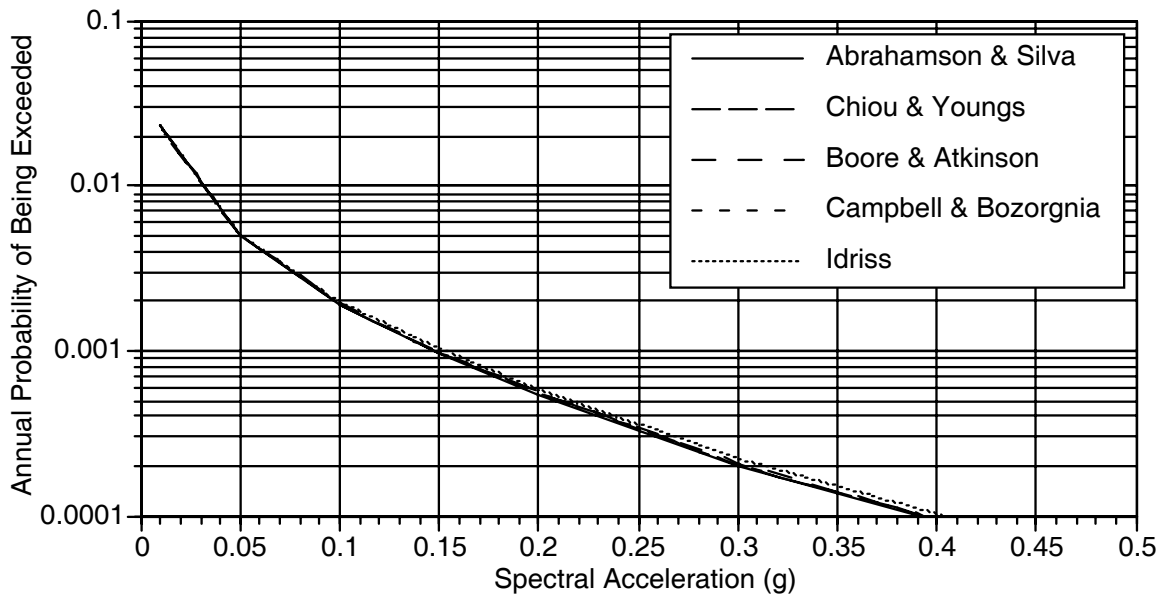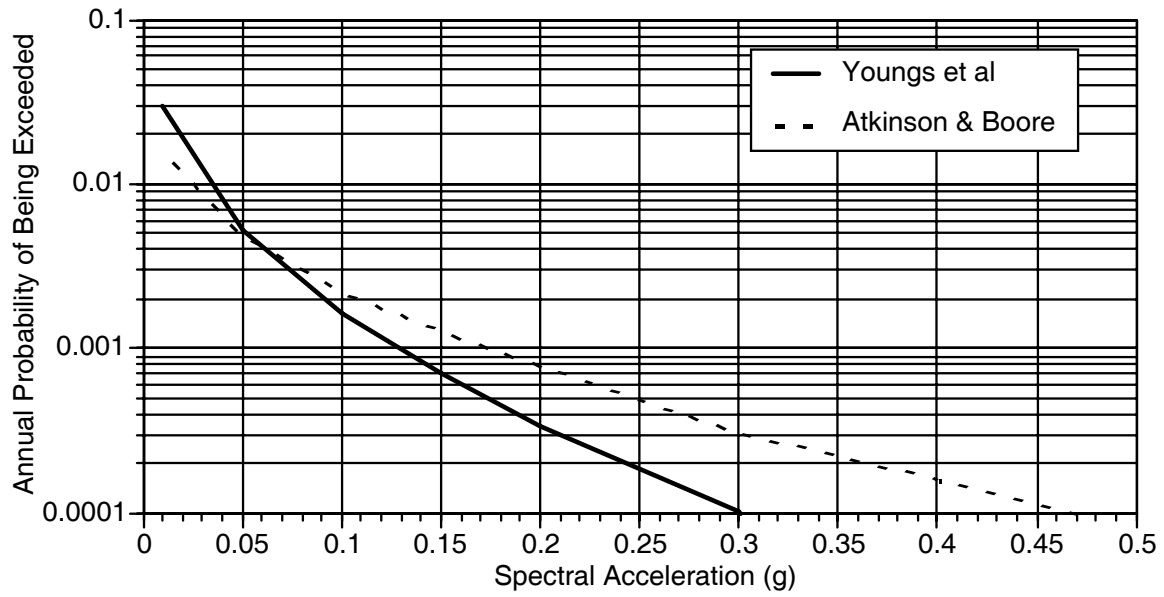
Figure B2-3b. Sensitivity of T=2 sec hazard to attenuation relation.
Top frame: subduction models. Bottom frame: crustal models
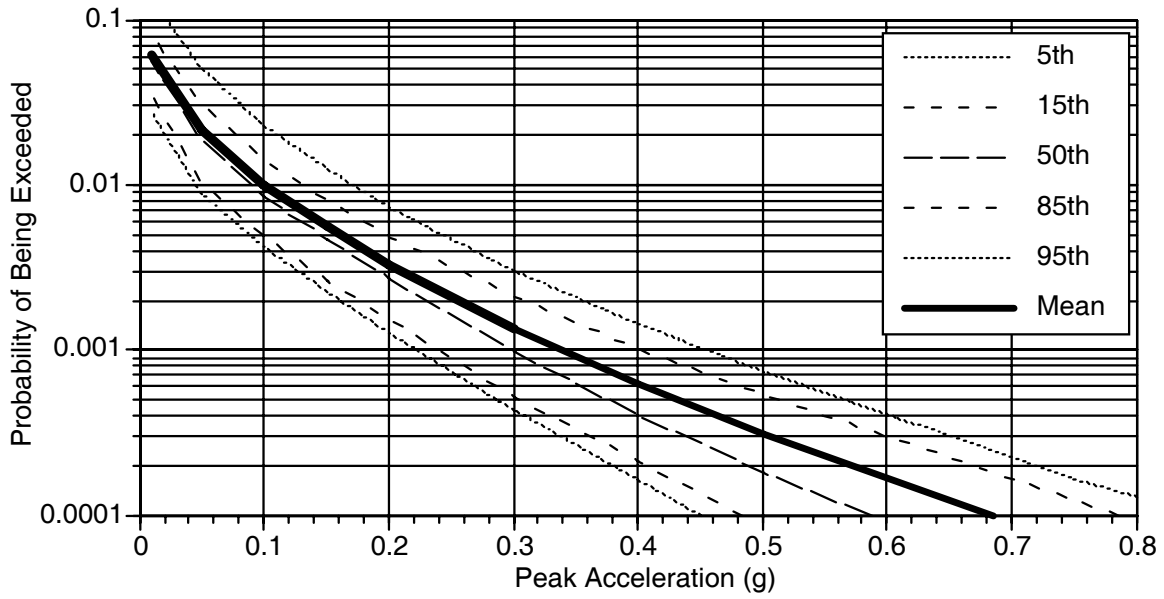
Figure 4a. Uncertainty fractiles of the PGA hazard
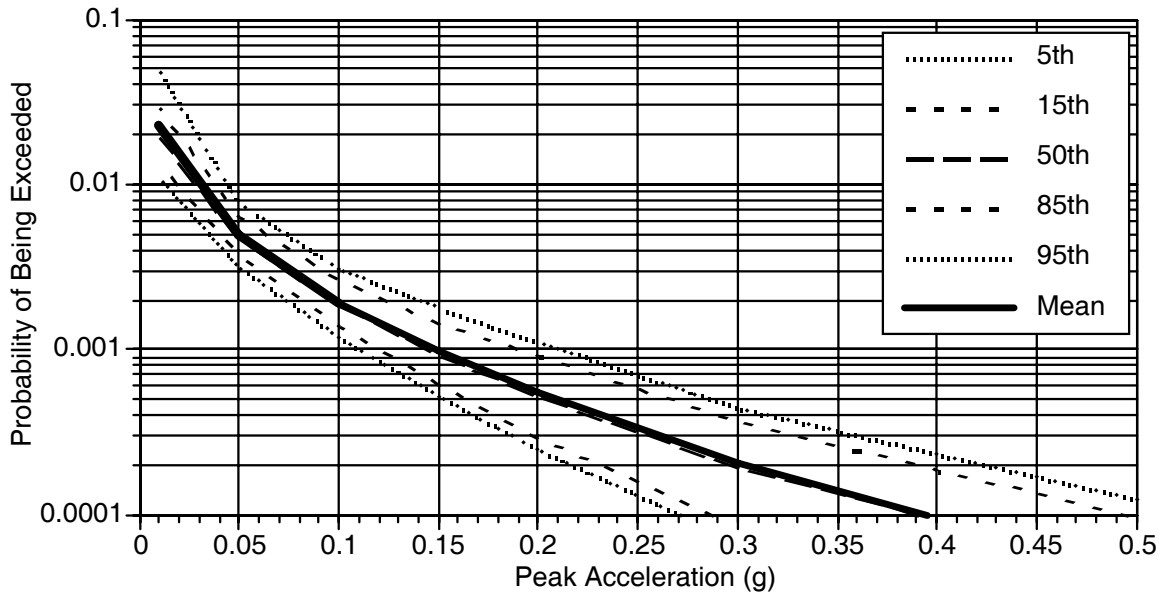
Figure B2-4b. Uncertainty fractiles of the T=2 sec hazard
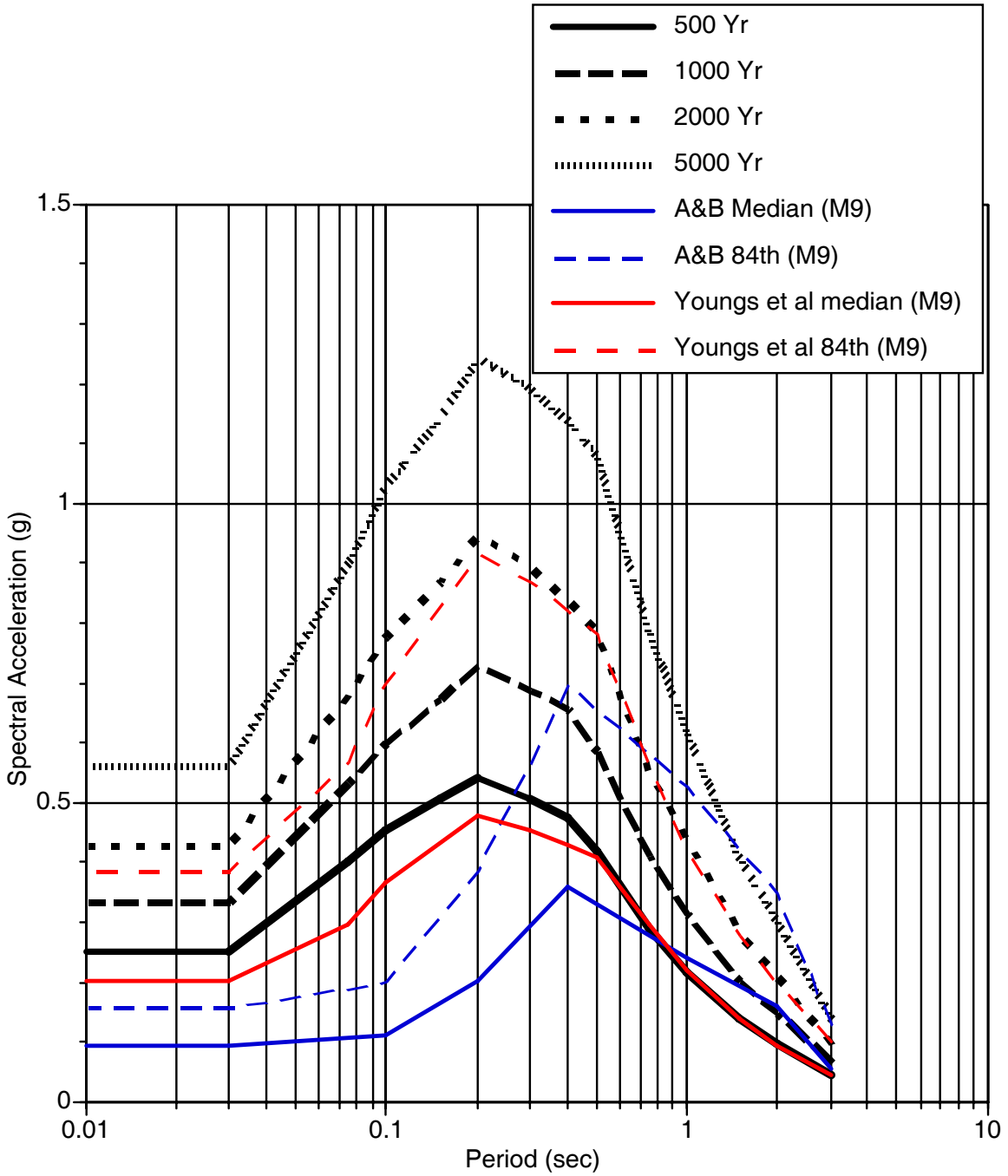
Figure B2-5a. UHS and deterministic (MCE) spectra for the M9 Cascadia source (R=55 km).
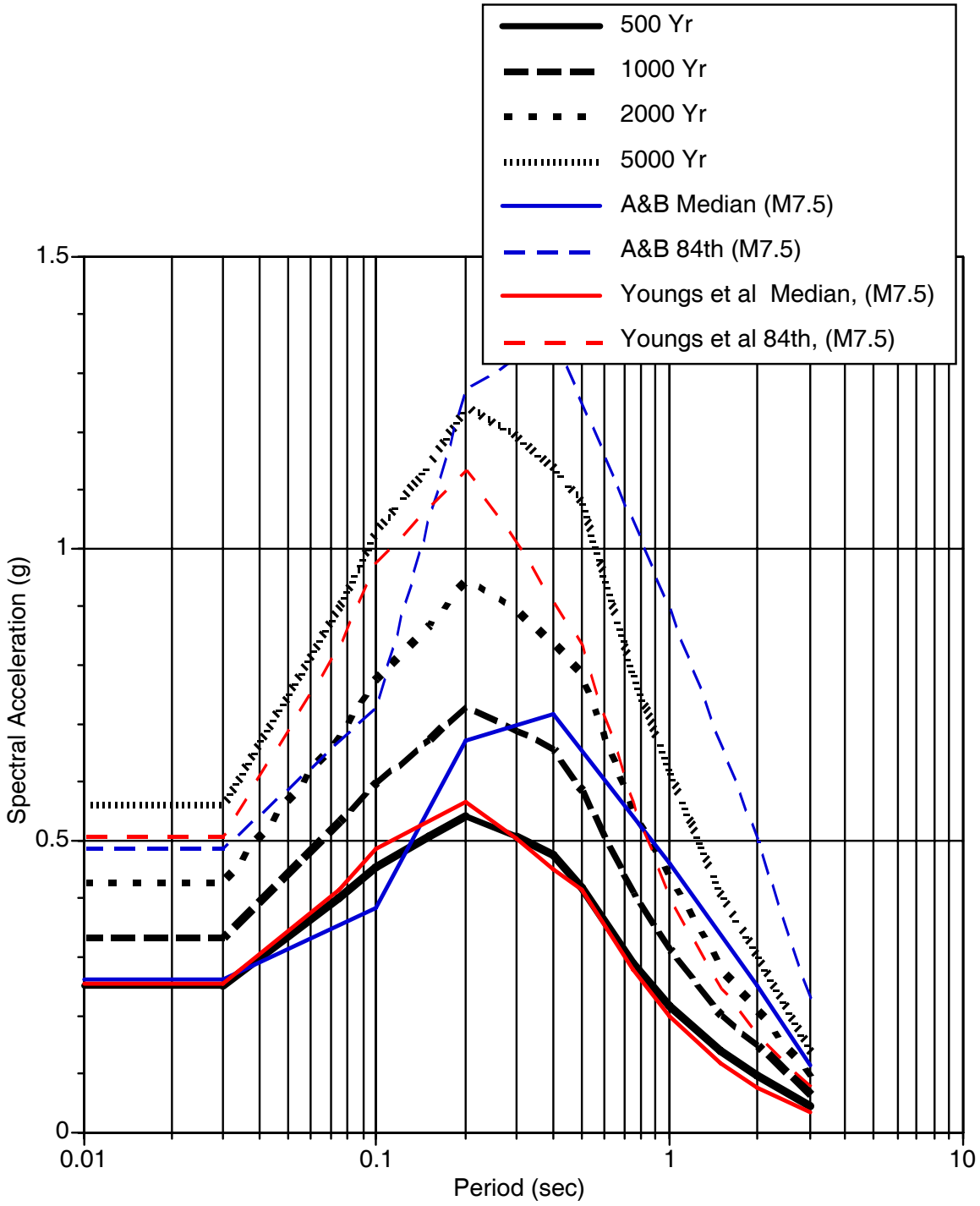
Figure B2-5b. UHS and deterministic (MCE) spectra for the M=7.6 Juan de Fuca source (R=40 km).
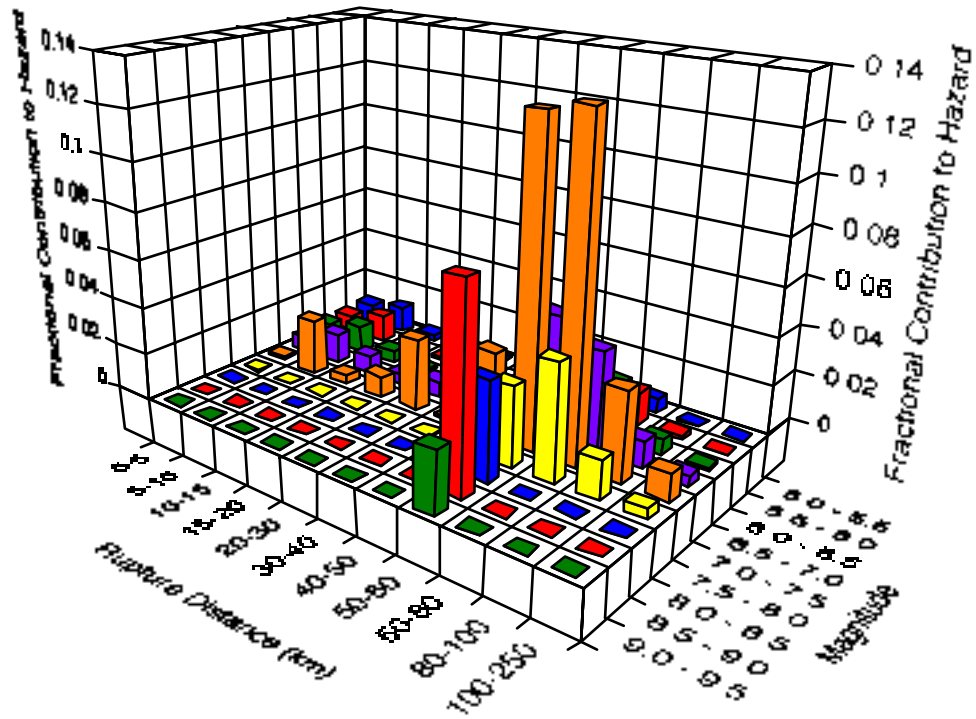
Figure 6a. Deaggreagation for PGA hazard for a return period of 2000 years.
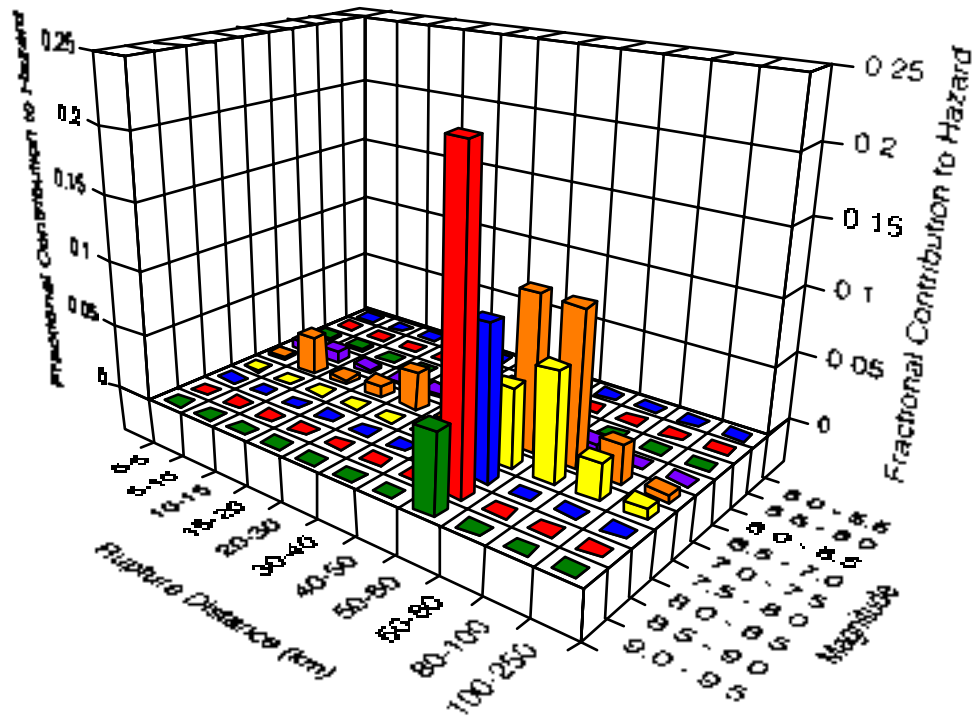
Figure B2-6b. Deaggregation for T=2 sec hazard for a return period of 2000 years.
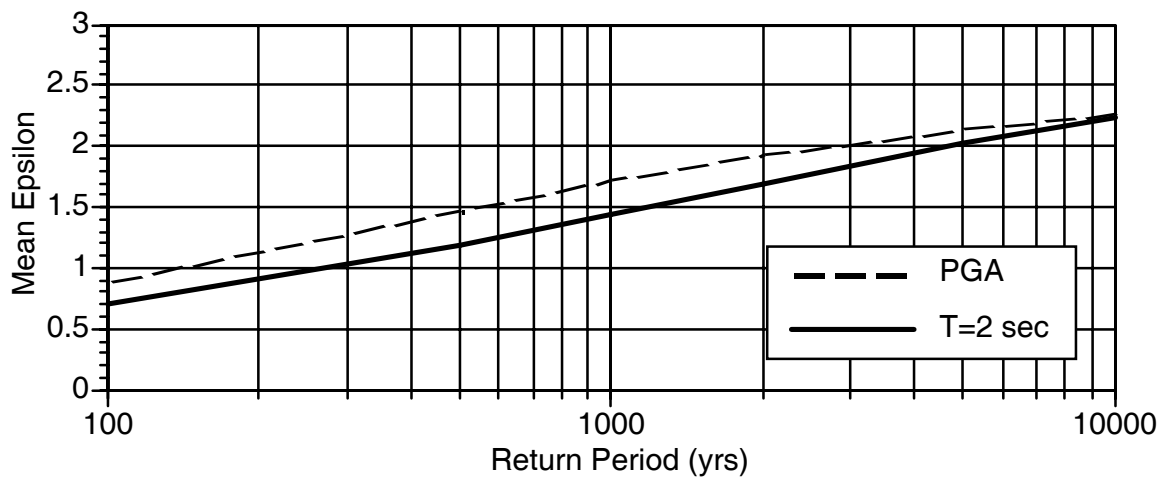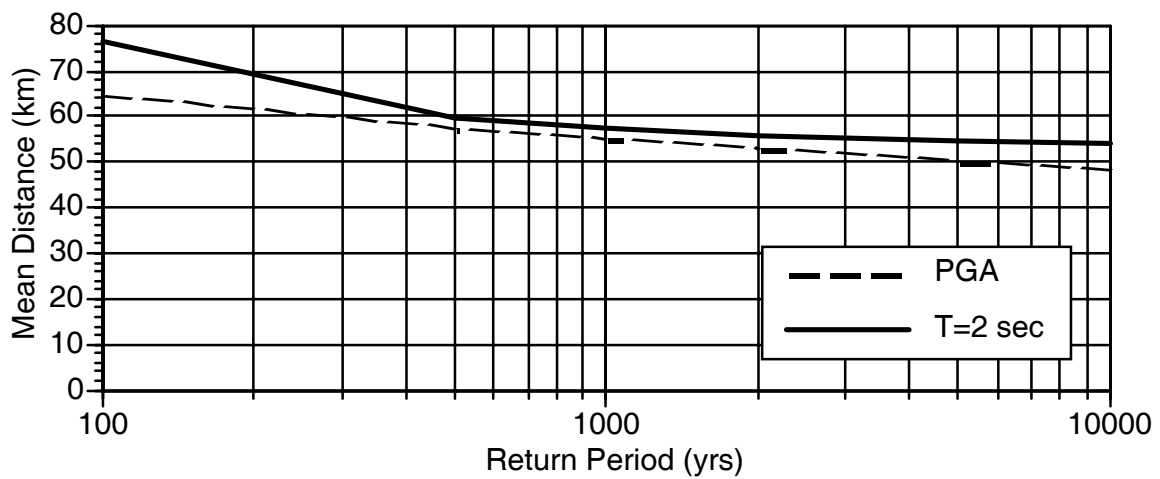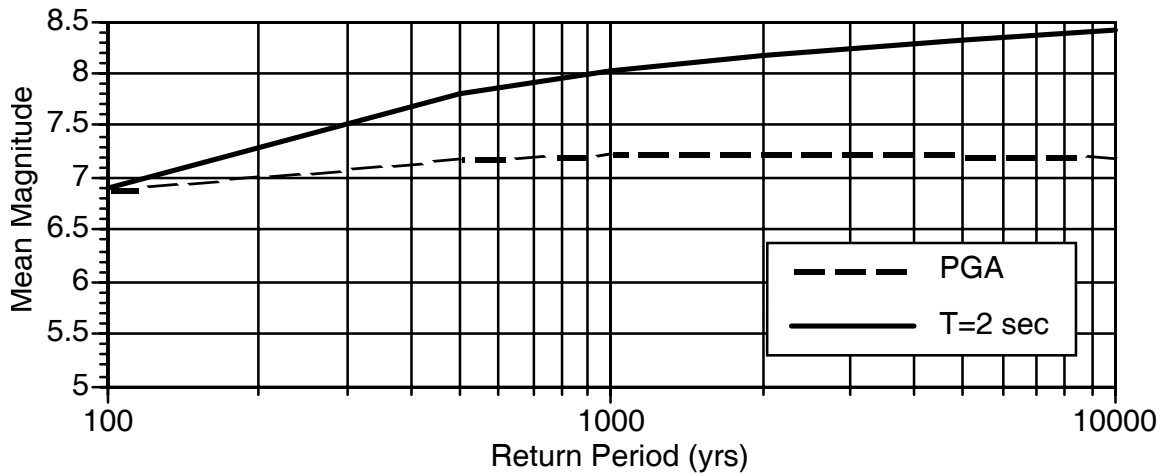
Figure B2-7. Return period dependence of the Mean M, R, epsilon from the deaggreagation for PGA and T=2 sec
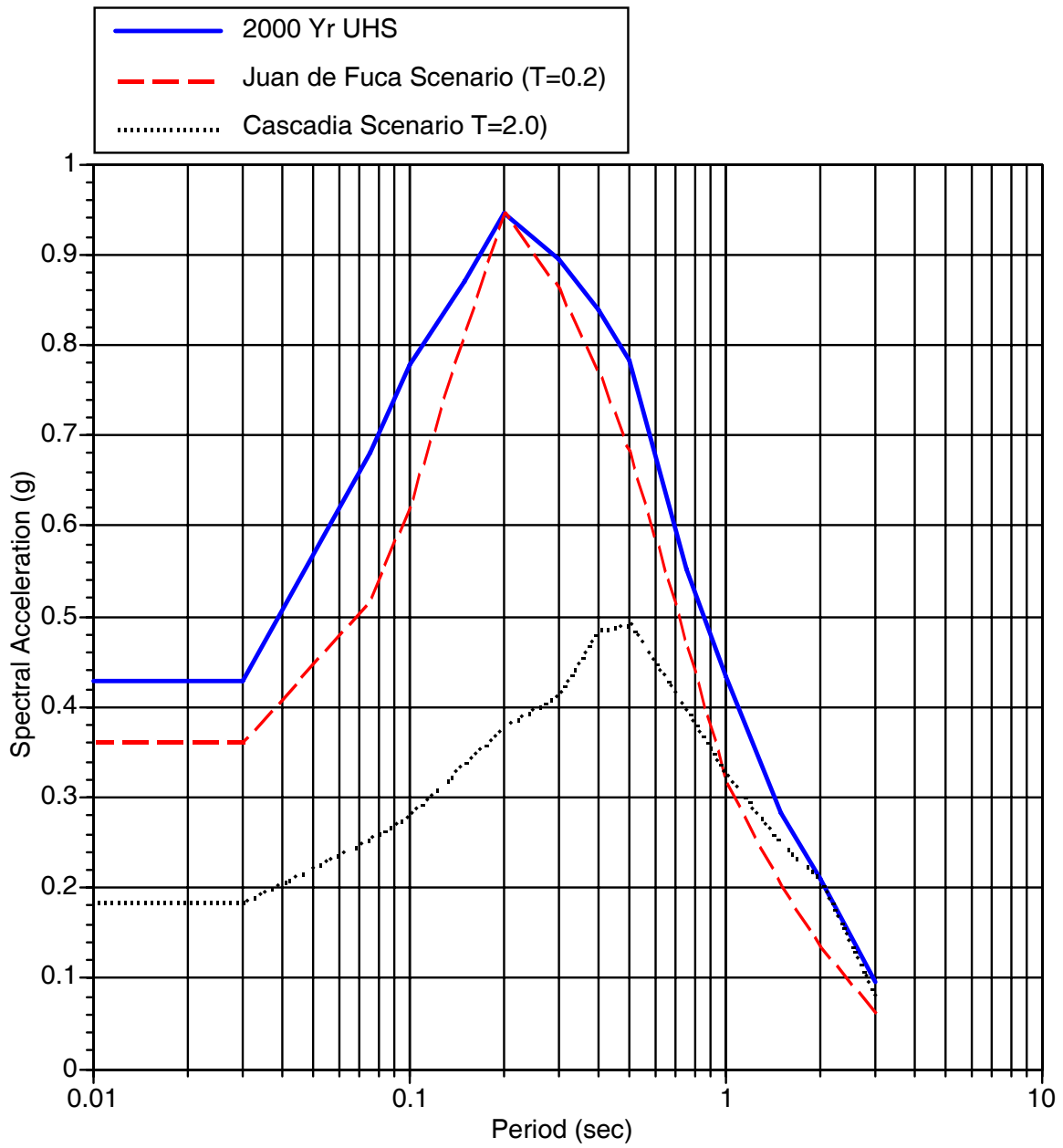
Figure B2-8. Expected spectra for scenario earthquakes for the UHS at T=0.2 and T=2.0 sec.
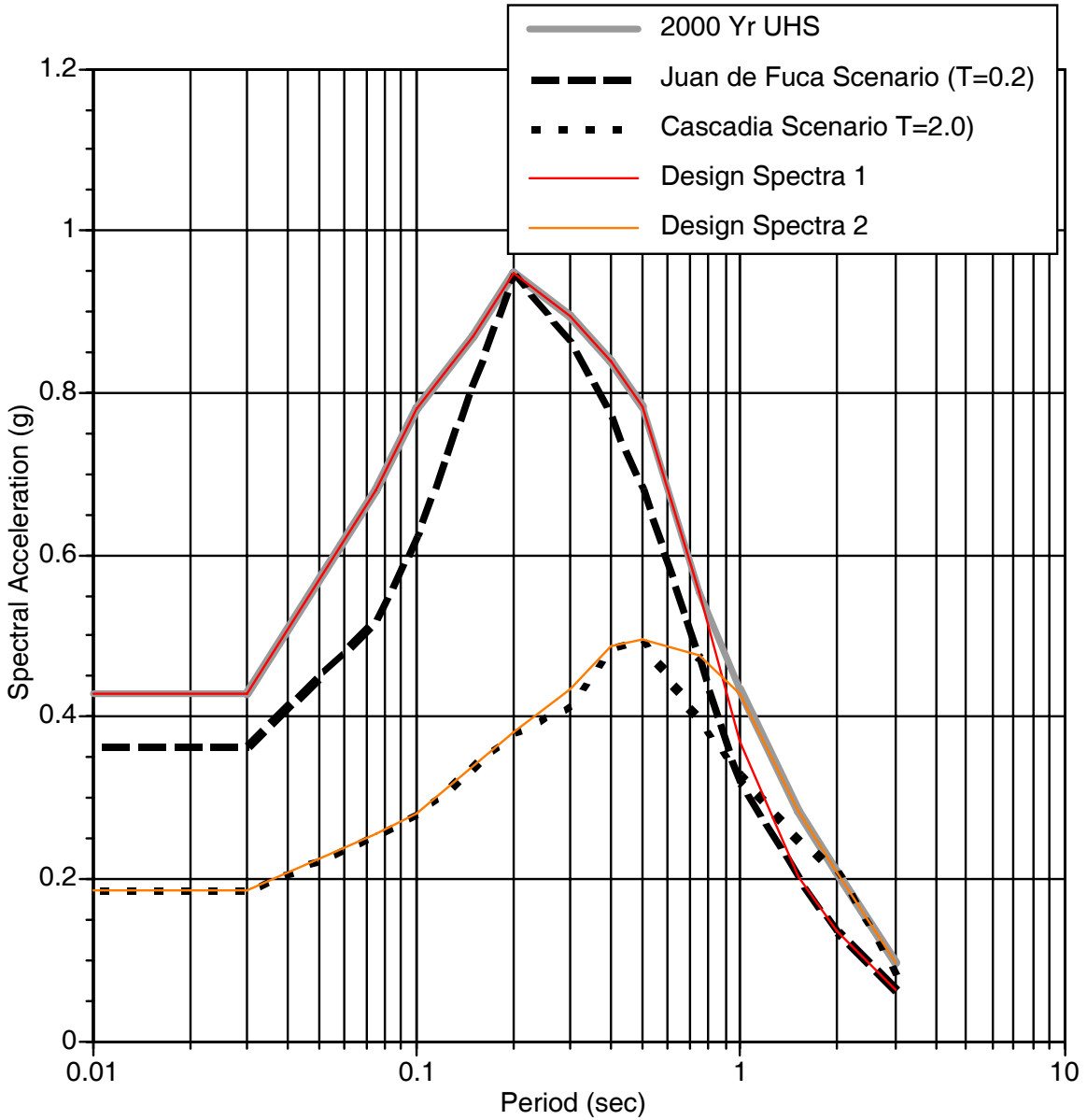
Figure B2-9. Example of broadening the expected spectra for scenario earthquakes into a small set of design spectra.

B2.9.2 *San Francisco bay area example*

The second example is for a site located in a high seismic region. A site located in the east bay in Northern California is used as the second example. Again, a return period of 2000 years is used.

Source Characterization
For this example, a simplified source characterization is used. Three fault sources are considered: the San Andreas, Hayward/Rodgers Creek, and Calaveras, . The location of the site with respect to the faults is shown in Figure B2-10. The parameters used for the sources are given in Table B2-5 . These are based on the USGS WG03 model. The objective of these examples is on the presentation of the hazard results, so a detailed description of the source models is not included here. In a complete hazard study, such detailed source descriptions should be included.

Ground Motion Models
For the crustal sources, the five NGA models recently developed as part of the PEER/Lifelines program are used. These new ground motion models include Abrahamson and Silva (2007), Boore and Atkinson (2006), Campbell and Bozorgnia (2006), Chiou and Youngs (2006), and Idriss (2007). For the Idriss model, the rock site class is used. For the other four models, a V_{S30} of 600 m/s is used. These five models are given equal weight.

Table B2-5. Source parameters for faults considered for the San Francisco Example

Fault System	Rupture	Mean Characteristic Magnitude	Recurrence Interval (yrs) of Characteristic Eqk	Style-of-Faulting
San Andreas	SAS	7.03 (0.8) 6.84 (0.1) 7.22 (0.1)	1,140(0.8) 260 (0.1) 100,000 (0.1)	Strike-Slip
San Andreas	SAP	7.15 (0.8) 6.95 (0.1) 7.32 (0.1)	670 (0.8) 160 (0.1) 100,000 (0.1)	Strike-Slip
San Andreas	SAN	7.45 (0.8) 7.28 (0.1) 7.61 (0.1)	3,320 (0.8) 800(0.1) 100,000 (0.1)	Strike-slip
San Andreas	SAO	7.29 (0.8) 7.12 (0.1) 7.44 (0.1)	3320 (0.8) 680 (0.1) 100,000 (0.1)	Strike-slip
San Andreas	SAS+SAP	7.42 (0.8) 7.26 (0.1) 7.56 (0.1)	840 (0.8) 30,000 (0.1) 280 (0.1)	Strike-slip
San Andreas	SAN+SAO	7.70 (0.8) 7.53 (0.1) 7.86 (0.1)	870 (0.8) 30,000 (0.1) 270 (0.1)	Strike-slip
San Andreas	SAS+SAP+SAN	7.76 (0.8) 7.59 (0.1) 7.92 (0.1)	30,000 (0.8) 10,000 (0.1) 100,000 (0.1)	Strike-slip
San Andreas	SAP+SAN+SAO	7.83 (0.8) 7.65 (0.1) 8.01 (0.1)	15,000 (0.8) 2700 (0.1) 100,000 (0.1)	Strike-slip
San Andreas	SAS+SAP+SAN+SAO	7.90 (0.8) 7.72 (0.1)	620 (0.8) 10,000 (0.1)	Strike-slip

		8.10 (0.1)	200 (0.1)	
San Andreas	Floating	6.9 (0.1)	410 (0.8) 7,500 (0.1) 100 (0.1)	Strike-slip
Hayward/RC	HS	6.67 (0.8) 6.36 (0.1) 6.93 (0.1)	250 (0.8) 1350 (0.1) 80 (0.1)	Strike-slip
	HN	6.49 (0.8) 6.18 (0.1) 6.78 (0.1)	230 (0.8) 1290 (0.1) 70 (0.1)	Strike-slip
	HS+HN	6.91 (0.8) 6.68 (0.1) 7.12 (0.1)	340 (0.8) 1560 (0.1) 110 (0.1)	Strike-slip
	RC	6.98 (0.8) 6.81 (0.1) 7.14 (0.1)	180 (0.8) 720 (0.1) 56 (0.1)	Strike-slip
	HN+RC	7.11 (0.8) 6.94 (0.1) 7.28 (0.1)	1650 (0.8) 440 (0.1) 100,000 (0.1)	Strike-slip
	HN+RS+RC	7.26 (0.8) 7.09 (0.1) 7.42 (0.1)	3,000(0.8) 30,000 (0.1) 900 (0.1)	Strike-slip
	Floating	6.90 (1.0)	4270 (0.8) 10,000 (0.1) 1860 (0.1)	Strike-slip
Calaveras	CS	5.79 (0.8) 5.0 (0.1) 6.14 (0.1)	125 (0.8) 40 (0.1) 100,000 (0.1)	Strike-slip
	CC	6.23 (0.8) 5.75 (0.1) 6.68 (0.1)	200 (0.8) 750 (0.1) 85 (0.1)	Strike-slip
	CS+CC	6.36 (0.8) 5.87 (0.1) 6.75 (0.1)	590 (0.8) 130 (0.1) 100,000 (0.1)	Strike-slip
	CN	6.78 (0.8) 6.58 (0.1) 6.97 (0.1)	230 (0.8) 990 (0.1) 70 (0.1)	Strike-slip
	CC+CN	6.90 (0.8) 6.68 (0.1) 7.11 (0.1)	10,000 (0.8) 820 (0.1) 100,000 (0.1)	Strike-slip
	CS+CC+CN	6.93 (0.8) 6.72 (0.1) 7.14 (0.1)	1490 (0.8) 370 (0.1) 100,000 (0.1)	Strike-slip
	Floating	6.20 (1.0)	390 (0.8) 1750 (0.1) 140 (0.1)	Strike-slip
	CS+CC_floating	6.2 (1.0)	100 (0.8) 570 (0.1) 40 (0.1)	Strike-slip

Hazard Results

The basic hazard results are shown in Figures B2-11a and B2-11b for PGA and T=1 sec, respectively. These figures also show how each source contributes to the hazard. Since the site is

located close to a high activity fault, the hazard is dominated by the nearby Hayward fault at both short and long spectral periods.

The sensitivity of the hazard to the attenuation relations is shown in Figure B2-12a and B2-12b for PGA and T=1 sec, respectively. As the return period increases (lower annual probability), the difference due to the attenuation relation increases. This is due to the different values of the standard deviations.

The epistemic uncertainty in the hazard is shown in Figures B2-13a and B2-13b for PGA and T=1 sec, respectively. In this case, the range of the fractiles is dominated by the epistemic uncertainty in the subduction attenuation relations.

The UHS for return periods of 500, 1000, 2000, and 5000 years is shown in Figure B2-14. This figure also compares the Hayward MCE (M=7.25, R=3.5 km) ground motions (median and 84th percentile) as used in deterministic analyses. At short spectral periods, the 84th percentile ground motion corresponds to a return period of about 700 years. This increases to a return period of 200 years at long spectral periods.

The deaggregation for a return period of 2000 years is shown in Figures B2-15a and B2-15b for PGA and T=1 sec, respectively. Figure B2-15a shows that for PGA, the mode of the deaggregation is M=6.5-7.0 at a distance of 0-5 km. Figure B2-15b shows that for T=1 sec, the mode of the deaggregation is still M=6.5-7.0 at a distance of 0-5 km, but the contribution of larger magnitudes (M=7.0-7.5) has increased. If the bin size were changed, the model may move to M=7. This shows how simply using the mode can miss some changes in the controlling source.

In addition to the mode, the deaggregation can be characterized by the mean magnitude, distance, and epsilon. These mean values are shown in Figure B2-16 as a function of return period for PGA and T=1 sec. With this type of plot, the differences in the magnitude for PGA and T=2 sec is apparent. As is typical for sites close to active faults, the mean magnitude is not very sensitive to the return period. At short spectral periods, the mean distance decreases quickly to the closest distance (3.5 km in this case). The main increase in the ground motion at long return periods is due to the increase in epsilon shown in the lower frame.

Expected Spectra for Scenario Earthquakes
From the deaggregation, the following scenario earthquakes were selected:

Source	M	Distance (km)	T_o (sec)
Hayward (SH)	6.75	4 km	0.2
Hayward (NS+SH)	7.0	5 km	1.0

The expected spectra are developed for these of these events. First, the median and standard deviation for the two scenarios listed above are computed using the five NGA ground motion models. The average of the median and the standard deviation for the two scenario earthquakes are listed in Tables B2-7a and B2-7b.

Next, the number of standard deviations needed to scale the median Sa to the UHS is determined. This value, ε_U, is shown in Table B2-6. The expected epsilon values at the other spectral periods are then computed (fifth column in Tables B2-7a and B2-7b) and the spectrum is then computed (sixth column in Tables B2-8a, and B2-8b).

The expected spectra for the scenarios are compared to the UHS in Figure B2-17. This figure shows that even if there is a single controlling source, the expected spectrum will still fall below the UHS at periods away from the reference period. This shows that it is not just the enveloping of earthquakes from different sources in the UHS, but also the enveloping of the variability at different spectral periods. A suite of these expected spectra will be enveloped by the UHS. The expected spectra are realistic ground motions for a future earthquake. To limit the number of scenarios considered, these expected spectra can be broadened so that they cover the UHS with a small number of scenarios. As an example, the two expected scenarios are broadened into two design spectra in Figure B2-18. The engineer conducting the analysis of the structure needs to determine to what degree it is worth broadening the expected spectra to reduce the number of scenarios considered.

Table B2-6. Computation of the epsilon needed to match the UHS.

Period (sec)	UHS 2000 Yr (g)	Median Sa(g)	σ	ε_U
0.2	2.56	0.904	0.619	1.68
1.0	0.97	0.313	0.660	1.72

Table B2-7a. Development for the expected spectrum for
T=0.2 sec and a return period of 2000 years.

Period (Sec)	c $(T_o=0.2)$	Median Sa(g)	σ	$\hat{\varepsilon}$	Expected Spectrum (g)
0.00	0.91	0.388	0.560	1.530	0.913
0.075	0.91	0.608	0.625	1.530	1.584
0.10	0.91	0.736	0.633	1.530	1.938
0.20	1.00	0.904	0.619	1.682	2.560
0.30	0.93	0.820	0.630	1.564	2.196
0.40	0.84	0.693	0.635	1.413	1.699
0.50	0.71	0.603	0.640	1.194	1.294
0.75	0.62	0.412	0.650	1.043	0.811
1.00	0.45	0.313	0.662	0.757	0.516
1.50	0.37	0.206	0.675	0.622	0.314
2.00	0.26	0.140	0.693	0.437	0.190
3.00	0.24	0.083	0.697	0.404	0.110

Table B2-7b. Development for the expected spectrum for
T=1.0 sec and a return period of 2000 years.

Period (Sec)	c (T$_o$=2.0)	Median Sa(g)	σ	$\hat{\varepsilon}$	Expected Spectrum (g)
0.00	0.68	0.374	0.554	1.167	0.745
0.075	0.54	0.587	0.620	0.927	1.086
0.10	0.5	0.703	0.626	0.858	1.267
0.20	0.48	0.876	0.613	0.824	1.505
0.30	0.63	0.801	0.625	1.081	1.620
0.40	0.71	0.677	0.630	1.218	1.502
0.50	0.77	0.600	0.636	1.321	1.404
0.75	0.92	0.410	0.650	1.579	1.149
1.00	1.00	0.322	0.660	1.716	0.974
1.50	0.87	0.213	0.675	1.493	0.565
2.00	0.81	0.150	0.691	1.390	0.368
3.00	0.77	0.090	0.696	1.321	0.208
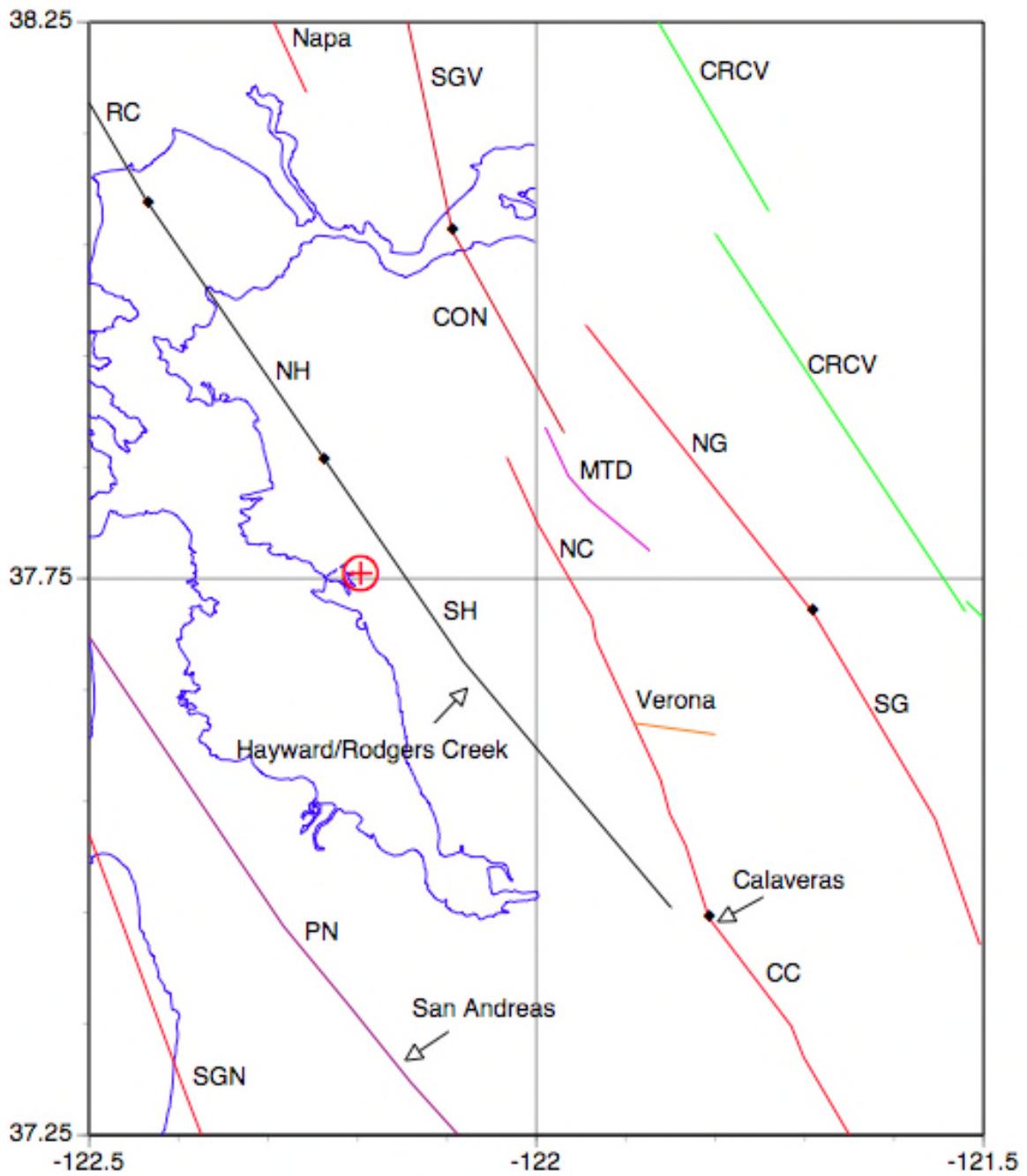
Figure B2-10. Faults and sources considered in the example.
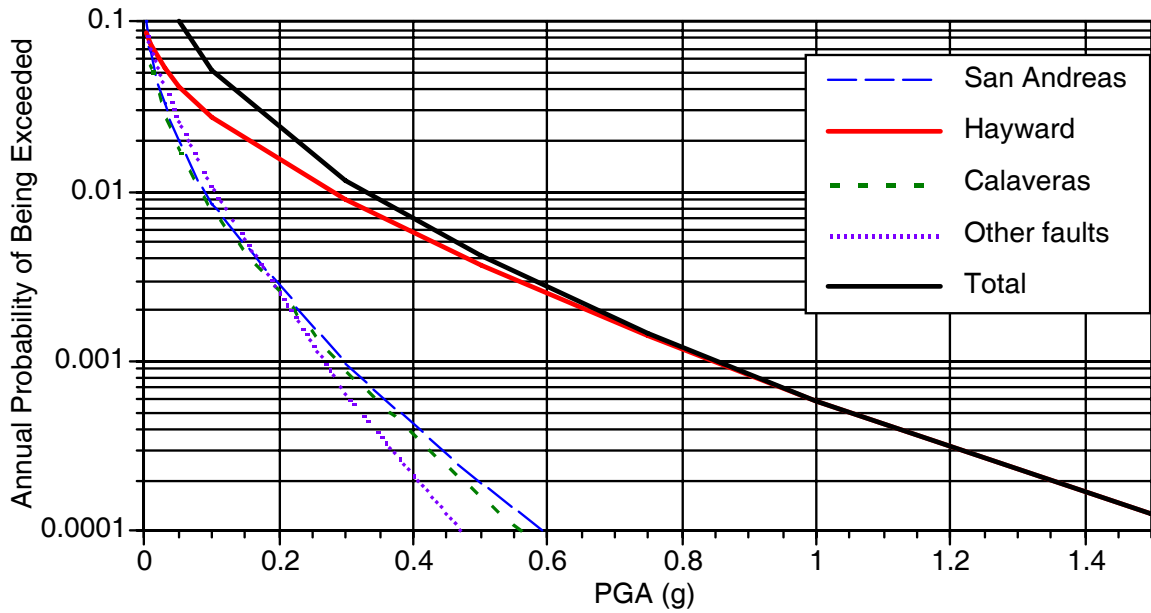
Figure B2-11a. Contribution to the PGA hazard by source.
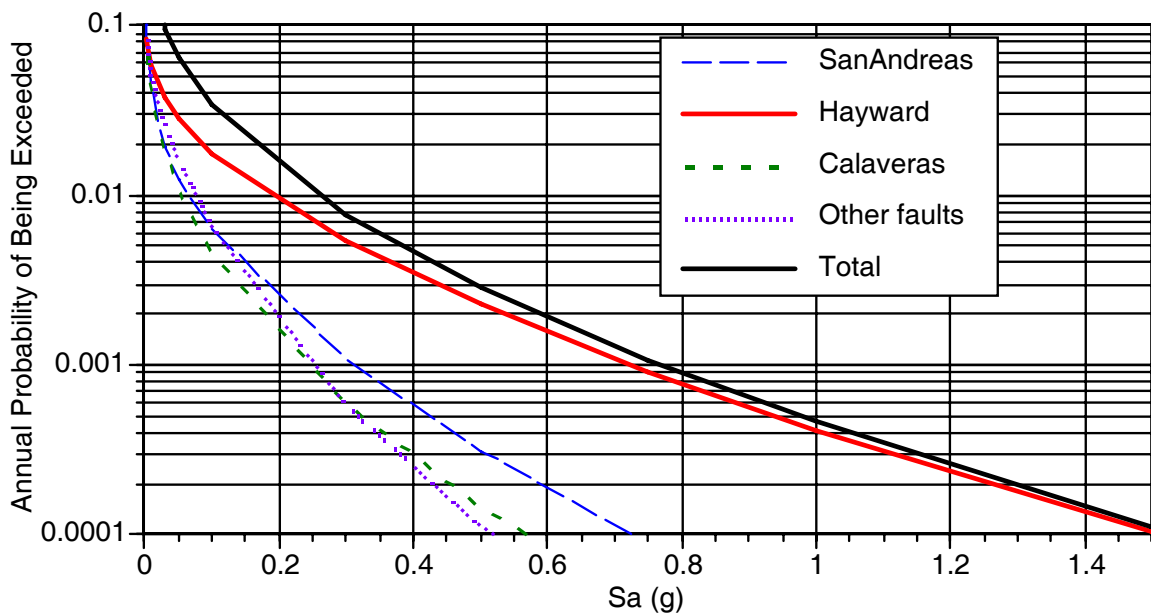
Figure B2-11b. Contribution to the T=1 sec hazard by source
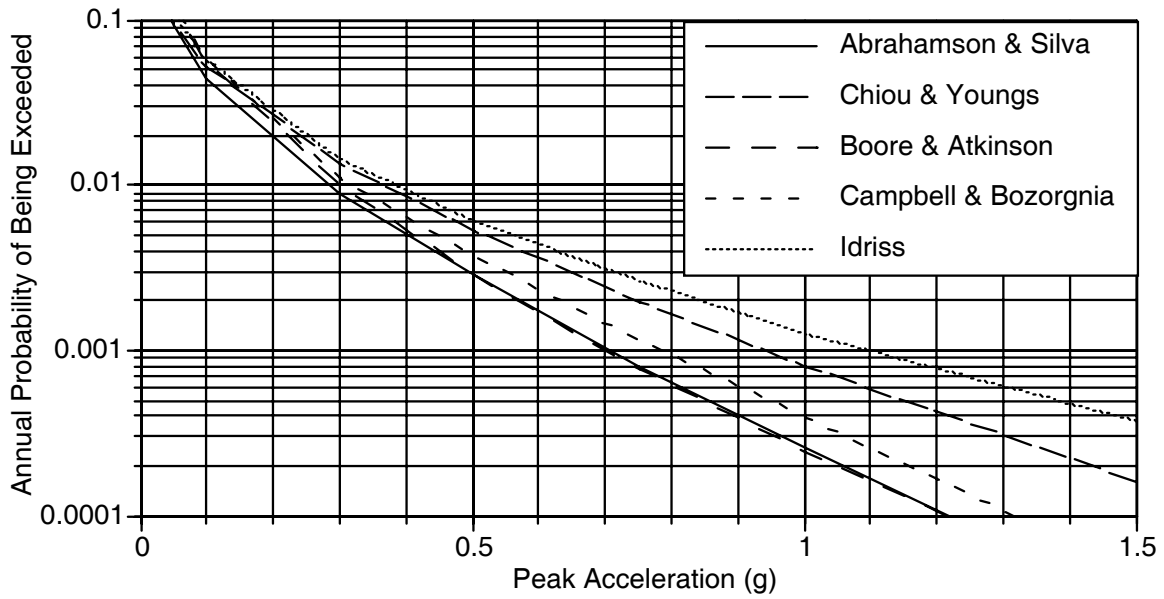
Figure B2-12a. Sensitivity of PGA hazard to attenuation relation.
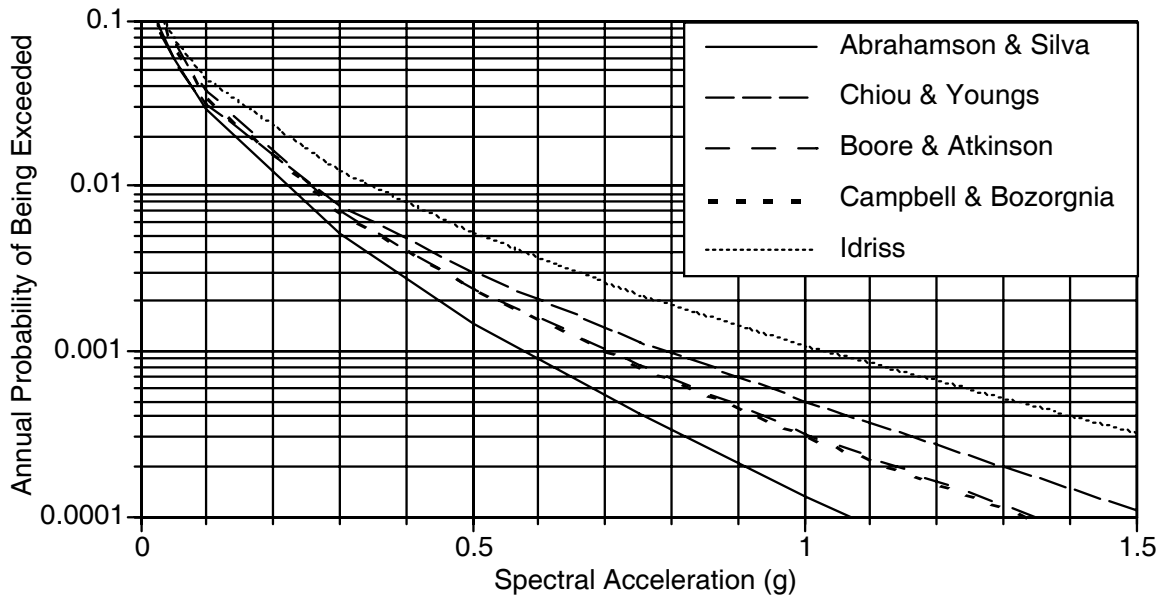
Figure B2-12b. Sensitivity of T=2 sec hazard to attenuation relation.
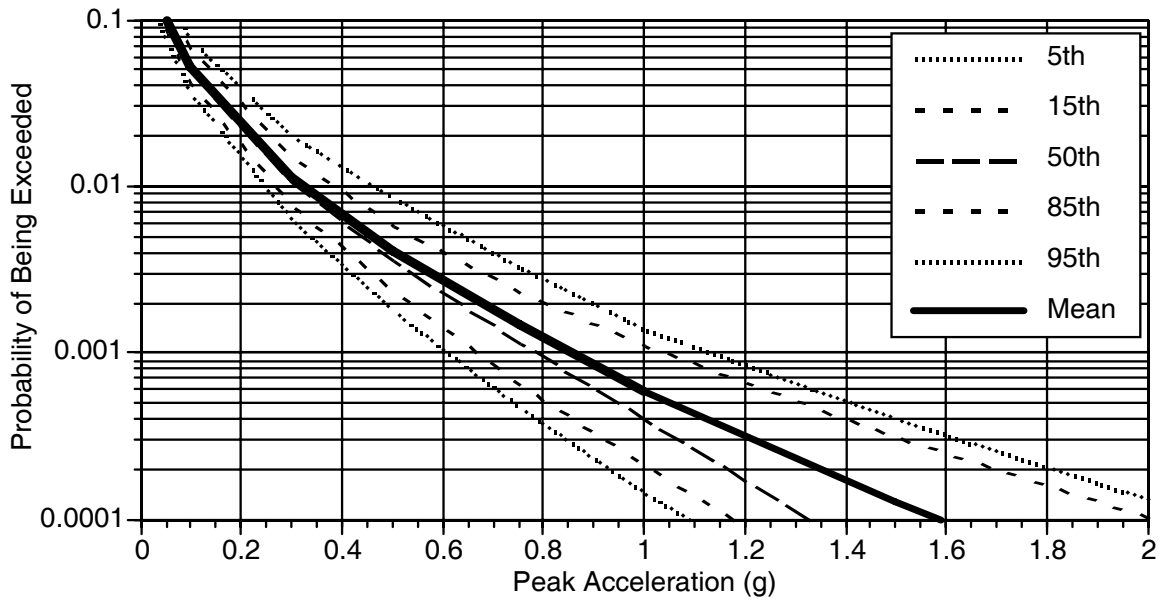
Figure B2-13a. Uncertainty fractiles of the PGA hazard
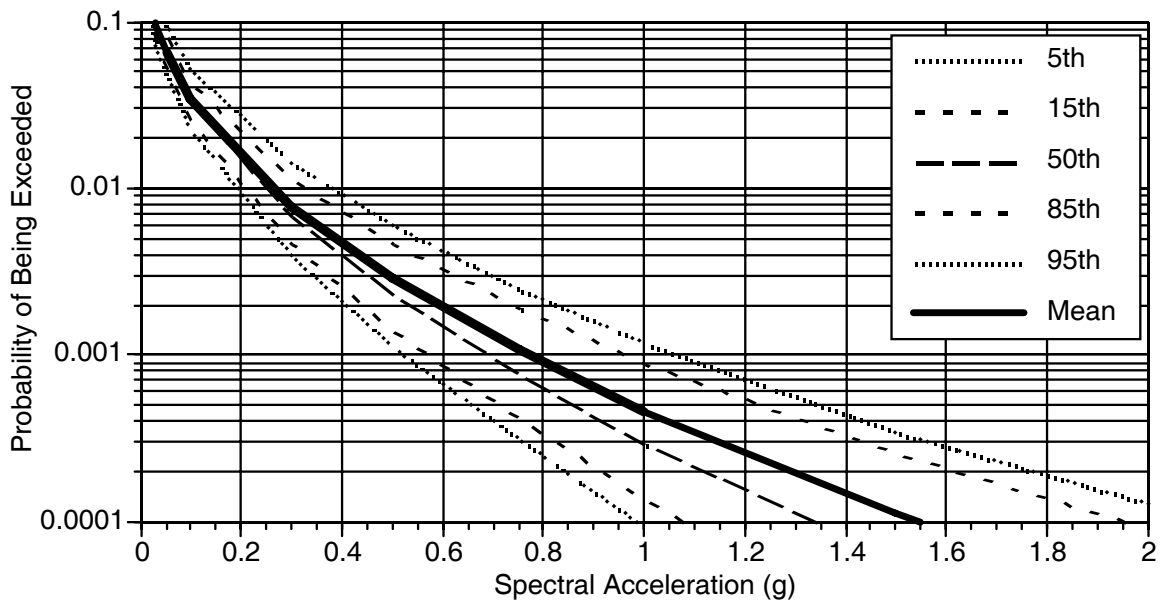
Figure B2-13b. Uncertainty fractiles of the T=2 sec hazard
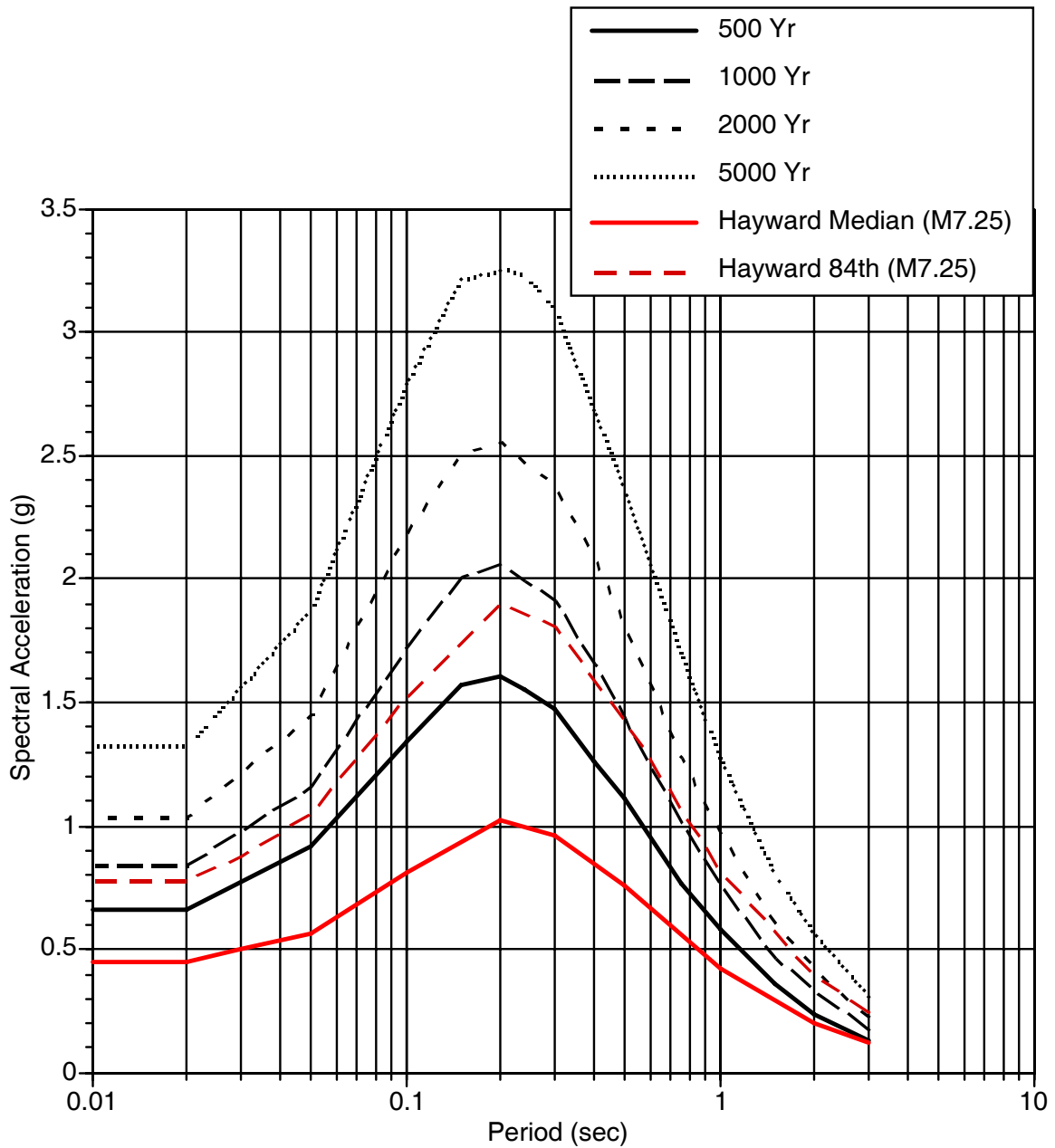
Figure B2-14. UHS and deterministic (MCE) spectra for the Hayward/Rodgers Creek source.
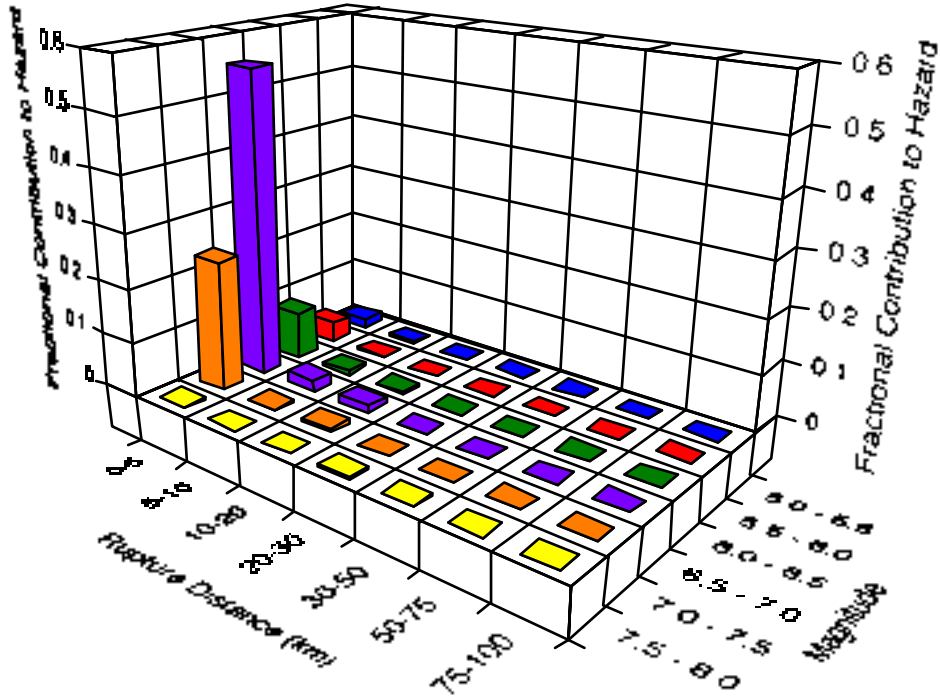
Figure B2-15a. Deaggregation for PGA hazard for a return period of 2000 years.
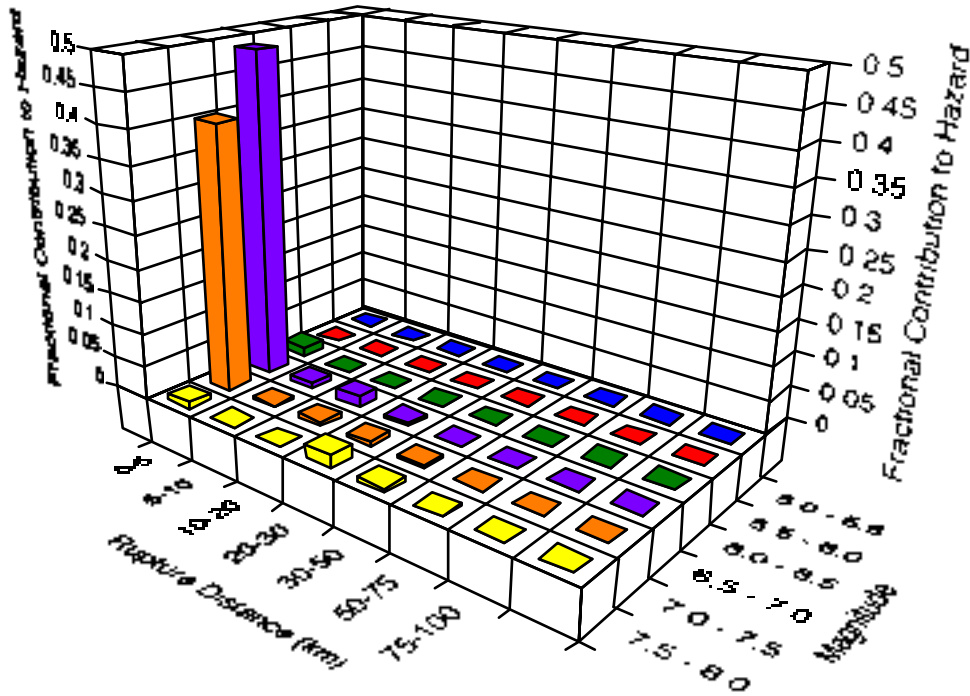
Figure B2-15b. Deaggregation for T=1 sec hazard for a return period of 2000 years.
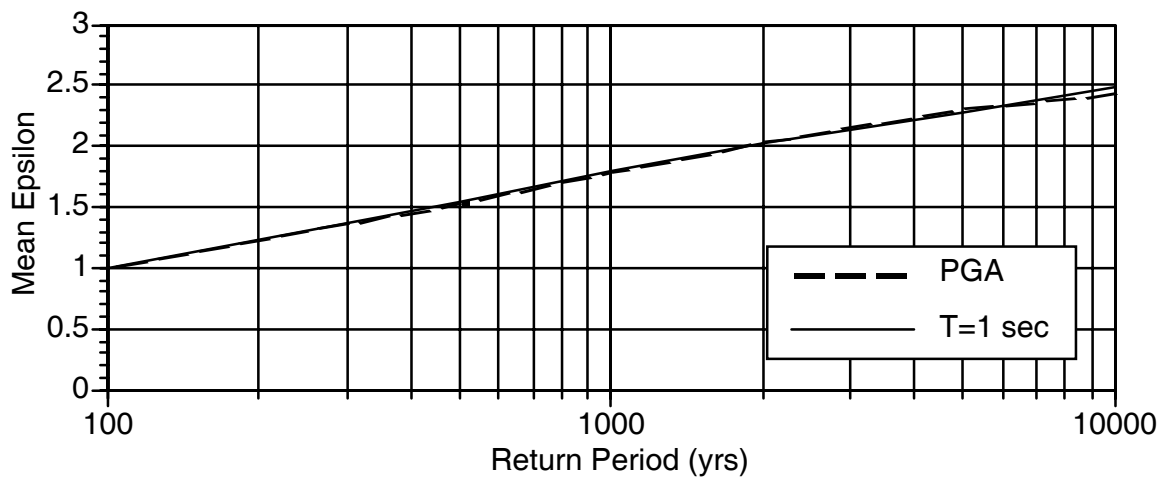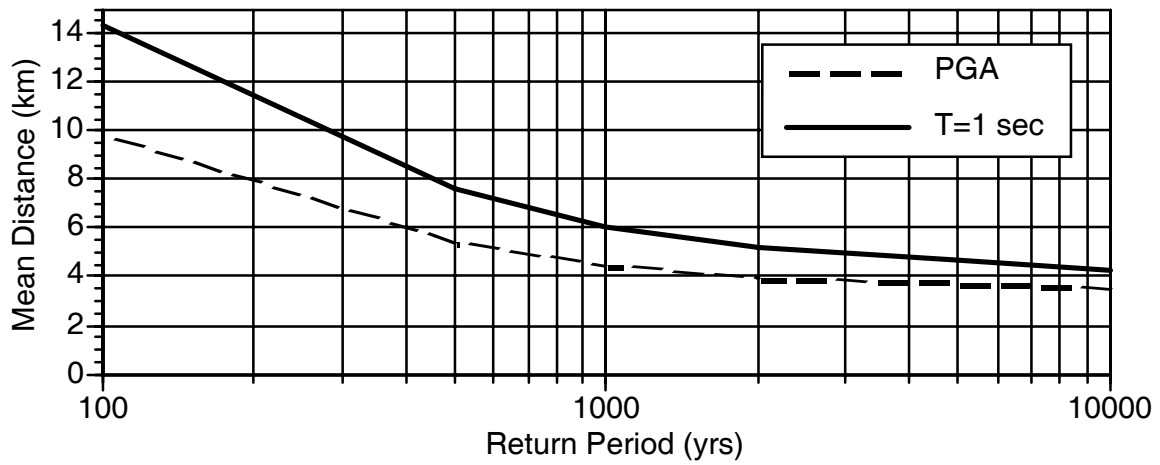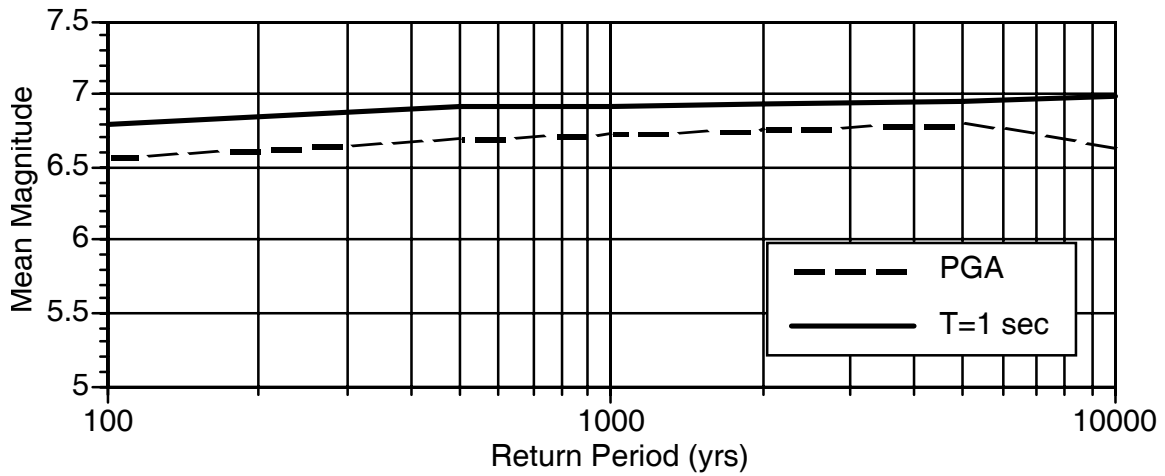
Figure B2-16. Return period dependence of the Mean M, R, epsilon from the deaggreagation for PGA and T=1 sec
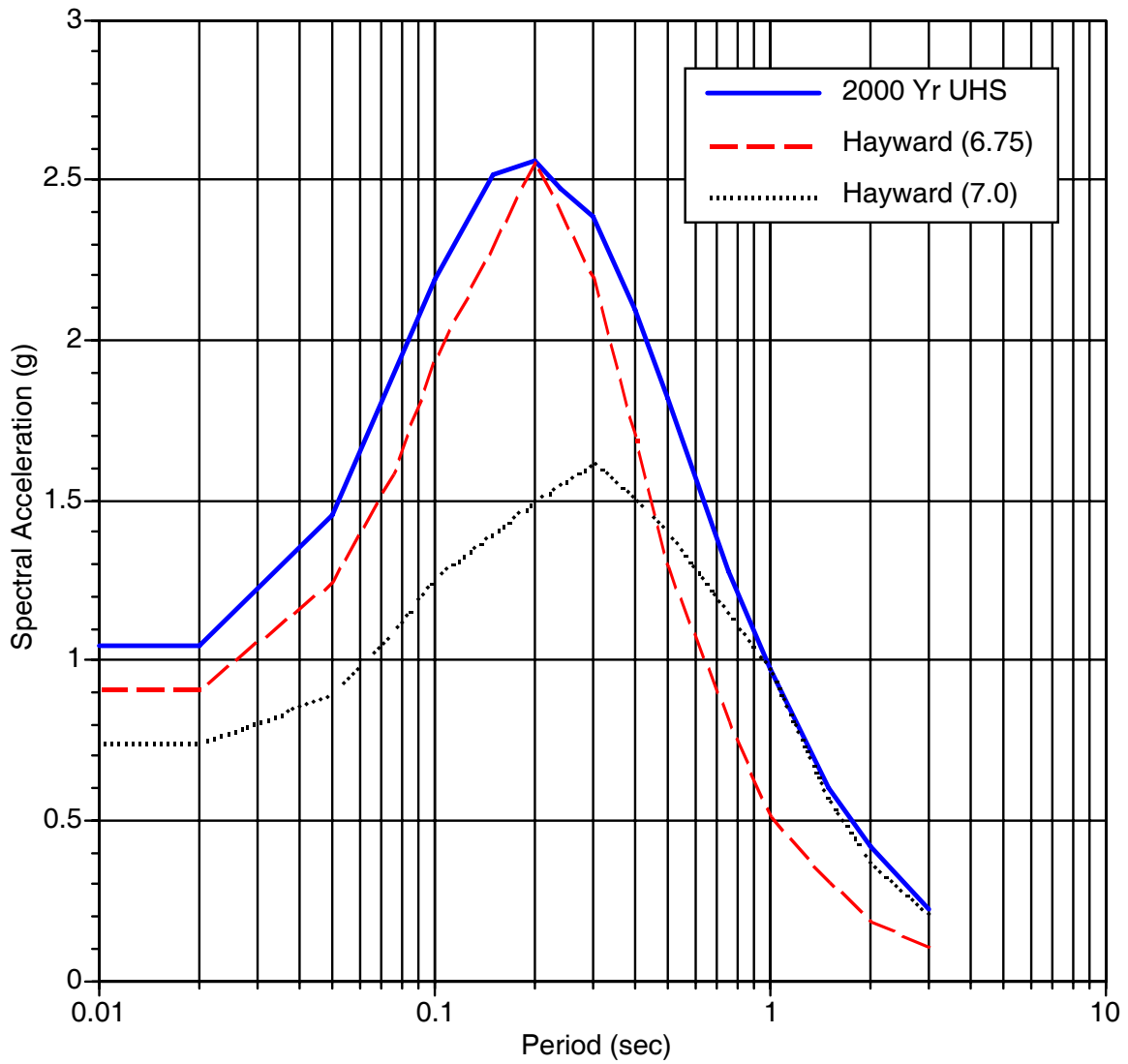
Figure B2-17. Expected spectra for scenario earthquakes for the UHS at T=0.2 and T=1.0 sec.
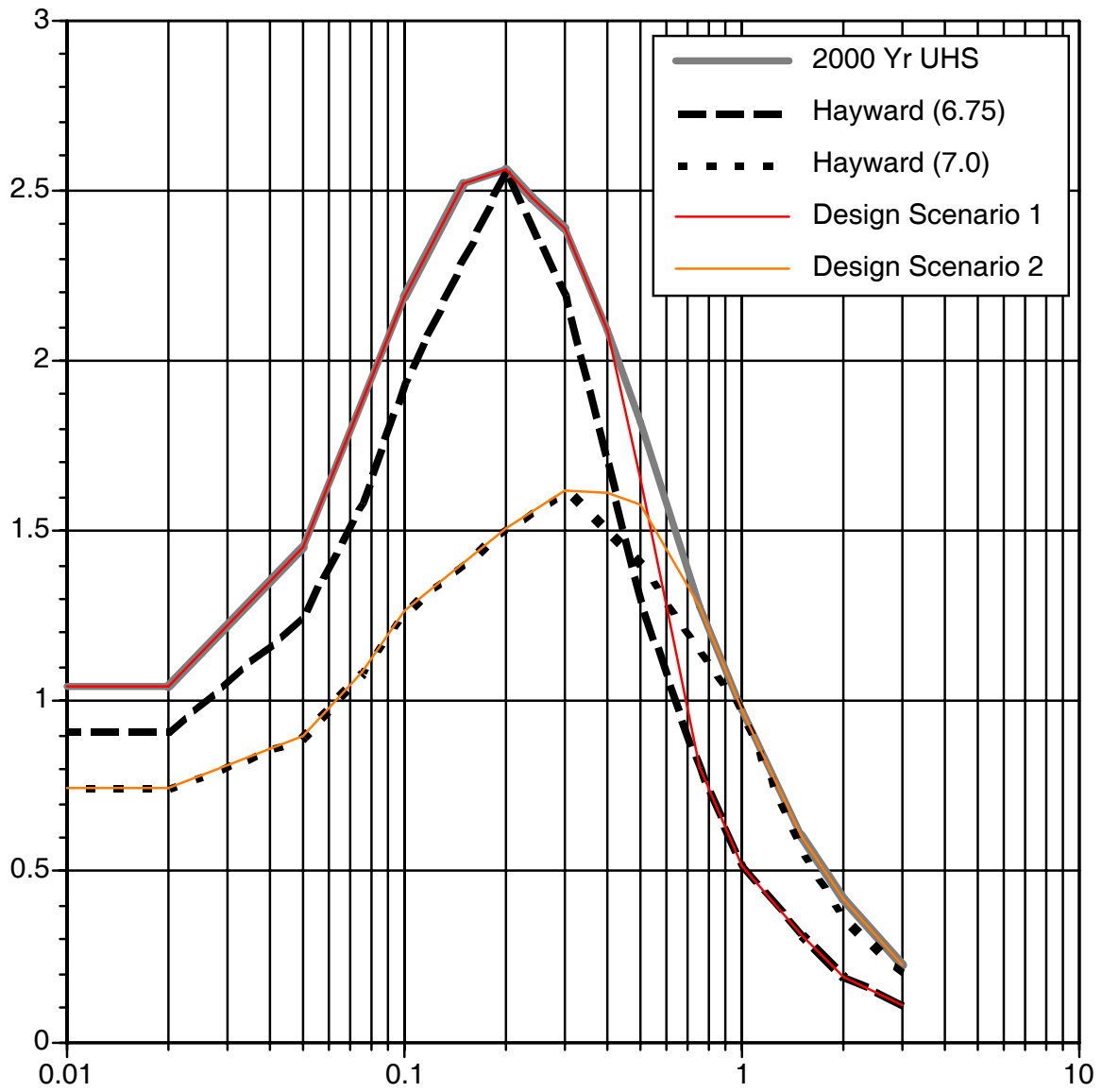
Figure B2-18. Example of broadening the expected spectra for scenario earthquakes into a small set of design spectra.

APPENDIX C
ATTENUATION RELATIONSHIPS FOR MOTIONS
IN WESTERN NORTH AMERICA (WNA)

The attenuation relationships derived by Abrahamson and Silva (1997), by Boore, Joyner and Fumal (1997), by Campbell (1997), by Idriss (2002), and by Sadigh et al (1997), are summarized in this Appendix.

C.1 ATTENUATION RELATIONSHIPS DERIVED BY ABRAHAMSON & SILVA (1997)

The functional form adopted by Abrahamson and Silva for spectral ordinates at rock sites is the following:

$$Ln(y) = f_1(M, r_{rup}) + Ff_3(M) + HWf_4(M, r_{rup}) \qquad \text{[C-1]}$$

in which, y is the median spectral acceleration in g (5% damping), or peak ground acceleration (pga), in g's, M is moment magnitude, r_{rup} is the closest distance to the rupture plane in km, F is the fault type (1 for reverse, 0.5 for reverse/oblique, and 0 otherwise), and HW is a dummy variable for sites located on the hanging wall (1 for sites over the hanging wall, 0 otherwise). The function $f_1(M, r_{rup})$ is given by.

for $M \leq c_1$

$$f_1(M, r_{rup}) = a_1 + a_2(M - c_1) + a_{12}(8.5 - M)^n + \left[a_3 + a_{13}(M - c_1) \right] Ln(R)$$

$$\text{[C-2]}$$

for $M \geq c_1$

$$f_1(M, r_{rup}) = a_1 + a_4(M - c_1) + a_{12}(8.5 - M)^n + \left[a_3 + a_{13}(M - c_1) \right] Ln(R)$$

Note that $R = \sqrt{r_{rup}^2 + c_4^2}$ in Eq. [C-2}.

The function $f_3(M)$ is described below:

$$f_3(M) = a_5 \text{ for } M \leq 5.8$$

$$f_3(M) = a_5 + \frac{(a_6 - a_5)}{c_1 - 5.8} \text{ for } 5.8 < M < c_1 \qquad \text{[C-3]}$$

$$f_3(M) = a_6 \text{ for } M \geq c_1$$

The function $f_4(M, r_{rup})$ is assumed to consist of the product of the following two functions, namely:

$$f_4(M, r_{rup}) = f_{HW}(M) f_{HW}(r_{rup}) \qquad \text{[C-4]}$$

The function $f_{HW}(M)$ is evaluated as follows:

$$f_{HW}(M) = 0 \text{ for } M \leq 5.5$$

$$f_{HW}(M) = M - 5.5 \text{ for } 5.5 < M < 6.5 \qquad \text{[C-5]}$$

$$f_{HW}(M) = 1 \text{ for } M \geq 6.5$$

The function $f_{HW}(r_{rup})$ is given by:

$$f_{HW}(r_{rup}) = 0 \text{ for } r_{rup} < 4$$

$$f_{HW}(r_{rup}) = a_9\left(\frac{r_{rup} - 4}{4}\right) \text{ for } 4 < r_{rup} < 8$$

$$f_{HW}(r_{rup}) = a_9 \text{ for } 8 < r_{rup} < 18 \qquad \text{[C-6]}$$

$$f_{HW}(r_{rup}) = a_9\left(1 - \frac{r_{rup} - 18}{7}\right) \text{ for } 18 < r_{rup} < 24$$

$$f_{HW}(r_{rup}) = 0 \text{ for } r_{rup} < 25$$

The standard error terms are given by the following equations:

$$\sigma_{total}(M) = b_5 \text{ for } M \leq 5$$

$$\sigma_{total}(M) = b_5 - b_6(M - 5) \text{ for } 5 < M < 7 \qquad \text{[C-7]}$$

$$\sigma_{total}(M) = b_5 - 2b_6 \text{ for } M \geq 7$$

Values of the coefficients $a_1 .. a_6$, $a_9 .. a_{13}$, c_1, c_4, c_5, and n are listed in Table C-1 for periods ranging from T = 0.01 sec (representing zpa) to T = 5 sec. Values of the coefficients b_5 and b_6 are listed in Table C-2 for the same periods.

Table C-1 Coefficients for the Median Spectral Ordinates Using Equations Derived by Abrahamson and Silva (1997)

Period	c_4	a_1	a_2	a_3	a_4	a_5	a_6	a_9	a_{10}	a_{11}	a_{12}
0.01	5.60	1.640	0.512	-1.1450	-0.144	0.610	0.260	0.370	-0.417	-0.230	0.0000
0.02	5.60	1.640	0.512	-1.1450	-0.144	0.610	0.260	0.370	-0.417	-0.230	0.0000
0.03	5.60	1.690	0.512	-1.1450	-0.144	0.610	0.260	0.370	-0.470	-0.230	0.0143
0.04	5.60	1.780	0.512	-1.1450	-0.144	0.610	0.260	0.370	-0.555	-0.251	0.0245
0.05	5.60	1.870	0.512	-1.1450	-0.144	0.610	0.260	0.370	-0.620	-0.267	0.0280
0.06	5.60	1.940	0.512	-1.1450	-0.144	0.610	0.260	0.370	-0.665	-0.280	0.0300
0.075	5.58	2.037	0.512	-1.1450	-0.144	0.610	0.260	0.370	-0.628	-0.280	0.0300
0.09	5.54	2.100	0.512	-1.1450	-0.144	0.610	0.260	0.370	-0.609	-0.280	0.0300
0.1	5.50	2.160	0.512	-1.1450	-0.144	0.610	0.260	0.370	-0.598	-0.280	0.0280
0.12	5.39	2.272	0.512	-1.1450	-0.144	0.610	0.260	0.370	-0.591	-0.280	0.0180
0.15	5.27	2.407	0.512	-1.1450	-0.144	0.610	0.260	0.370	-0.577	-0.280	0.0050
0.17	5.19	2.430	0.512	-1.1350	-0.144	0.610	0.260	0.370	-0.522	-0.265	-0.0040
0.2	5.10	2.406	0.512	-1.1150	-0.144	0.610	0.260	0.370	-0.445	-0.245	-0.0138
0.24	4.97	2.293	0.512	-1.0790	-0.144	0.610	0.232	0.370	-0.350	-0.223	-0.0238
0.3	4.80	2.114	0.512	-1.0350	-0.144	0.610	0.198	0.370	-0.219	-0.195	-0.0360
0.36	4.62	1.955	0.512	-1.0052	-0.144	0.610	0.170	0.370	-0.123	-0.173	-0.0460
0.4	4.52	1.860	0.512	-0.9880	-0.144	0.610	0.154	0.370	-0.065	-0.160	-0.0518
0.46	4.38	1.717	0.512	-0.9652	-0.144	0.592	0.132	0.370	0.020	-0.136	-0.0594
0.5	4.30	1.615	0.512	-0.9515	-0.144	0.581	0.119	0.370	0.085	-0.121	-0.0635
0.6	4.12	1.428	0.512	-0.9218	-0.144	0.557	0.091	0.370	0.194	-0.089	-0.0740
0.75	3.90	1.160	0.512	-0.8852	-0.144	0.528	0.057	0.331	0.320	-0.050	-0.0862
0.85	3.81	1.020	0.512	-0.8648	-0.144	0.512	0.038	0.309	0.370	-0.028	-0.0927
1	3.70	0.828	0.512	-0.8383	-0.144	0.490	0.013	0.281	0.423	0.000	-0.1020
1.5	3.55	0.260	0.512	-0.7721	-0.144	0.438	-0.049	0.210	0.600	0.040	-0.1200
2	3.50	-0.150	0.512	-0.7250	-0.144	0.400	-0.094	0.160	0.610	0.040	-0.1400
3	3.50	-0.690	0.512	-0.7250	-0.144	0.400	-0.156	0.089	0.630	0.040	-0.1726
4	3.50	-1.130	0.512	-0.7250	-0.144	0.400	-0.200	0.039	0.640	0.040	-0.1956
5	3.50	-1.460	0.512	-0.7250	-0.144	0.400	-0.200	0.000	0.664	0.040	-0.2150

The coefficients $a_{13} = 0.17$, $c_1 = 6.4$, $c_5 = 0.03$, and $n = 2$ for all periods.

Table C-2 Coefficients for Standard Error Terms Using Equations Derived by Abrahamson and Silva (1997)

Period - sec	b_5	b_6
0.01	0.70	0.135
0.02	0.70	0.135
0.03	0.70	0.135
0.04	0.71	0.135
0.05	0.71	0.135
0.06	0.72	0.135
0.075	0.73	0.135
0.09	0.74	0.135
0.1	0.74	0.135
0.12	0.75	0.135
0.15	0.75	0.135
0.17	0.76	0.135
0.2	0.77	0.135
0.24	0.77	0.135
0.3	0.78	0.135
0.36	0.79	0.135
0.4	0.79	0.135
0.46	0.80	0.132
0.5	0.80	0.130
0.6	0.81	0.127
0.75	0.81	0.123
0.85	0.82	0.121
1	0.83	0.118
1.5	0.84	0.110
2	0.85	0.105
3	0.87	0.097
4	0.88	0.092
5	0.89	0.087

C.2 ATTENUATION RELATIONSHIPS DERIVED BY BOORE, JOYNER AND FUMAL (1997)

The following equation was derived by Boore et al for spectral ordinates at rock sites:

$$Ln(y) = b_1 + b_2 (M - 6) + b_3 (M - 6)^2 + b_5 Ln(r) + b_V Ln\left(\frac{V_S}{V_A}\right)$$

$$r = \sqrt{r_{jb}^2 + h^2}$$

[C-8]

$$b_1 = \begin{cases} b_{1SS} & \text{for strike-slip earthquakes} \\ b_{1RV} & \text{for reverse-slip earthquakes} \\ b_{1ALL} & \text{if mechanism is not specified} \end{cases}$$

[C-9]

The variable y is spectral acceleration (5% damping) in g's; M is moment magnitude, V_s is the average shear wave velocity (in m/sec)in the upper 30 m of the profile under consideration, V_A is reference shear wave velocity (in m/sec), and r_{jb} is the closest horizontal distance (in km) from the site to the surface projection of the source. Values of the coefficients b_{1SS}, b_{1RV}, b_{1ALL}, b_2, b_3, b_5, b_V, V_A, and h (in km) are listed in Table C-3. Also listed in Table C-3 are the values of the standard error terms.

Table C-3
Coefficients Derived by Boore, Fumal and Joyner (1997)

Period	b_{1ss}	b_{1RV}	b_{1ALL}	b_2	b_3	b_5	b_V	V_A	h	SE
0	-0.313	-0.117	-0.242	0.527	0.000	-0.778	-0.371	1396	5.57	0.520
0.10	1.006	1.087	1.059	0.753	-0.226	-0.934	-0.212	1112	6.27	0.479
0.11	1.072	1.164	1.130	0.732	-0.230	-0.937	-0.211	1291	6.65	0.481
0.12	1.109	1.215	1.174	0.721	-0.233	-0.939	-0.215	1452	6.91	0.485
0.13	1.128	1.246	1.200	0.711	-0.233	-0.939	-0.221	1596	7.08	0.486
0.14	1.135	1.261	1.208	0.707	-0.230	-0.938	-0.228	1718	7.18	0.489
0.15	1.128	1.264	1.204	0.702	-0.228	-0.937	-0.238	1820	7.23	0.492
0.16	1.112	1.257	1.192	0.702	-0.226	-0.935	-0.248	1910	7.24	0.495
0.17	1.090	1.242	1.173	0.702	-0.221	-0.933	-0.258	1977	7.21	0.497
0.18	1.063	1.222	1.151	0.705	-0.216	-0.930	-0.270	2037	7.16	0.499
0.19	1.032	1.198	1.122	0.709	-0.212	-0.927	-0.281	2080	7.10	0.501
0.20	0.999	1.170	1.089	0.711	-0.207	-0.924	-0.292	2118	7.02	0.502
0.22	0.925	1.104	1.019	0.721	-0.198	-0.918	-0.315	2158	6.83	0.508
0.24	0.847	1.033	0.941	0.732	-0.189	-0.912	-0.338	2178	6.62	0.511
0.26	0.764	0.958	0.861	0.744	-0.180	-0.906	-0.360	2173	6.39	0.514
0.28	0.681	0.881	0.780	0.758	-0.168	-0.899	-0.381	2158	6.17	0.518
0.30	0.598	0.803	0.700	0.769	-0.161	-0.893	-0.401	2133	5.94	0.522
0.32	0.518	0.725	0.619	0.783	-0.152	-0.888	-0.420	2104	5.72	0.525
0.34	0.439	0.648	0.540	0.794	-0.143	-0.882	-0.438	2070	5.50	0.530
0.36	0.361	0.570	0.462	0.806	-0.136	-0.877	-0.456	2032	5.30	0.532
0.38	0.286	0.495	0.385	0.820	-0.127	-0.872	-0.472	1995	5.10	0.536
0.40	0.212	0.423	0.311	0.831	-0.120	-0.867	-0.487	1954	4.91	0.538
0.42	0.140	0.352	0.239	0.840	-0.113	-0.862	-0.502	1919	4.74	0.542
0.44	0.073	0.282	0.169	0.852	-0.108	-0.858	-0.516	1884	4.57	0.545
0.46	0.005	0.217	0.102	0.863	-0.101	-0.854	-0.529	1849	4.41	0.549
0.48	-0.058	0.151	0.036	0.873	-0.097	-0.850	-0.541	1816	4.26	0.551
0.50	-0.122	0.087	-0.025	0.884	-0.090	-0.846	-0.553	1782	4.13	0.556
0.55	-0.268	-0.063	-0.176	0.907	-0.078	-0.837	-0.579	1710	3.82	0.562
0.60	-0.401	-0.203	-0.314	0.928	-0.069	-0.830	-0.602	1644	3.57	0.569
0.65	-0.523	-0.331	-0.440	0.946	-0.060	-0.823	-0.622	1592	3.36	0.575
0.70	-0.634	-0.452	-0.555	0.962	-0.053	-0.818	-0.639	1545	3.20	0.582
0.75	-0.737	-0.562	-0.661	0.979	-0.046	-0,813	-0.653	1507	3.07	0.587
0.80	-0.829	-0.666	-0.760	0.992	-0.041	-0.809	-0.666	1476	2.98	0.593
0.85	-0.915	-0.761	-0.851	1.006	-0.037	-0.805	-0.676	1452	2.92	0.598
0.90	-0.993	-0.848	-0.933	1.018	-0.035	-0.802	-0.685	1432	2.89	0.604
0.95	-1.066	-0.932	-1.010	1.027	-0.032	-0.800	-0.692	1416	2.88	0.609
1.00	-1.133	-1.009	-1.080	1.036	-0.032	-0.798	-0.698	1406	2.90	0.613
1.10	-1.249	-1.145	-1.208	1.052	-0.030	-0.795	-0.706	1396	2.99	0.622
1.20	-1.345	-1.265	-1.315	1.064	-0.032	-0.794	-0.710	1400	3.14	0.629
1.30	-1.428	-1.370	-1.407	1.073	-0.035	-0.793	-0.711	1416	3.36	0.637
1.40	-1.495	-1.460	-1.483	1.080	-0.039	-0.794	-0.709	1442	3.62	0.643
1.50	-1.552	-1.538	-1.550	1.085	-0.044	-0.796	-0.704	1479	3.92	0.649
1.60	-1.598	-1.608	-1.605	1.087	-0.051	-0.798	-0.697	1524	4.26	0.654
1.70	-1.634	-1.668	-1.652	1.089	-0.058	-0.801	-0.689	1581	4.62	0.660
1.80	-1.663	-1.718	-1.689	1.087	-0.067	-0.804	-0.679	1644	5.01	0.664
1.90	-1.685	-1.763	-1.720	1.087	-0.074	-0.808	-0.667	1714	5.42	0.669
2.00	-1.699	-1.801	-1.743	1.085	-0.085	-0.812	-0.655	1795	5.85	0.672

C.3 ATTENUATION RELATIONSHIPS DERIVED BY CAMPBELL (1997)

The following equations were derived by Campbell for the median value of peak horizontal acceleration (A_H in g's) and the median value of horizontal spectral ordinates (SA_H in g's) for 5% spectral damping:

$$
\begin{aligned}
Ln(A_H) = & -3.512 + 0.904M \\
& - 1.328 Ln \left\{ \sqrt{R_{SEIS}^2 + \left[0.149 \exp(0.647M) \right]^2} \right\} \\
& + \left[1.125 - 0.112 Ln(R_{SEIS}) - 0.0957M \right] F \\
& + \left[0.440 - 0.171 Ln(R_{SEIS}) \right] S_{SR} \\
& + \left[0.405 - 0.222 Ln(R_{SEIS}) \right] S_{HR}
\end{aligned}
\qquad \text{[C-10]}
$$

$$
\begin{aligned}
Ln(SA_H) = & Ln(A_H) + c_1 + c_2 \tanh \left[c_3(M - 4.7) \right] \\
& + (c_4 + c_5 M) R_{SEIS} + 0.5 c_6 S_{SR} + c_6 S_{HR} \\
& + c_7 \tanh(c_8 D)(1 - S_{HR}) + f_{SA}(D)
\end{aligned}
\qquad \text{[C-11]}
$$

In these equations, M is moment magnitude, and the source-to-site distance, R_{SEIS}, is the shortest distance between the recording site and the assumed zone of seismogenic rupture on the fault. Campbell indicates, based on the work of Marone and Scholz (1988), that the upper 2 to 4 km of the fault zone is typically non-seismogenic. The style of faulting variable, F, is equal to zero for strike slip faulting and is equal to unity for all other style of faulting. The parameters S_{SR} and S_{HR} define the local site conditions as follows:

$$S_{SR} = 1 \quad \& \quad S_{HR} = 0 \qquad \text{for soft rock sites; and}$$

$$S_{SR} = 0 \quad \& \quad S_{HR} = 1 \qquad \text{for hard rock sites.}$$

The parameter D is depth to basement rock below the site. The function $f_{SA}(D)$ is given by:

$$
\begin{aligned}
& \text{For } D \geq 1 \text{ km} \\
& \qquad f_{SA}(D) = 0 \\
& \text{For } D < 1 \\
& \qquad f_{SA}(D) = c_6(1 - S_{HR})(1 - D) + 0.5 c_6(1 - D) S_{SR}
\end{aligned}
\qquad \text{[C-12]}
$$

The values of the coefficients $c_1 ...... c_8$ are provided in Table C-4.

Campbell derived relationships for the standard error of estimate of $Ln(A_H)$ as a function of mean predicted value of $Ln(A_H)$ and mean earthquake magnitude. Thus:

$$\text{For } A_H < 0.068g$$
$$SE = 0.55 \qquad \qquad \text{[C-13]}$$
$$\text{For } 0.068g \leq A_H \leq 0.21g$$
$$SE = 0.173 - 0.14Ln(A_H)$$
$$\text{For } A_H > 0.21g$$
$$SE = 0.39$$

$$\text{For } M < 7.4$$
$$SE = 0.889 - 0.0691M \qquad \qquad \text{[C-14]}$$
$$\text{For } M \geq 7.4$$
$$SE = 0.38$$

Campbell suggests that Eq. C-13 is more statistically robust than Eq. C-14.

Table C-4
Coefficients Derived by Campbell (1997)

Period	c_1	c_2	c_3	c_4	c_5	c_6	c_7	c_8
0.05	0.05	0	0	-0.0011	0.000055	0.20	0	0
0.075	0.27	0	0	-0.0024	0.000095	0.22	0	0
0.1	0.48	0	0	-0.0024	0.000007	0.14	0	0
0.15	0.72	0	0	-0.0010	-0.00027	-0.02	0	0
0.2	0.79	0	0	0.0011	-0.00053	-0.18	0	0
0.3	0.77	0	0	0.0035	-0.00072	-0.40	0	0
0.5	-0.28	0.74	0.66	0.0068	-0.001	-0.42	0.25	0.62
0.75	-1.08	1.23	0.66	0.0077	-0.001	-0.44	0.37	0.62
1	-1.79	1.59	0.66	0.0085	-0.001	-0.38	0.57	0.62
1.5	-2.65	1.98	0.66	0.0094	-0.001	-0.32	0.72	0.62
2	-3.28	2.23	0.66	0.0100	-0.001	-0.36	0.83	0.62
3	-4.07	2.39	0.66	0.0108	-0.001	-0.22	0.86	0.62
4	-4.26	2.03	0.66	0.0112	-0.001	-0.30	1.05	0.62

C.4 ATTENUATION RELATIONSHIPS DERIVED BY IDRISS (2002)

The following equation was derived by Idriss for spectral ordinates at rock sites:

$$Ln(y) = (\alpha_1 + \alpha_2 M) - (\beta_1 + \beta_2 M) Ln(R + 10) + \varphi F \qquad \text{[C-15]}$$

y is the median spectral acceleration in g (5% damping), or peak ground acceleration (pga), in g's, M is moment magnitude, R is the closest distance to the rupture plane in km, F is the fault type (1 for reverse and reverse/oblique, and 0 otherwise), and $\alpha_1, \alpha_2, \beta_1, \beta_2$ are coefficients, whose values are listed in Table C-5a, C-5b; and C-5c. Table 5a provides values of these coefficients for $M < 6$. Values for $M = 6$ to $M = 6.5$ are listed in Table 5b, and those for $M > 6.5$ in table 5c.

Standard error terms are obtained using the following expressions:

$$SE = \begin{cases} \varepsilon_{max} & \text{for } M \leq 5 \\ \varepsilon_1 - 0.12M & \text{for } 5 \leq M \leq 7 \\ \varepsilon_{min} & \text{for } M \geq 7 \end{cases} \qquad \text{[C-16]}$$

The values of $\varphi, \varepsilon_1, \varepsilon_{min}$, and ε_{max} are listed in Table C-6.

Table C-5a Coefficients for the Median Spectral Ordinates Using Equations
Derived by Idriss (2002) for **M < 6**

Period - sec	α_1	α_2	β_1	β_2
M < 6				
0.01	2.5030	0.1337	2.8008	-0.1970
0.03	2.5030	0.1337	2.8008	-0.1970
0.04	2.9873	0.0290	2.7850	-0.2081
0.05	3.2201	0.0099	2.7802	-0.2092
0.06	3.2988	0.0187	2.7784	-0.2083
0.07	3.2935	0.0378	2.7777	-0.2072
0.075	3.2702	0.0489	2.7774	-0.2068
0.08	3.2381	0.0606	2.7773	-0.2065
0.09	3.1522	0.0845	2.7770	-0.2061
0.1	3.0467	0.1083	2.7767	-0.2060
0.11	2.9308	0.1316	2.7763	-0.2061
0.12	2.8093	0.1541	2.7759	-0.2063
0.13	2.6859	0.1758	2.7754	-0.2066
0.14	2.5579	0.1966	2.7748	-0.2070
0.15	2.4301	0.2166	2.7741	-0.2074
0.16	2.3026	0.2357	2.7733	-0.2079
0.17	2.1785	0.2541	2.7724	-0.2083
0.18	2.0543	0.2718	2.7714	-0.2088
0.19	1.9324	0.2888	2.7704	-0.2092
0.2	1.8129	0.3051	2.7693	-0.2096
0.22	1.5794	0.3360	2.7668	-0.2105
0.24	1.3575	0.3646	2.7641	-0.2112
0.25	1.2490	0.3782	2.7626	-0.2116
0.26	1.1435	0.3913	2.7611	-0.2119
0.28	0.9381	0.4161	2.7580	-0.2126
0.3	0.7437	0.4394	2.7548	-0.2132
0.32	0.5553	0.4612	2.7514	-0.2137
0.34	0.3755	0.4816	2.7480	-0.2143
0.35	0.2883	0.4914	2.7462	-0.2145
0.36	0.2049	0.5008	2.7445	-0.2147
0.38	0.0362	0.5190	2.7410	-0.2152
0.4	-0.1223	0.5361	2.7374	-0.2156
0.45	-0.4985	0.5749	2.7285	-0.2167
0.5	-0.8415	0.6091	2.7197	-0.2176
0.55	-1.1581	0.6393	2.7112	-0.2185
0.6	-1.7051	0.7087	2.7030	-0.2194
0.7	-1.9821	0.7127	2.6878	-0.2211
0.8	-2.4510	0.7514	2.6742	-0.2228
0.9	-2.8715	0.7847	2.6624	-0.2244
1	-3.2511	0.8139	2.6522	-0.2259
1.5	-4.7813	0.9288	2.6206	-0.2326
2	-5.9481	1.0246	2.6097	-0.2368
3	-7.7976	1.2121	2.6086	-0.2385
4	-9.3398	1.4047	2.6012	-0.2336
5	-10.7364	1.5973	2.5703	-0.2250

Table C-5b Coefficients for the Median Spectral Ordinates Using Equations
Derived by Idriss (2002) for **M = 6 to M = 6.5**

Period - sec	α_1	α_2	β_1	β_2
M = 6 to M = 6.5				
0.01	4.3387	-0.1754	3.2564	-0.2739
0.03	4.3387	-0.1754	3.2564	-0.2739
0.04	3.9748	-0.1244	3.0378	-0.2468
0.05	3.9125	-0.0972	2.9689	-0.2381
0.06	3.8984	-0.0777	2.9481	-0.2355
0.07	3.8852	-0.0613	2.9448	-0.2352
0.075	3.8748	-0.0536	2.9458	-0.2354
0.08	3.8613	-0.0462	2.9477	-0.2358
0.09	3.8249	-0.0319	2.9527	-0.2367
0.1	3.7774	-0.0181	2.9578	-0.2376
0.11	3.7206	-0.0046	2.9623	-0.2385
0.12	3.6562	0.0086	2.9659	-0.2393
0.13	3.5860	0.0215	2.9685	-0.2401
0.14	3.5111	0.0341	2.9703	-0.2407
0.15	3.4327	0.0464	2.9712	-0.2412
0.16	3.3515	0.0586	2.9713	-0.2416
0.17	3.2683	0.0704	2.9708	-0.2420
0.18	3.1837	0.0821	2.9697	-0.2423
0.19	3.0980	0.0934	2.9681	-0.2425
0.2	3.0117	0.1046	2.9660	-0.2426
0.22	2.8382	0.1263	2.9608	-0.2428
0.24	2.6648	0.1471	2.9544	-0.2428
0.25	2.5786	0.1572	2.9509	-0.2428
0.26	2.4929	0.1671	2.9472	-0.2427
0.28	2.3231	0.1863	2.9393	-0.2425
0.3	2.1559	0.2049	2.9310	-0.2423
0.32	1.9916	0.2228	2.9224	-0.2419
0.34	1.8306	0.2400	2.9135	-0.2416
0.35	1.7512	0.2484	2.9091	-0.2414
0.36	1.6728	0.2567	2.9045	-0.2412
0.38	1.5183	0.2728	2.8955	-0.2407
0.4	1.3671	0.2883	2.8864	-0.2403
0.45	1.0036	0.3251	2.8639	-0.2391
0.5	0.6598	0.3591	2.8419	-0.2379
0.55	0.3347	0.3906	2.8206	-0.2367
0.6	0.0271	0.4200	2.8002	-0.2356
0.7	-0.5407	0.4729	2.7624	-0.2334
0.8	-1.0522	0.5193	2.7283	-0.2315
0.9	-1.5147	0.5603	2.6980	-0.2298
1	-1.9343	0.5966	2.6712	-0.2284
1.5	-3.5364	0.7255	2.5803	-0.2246
2	-4.5538	0.7945	2.5443	-0.2252
3	-5.5133	0.8254	2.5790	-0.2354
4	-5.5624	0.7672	2.7072	-0.2537
5	-5.0154	0.6513	2.8979	-0.2773

Table C-5c Coefficients for the Median Spectral Ordinates Using Equations
Derived by Idriss (2002) for **M > 6.5**

Period - sec	α_1	α_2	β_1	β_2
M > 6.5
0.01	6.5668	-0.5164	3.2606	-0.2740
0.03	6.5668	-0.5164	3.2606	-0.2740
0.04	6.1747	-0.4717	3.0156	-0.2461
0.05	6.2734	-0.4675	2.9671	-0.2400
0.06	6.4228	-0.4696	2.9677	-0.2396
0.07	6.5418	-0.4704	2.9791	-0.2406
0.075	6.5828	-0.4698	2.9850	-0.2413
0.08	6.6162	-0.4685	2.9904	-0.2419
0.09	6.6541	-0.4642	2.9989	-0.2429
0.1	6.6594	-0.4580	3.0044	-0.2437
0.11	6.6436	-0.4504	3.0071	-0.2442
0.12	6.6084	-0.4419	3.0077	-0.2446
0.13	6.5639	-0.4328	3.0067	-0.2448
0.14	6.5085	-0.4233	3.0044	-0.2448
0.15	6.4448	-0.4137	3.0012	-0.2448
0.16	6.3778	-0.4040	2.9974	-0.2447
0.17	6.3077	-0.3945	2.9931	-0.2446
0.18	6.2366	-0.3850	2.9885	-0.2444
0.19	6.1623	-0.3758	2.9836	-0.2442
0.2	6.0872	-0.3668	2.9786	-0.2440
0.22	5.9380	-0.3494	2.9684	-0.2436
0.24	5.7915	-0.3331	2.9580	-0.2431
0.25	5.7213	-0.3253	2.9529	-0.2428
0.26	5.6485	-0.3178	2.9477	-0.2426
0.28	5.5097	-0.3035	2.9376	-0.2421
0.3	5.3744	-0.2900	2.9276	-0.2417
0.32	5.2428	-0.2774	2.9178	-0.2412
0.34	5.1167	-0.2656	2.9082	-0.2408
0.35	5.0563	-0.2600	2.9034	-0.2405
0.36	4.9957	-0.2545	2.8987	-0.2403
0.38	4.8752	-0.2441	2.8894	-0.2399
0.4	4.7604	-0.2342	2.8803	-0.2395
0.45	4.4900	-0.2119	2.8581	-0.2384
0.5	4.2369	-0.1922	2.8367	-0.2374
0.55	4.0027	-0.1747	2.8160	-0.2363
0.6	3.7826	-0.1589	2.7960	-0.2353
0.7	3.3750	-0.1314	2.7580	-0.2333
0.8	3.0078	-0.1078	2.7227	-0.2314
0.9	2.6734	-0.0870	2.6901	-0.2295
1	2.3648	-0.0683	2.6603	-0.2278
1.5	1.1109	0.0068	2.5501	-0.2211
2	0.1818	0.0649	2.4928	-0.2176
3	-1.1016	0.1532	2.4711	-0.2168
4	-1.9306	0.2153	2.4953	-0.2190
5	-2.5042	0.2579	2.5107	-0.2199

Table C-6 Style of Faulting and Standard Error Coefficients for Spectral Ordinates
Using Equations Derived by Idriss (2002)

Period - sec	φ	ε_{max}	ε_1	ε_{min}
0.01	0.320	0.720	1.320	0.450
0.03	0.320	0.720	1.320	0.450
0.04	0.320	0.720	1.320	0.450
0.05	0.320	0.720	1.320	0.450
0.06	0.320	0.730	1.330	0.460
0.07	0.320	0.739	1.339	0.469
0.075	0.320	0.743	1.343	0.473
0.08	0.320	0.747	1.347	0.477
0.09	0.320	0.753	1.353	0.483
0.1	0.320	0.760	1.360	0.490
0.11	0.324	0.765	1.365	0.495
0.12	0.327	0.770	1.370	0.500
0.13	0.330	0.775	1.375	0.505
0.14	0.332	0.779	1.379	0.509
0.15	0.335	0.783	1.383	0.513
0.16	0.337	0.787	1.387	0.517
0.17	0.339	0.791	1.391	0.521
0.18	0.341	0.794	1.394	0.524
0.19	0.343	0.797	1.397	0.527
0.2	0.345	0.800	1.400	0.530
0.22	0.348	0.806	1.406	0.536
0.24	0.352	0.811	1.411	0.541
0.25	0.353	0.814	1.414	0.544
0.26	0.355	0.816	1.416	0.546
0.28	0.357	0.820	1.420	0.550
0.3	0.360	0.825	1.425	0.555
0.32	0.360	0.829	1.429	0.559
0.34	0.360	0.832	1.432	0.562
0.35	0.360	0.834	1.434	0.564
0.36	0.360	0.836	1.436	0.566
0.38	0.360	0.839	1.439	0.569
0.4	0.360	0.842	1.442	0.572
0.45	0.360	0.849	1.449	0.579
0.5	0.360	0.856	1.456	0.586
0.55	0.350	0.862	1.462	0.592
0.6	0.340	0.867	1.467	0.597
0.7	0.322	0.877	1.477	0.607
0.8	0.307	0.885	1.485	0.615
0.9	0.294	0.893	1.493	0.623
1	0.282	0.900	1.500	0.630
1.5	0.236	0.900	1.500	0.630
2	0.204	0.900	1.500	0.630
3	0.158	0.900	1.500	0.630
4	0.125	0.900	1.500	0.630
5	0.100	0.900	1.500	0.630

C.5 ATTENUATION RELATIONSHIPS DERIVED BY SADIGH, CHANG, EGAN, MAKDISI, AND YOUNGS (1997)

The following equation was derived by Sadigh et al for spectral ordinates at rock sites:

$$Ln(y) = C_1 + C_2 M + C_3 (8.5 - M)^{2.5} + C_4 Ln\left[r_{rup} + exp(C_5 + C_6 M) \right]$$
$$+ C_7 Ln(r_{rup} + 2)$$

[C-17]

y is the median spectral acceleration in g (5% damping), or peak ground acceleration (pga), in g's, M is moment magnitude, r_{rup} is the closest distance to the rupture plane in km, and $C_1...C_7$ are coefficients. The values of the standard error terms are listed in Table C-7. The values of the coefficients $C_1...C_7$ are provided in Table C-8.

Table C-7 Coefficients for Standard Error Terms Using
Equations Derived by Sadigh et al (1997)

Period - sec	Standard Error Term	Minimum Value for $M \geq 7.21$
zpa	$1.39 - 0.14M$	0.38
0.07	$1.40 - 0.14M$	0.39
0.10	$1.41 - 0.14M$	0.40
0.20	$1.43 - 0.14M$	0.42
0.30	$1.45 - 0.14M$	0.44
0.40	$1.48 - 0.14M$	0.47
0.50	$1.50 - 0.14M$	0.49
0.75	$1.52 - 0.14M$	0.51
≥ 1.00	$1.53 - 0.14M$	0.52

Table C-8 Coefficients for the Median Spectral Ordinates Using Equations
Derived by Sadigh et al (1997)

Period	C_1	C_2	C_3	C_4	C_5	C_6	C_7
$M \leq 6.5$							
zpa	-0.624	1	0.000	-2.100	1.29649	0.250	0.000
0.03	-0.624	1	0.000	-2.100	1.29649	0.250	0.000
0.07	0.110	1	0.006	-2.128	1.29649	0.250	-0.082
0.1	0.275	1	0.006	-2.148	1.29649	0.250	-0.041
0.2	0.153	1	-0.004	-2.080	1.29649	0.250	0.000
0.3	-0.057	1	-0.017	-2.028	1.29649	0.250	0.000
0.4	-0.298	1	-0.028	-1.990	1.29649	0.250	0.000
0.5	-0.588	1	-0.040	-1.945	1.29649	0.250	0.000
0.75	-1.208	1	-0.050	-1.865	1.29649	0.250	0.000
1	-1.705	1	-0.055	-1.800	1.29649	0.250	0.000
1.5	-2.407	1	-0.065	-1.725	1.29649	0.250	0.000
2	-2.945	1	-0.070	-1.670	1.29649	0.250	0.000
3	-3.700	1	-0.080	-1.610	1.29649	0.250	0.000
4	-4.230	1	-0.100	-1.570	1.29649	0.250	0.000
$M > 6.5$							
zpa	-1.237	1.1	0.000	-2.100	-0.48451	0.524	0.000
0.03	-1.237	1.1	0.000	-2.100	-0.48451	0.524	0.000
0.07	-0.540	1.1	0.006	-2.128	-0.48451	0.524	-0.082
0.1	-0.375	1.1	0.006	-2.148	-0.48451	0.524	-0.041
0.2	-0.497	1.1	-0.004	-2.080	-0.48451	0.524	0.000
0.3	-0.707	1.1	-0.017	-2.028	-0.48451	0.524	0.000
0.4	-0.948	1.1	-0.028	-1.990	-0.48451	0.524	0.000
0.5	-1.238	1.1	-0.040	-1.945	-0.48451	0.524	0.000
0.75	-1.858	1.1	-0.050	-1.865	-0.48451	0.524	0.000
1	-2.355	1.1	-0.055	-1.800	-0.48451	0.524	0.000
1.5	-3.057	1.1	-0.065	-1.725	-0.48451	0.524	0.000
2	-3.595	1.1	-0.070	-1.670	-0.48451	0.524	0.000
3	-4.350	1.1	-0.080	-1.610	-0.48451	0.524	0.000
4	-4.880	1.1	-0.100	-1.570	-0.48451	0.524	0.000

Note that the above coefficients are applicable to ground motions generated by a strike slip event. Sadigh et al suggest that the calculated spectral ordinates be multiplied by a factor of 1.2 for reverse / thrust events.

APPENDIX D
ATTENUATION RELATIONSHIPS FOR MOTIONS
IN EASTERN NORTH AMERICA (ENA)

The attenuation relationships derived by Toro et al (1997) and those by Atkinson & Boore (1997) are summarized in this Appendix. Also included in this appendix is the attenuation relationship developed by Nuttli (1986).

D.1 ATTENUATION RELATIONSHIPS BY TORO, ABRAHAMSON AND SCHNEIDER (1997)

The functional form adopted by Toro et al is the following:

$$Ln(y) = C_1 + C_2(M-6) + C_3(M-6)^2 - C_4 Ln(R_M)$$
$$- (C_5 - C_4) max\left[Ln\left(\frac{R_M}{100}\right), 0 \right] - C_6 R_M \qquad \text{[D-1]}$$

$$R_M = \sqrt{R_{jb}^2 + C_7^2} \qquad \text{[D-2]}$$

in which, y is the median spectral acceleration in g (5% damping) or peak ground acceleration (pga) in g's, M is either Lg magnitude (m_{bLg}) or moment magnitude M, C_1 through C_7 are coefficients that depend on the frequency and on the region under consideration, and R_{jb} is the closest horizontal distance to the rupture surface if this surface is projected to the ground surface (i.e., the Joyner-Boore distance) in km.

Two regions were considered by Toro et al (1997) in deriving attenuation relationships for Eastern North America (ENA), namely the Mid-Continent and the Gulf Crustal Regions. The extent of each region is depicted in Fig. D-1. The coefficients $C_1 ... C_7$ for various frequencies and for zpa and applicable to each region are listed in Table D-1 for equations using moment magnitude and for equations using Lg magnitude.

D.2 ATTENUATION RELATIONSHIPS BY ATKINSON AND BOORE (1997)

The following functional form was used by Atkinson & Bore (1997) to calculate the median spectral acceleration

$$Ln(y) = C_1 + C_2(M-6) + C_3(M-6)^2 - Ln(R) - C_4 R \qquad \text{[D-3]}$$

in which, y is the median spectral acceleration in g (5% damping) or peak ground acceleration (pga) in g's, M is moment magnitude C_1 through C_4 are coefficients that depend on frequency, and R is the hypocentral distance in km. The coefficients $C_1 ... C_4$ for various frequencies and for pga are listed in Table D-2.

D.3 ATTENUATION RELATIONSHIPS BY NUTTLI (1986)
(TBC)

Table D-1 Coefficients of Attenuation Equations Derived by Toro et al (1997)

Frequency (Hz)	Coefficient						
	C_1	C_2	C_3	C_4	C_5	C_6	C_7
Mid-Continent Region – Equations Using Moment Magnitude							
0.5	-0.74	1.86	-0.31	0.92	0.46	0.0017	6.9
1	0.09	1.42	-0.20	0.90	0.49	0.0023	6.8
2.5	1.07	1.05	-0.10	0.93	0.56	0.0033	7.1
5	1.73	0.84	0	0.98	0.66	0.0042	7.5
10	2.37	0.81	0	1.10	1.02	0.0040	8.3
25	3.68	0.80	0	1.46	1.77	0.0013	10.5
35	4.00	0.79	0	1.57	1.83	0.0008	11.1
pga	2.20	0.81	0	1.27	1.16	0.0021	9.3
Mid-Continent Region – Equations Using Lg Magnitude							
0.5	-0.97	2.52	-0.47	0.93	0.60	0.0012	7.0
1	-0.12	2.05	-0.34	0.90	0.59	0.0019	6.8
2.5	0.90	1.70	-0.26	0.94	0.65	0.0030	7.2
5	1.60	1.24	0	0.98	0.74	0.0039	7.5
10	2.36	1.23	0	1.12	1.05	0.0043	8.5
25	3.54	1.19	0	1.46	1.84	0.0010	10.5
35	3.87	1.19	0	1.58	1.90	0.0005	11.1
pga	2.07	1.20	0	1.28	1.23	0.0018	9.3
Gulf Region – Equations Using Moment Magnitude							
0.5	-0.81	-1.60	-0.26	0.74	0.71	0.0025	6.6
1	0.24	-0.60	-0.15	0.79	0.82	0.0034	7.2
2.5	1.64	0.80	-0.08	0.99	1.27	0.0036	8.9
5	3.10	2.26	0	1.34	1.95	0.0017	11.4
10	5.08	4.25	0	1.87	2.52	0.0002	14.1
25	5.19	4.35	0	1.96	1.96	0.0004	12.9
35	4.81	3.97	0	1.89	1.80	0.0008	11.9
pga	2.91	2.07	0	1.49	1.61	0.0014	10.9
Gulf Region – Equations Using Lg Magnitude							
0.5	-1.01	2.38	-0.42	0.75	0.83	0.0032	6.8
1	0.06	1.97	-0.32	0.80	0.92	0.0030	7.3
2.5	1.49	1.74	-0.26	1.00	1.36	0.0032	9.0
5	3.00	1.31	0	1.35	2.03	0.0014	11.4
10	4.65	1.30	0	1.78	2.41	0.0000	13.8
25	5.08	1.29	0	1.97	2.04	0.0000	12.9
35	4.68	1.30	0	1.89	1.88	0.0005	11.9
pga	2.80	1.31	0	1.49	1.68	0.0017	10.9

Table D-2 Coefficients of Attenuation Equations Derived by Atkinson & Boore (1997)

Frequency (Hz)	Coefficient			
	C_1	C_2	C_3	C_4
0.5	-1.660	1.460	-0.039	0
0.8	-0.900	1.462	-0.071	0
1.0	-0.508	1.428	-0.094	0
1.3	-0.094	1.391	-0.118	0
2.0	0.620	1.267	-0.147	0
3.2	1.265	1.094	-0.165	0.00024
5.0	1.749	0.963	-0.148	0.00105
7.9	2.140	0.864	-0.129	0.00207
10	2.301	0.829	-0.121	0.00279
13	2.463	0.797	-0.113	0.00352
20	2.762	0.755	-0.110	0.00520
pga	1.841	0.686	-0.123	0.00311
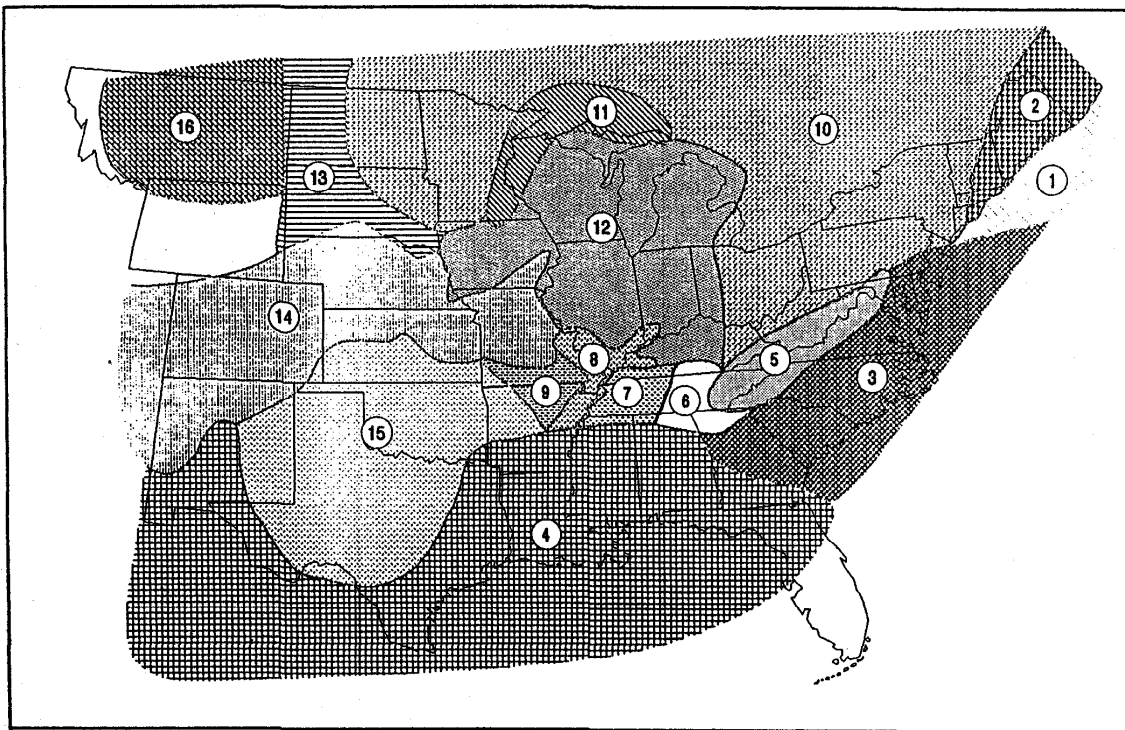
Regionalization of crustal structure for CENA. Attenuation equations are developed for the Mid-continent and Gulf crustal regions (regions 12 and 4, respectively). The equations for the Mid-continent are applicable to regions 1 through 3 and 5 through 16

Fig. D-1 Regions Considered by Toro et al (1997) in Deriving Attenuation Relationships for Eastern North America (ENA)

APPENDIX E
ATTENUATION RELATIONSHIPS FOR SUBDUCTION EARTHQUAKES

The attenuation relationships derived by Youngs et al (1997) and those by Atkinson & Boore (2003) are summarized in this Appendix.

E.1 ATTENUATION RELATIONSHIPS DERIVED BY YOUNGS, CHIOU, SILVA AND HUMPHREY (1997)

The following attenuation relationship was derived by Youngs et al (1997):

$$Ln(y) = 0.2418 + 1.414M + C_1 + C_2(10 - M)^3 + C_3 Ln(R_{rup} + C_M)$$
$$+ 0.00607H + 0.3846Z_r$$
[E-1]

$$C_M = 1.7818 \exp(0.554M)$$
[E-2]

$$\text{Standard error term, } SE = C_4 + C_5 M$$
[E-3]

y is spectral acceleration in g's, M is moment magnitude, R_{rup} is closest distance from site to rupture surface in km, H is depth in km, and $Z_r = 0$ for interface events (such as the Cascadia Zone) and $Z_r = 1$ for intra-slab events (such as the Juan de Fuca).

Note that for magnitudes greater than 8, the SE term for $M = 8$ is to be used.

The values of the coefficients $C_1 ... C_5$ are listed in Table E-1.

Table E-1 Coefficients of Attenuation Equations Derived by Young et al (1997)

Period - sec	C_1	C_2	C_3	C_4	C_5
0.01	0	0	-2.552	1.45	-0.1
0.075	1.275	0	-2.707	1.45	-0.1
0.1	1.188	-0.0011	-2.655	1.45	-0.1
0.2	0.722	-0.0027	-2.528	1.45	-0.1
0.3	0.246	-0.0036	-2.454	1.45	-0.1
0.4	-0.115	-0.0043	-2.401	1.45	-0.1
0.5	-0.400	-0.0048	-2.360	1.45	-0.1
0.75	-1.149	-0.0057	-2.286	1.45	-0.1
1	-1.736	-0.0064	-2.234	1.45	-0.1
1.5	-2.634	-0.0073	-2.160	1.50	-0.1
2	-3.328	-0.0080	-2.107	1.55	-0.1
3	-4.511	-0.0089	-2.033	1.65	-0.1

E.2 ATTENUATION RELATIONSHIPS DERIVED BY ATKINSON AND BOORE (2003)
(TBC)
E.3 ATTENUATION RELATIONSHIPS DERIVED BY ZHAO ET AL.(2006)
(TBC)

APPENDIX F
EFFECTS OF RUPTURE DIRECTIVITY ON EARTHQUAKE GROUND MOTIONS

F.1 INTRODUCTION

Rupture directivity effects can lead to large long period pulses in the ground motion. Recently, models have been developed to quantify the directivity effect (e.g. Somerville et al, 1997). With these models of the rupture directivity effect, directivity can be included in either deterministic or probabilistic seismic hazard analyses. This paper demonstrates the effect of rupture directivity on probabilistic seismic hazard analyses.

F.2 ATTENUATION RELATIONS AND RUPTURE DIRECTIVITY

For design of long-period structures such as bridges, characterization of long-period motion is essential. Attenuation relations commonly used in California do not explicitly include rupture directivity effects but they can adjusted to account for near-fault directivity effects using the Somerville et al. (1997) fault-rupture directivity model. The Somerville et al. (1997) model comprises two period-dependent scaling factors that may be applied to horizontal attenuation relationship. One of the factors accounts for the change in shaking intensity in the average horizontal component of motion due to near-fault rupture directivity effects (higher ground motions for rupture toward the site and lower ground motions for rupture away from the site). The second factor reflects the directional nature of the shaking intensity using two ratios: fault normal (FN) and fault parallel (FP) versus the average (FA)

APPENDIX G
EFFECTS OF HANGING WALL/FOOTWALL ON EARTHQUAKE GROUND MOTIONS

APPENDIX H
ESTIMATION OF TARGET SPECTRUM AT
SPECTRAL DAMPING RATIOS OTHER THAN 5%

The equations listed in Appendices C through E are for a spectral damping ratio of 5%. Attenuation relationships at other damping ratios have not usually been derived. Instead, a factor to adjust from 5% damping to other damping ratios is used. For example, Newmark and Hall (1981) provided the following relationships for the median spectral amplification factors (SAF):

Region	Approximate Range of Periods, T - sec	Spectrum Amplification Factor (SAF)	SAF Normalized with respect to $\beta = 5\%$
Acceleration	$0.125 \leq T < 0.3$ to 0.4	$3.21 - 0.68Ln(\beta)$	$1.517 - 0.321Ln(\beta)$
Velocity	0.3 to $0.4 \leq T < 1.5$ to 3	$2.31 - 0.41Ln(\beta)$	$1.40 - 0.248Ln(\beta)$
Displacement	$T \geq 1.5$ to 3	$0.82 - 0.27Ln(\beta)$	$1.314 - 0.195Ln(\beta)$

Note: The approximate range of periods listed above depends on the values selected for peak particle acceleration, velocity and displacement.

For example, the spectral ordinates shown in Fig. H-1 are for peak particle acceleration of 1 g, v/a ratio equal to 75 cm/sec/g and a value of ad/v^2 equal to 4; the resulting range of periods is as follows:

Acceleration Region:	$0.125 \leq T < 0.35$ to 0.4
Velocity Region:	0.35 to $0.4 \leq T < 1.5$ to 1.7
Displacement Region:	$T \geq 1.5$ to 1.7

The values of $v/a = 75$ and $ad/v^2 = 4$ were selected to represent motions at a rock site generated by a nearby earthquake having a magnitude of about 6½ to 7½.

Recordings from the San Fernando (SF) and the Imperial Valley (IV) earthquakes were also used to derive adjustment factors normalized with respect to 5 percent spectral damping. Expressions similar to those utilized by Newmark and Hall (1981) were used to derive the coefficients for two sets of expressions. One set relates spectral values at damping ratios less than 5 percent to spectral values at damping of 5 percent, and the other set for spectral damping ratios higher than 5 percent. Thus,

$$Ratio = a_1 - b_1 Ln(\beta) \quad \text{for } \beta \leq 5\% \qquad \text{[F-1]}$$

$$Ratio = a_2 - b_2 Ln(\beta) \quad \text{for } \beta \geq 5\% \qquad \text{[F-2]}$$

The values of the coefficients a_1, b_1, a_2 and b_2 for a selected number of periods are listed Table H-1

Table H-1 Parameters a_1, b_1, a_2 and b_2

Period - sec	a_1	b_1	a_2	b_2
0.03	1	0	1	0
0.05	1.1142	0.0709	1.083	0.0505
0.075	1.3513	0.2183	1.2902	0.1803
0.1	1.4918	0.3056	1.4179	0.2597
0.15	1.5796	0.3601	1.4992	0.3102
0.2	1.6148	0.382	1.534	0.3318
0.25	1.6148	0.382	1.534	0.3318
0.3	1.6148	0.382	1.534	0.3318
0.35	1.606	0.3765	1.5224	0.3246
0.4	1.5972	0.3711	1.5108	0.3174
0.5	1.5796	0.3605	1.4992	0.3102
0.6	1.5445	0.3383	1.4876	0.303
0.7	1.5269	0.3274	1.4876	0.303
0.8	1.5094	0.3165	1.476	0.2958
0.9	1.4918	0.3056	1.469	0.2914
1	1.4742	0.2947	1.4644	0.2885
1.5	1.4391	0.2728	1.4644	0.2885
2	1.4216	0.2619	1.4644	0.2885
3	1.404	0.251	1.4644	0.2885
4	1.404	0.251	1.4644	0.2885
5	1.404	0.251	1.4644	0.2885

Note: The values of the parameters a_1, b_1, a_2 and b_2 given above are reported up to the fourth decimal point to provide smooth curves for the calculated spectral ratios; this degree of precision does not imply any increase in accuracy.

Values of the spectral ordinates for damping ratios of 2, 4, 7 and 10% divided by those for a damping ratio of 5% are presented in Fig. H-2 using the above equations and the corresponding values of the coefficients a_1, b_1, a_2 and b_2. Also shown in Fig. H-2 are the values using the expressions proposed by Newmark and Hall for a peak acceleration of 1 g, $v/a = 75$ and ad/v^2 = 4. The results shown in Fig. H-2 indicate that the relationships proposed by Newmark and Hall and the expressions based on recorded data provide comparable results. Therefore, either set of equations can be used for obtaining target spectra at damping ratios other than 5 percent.
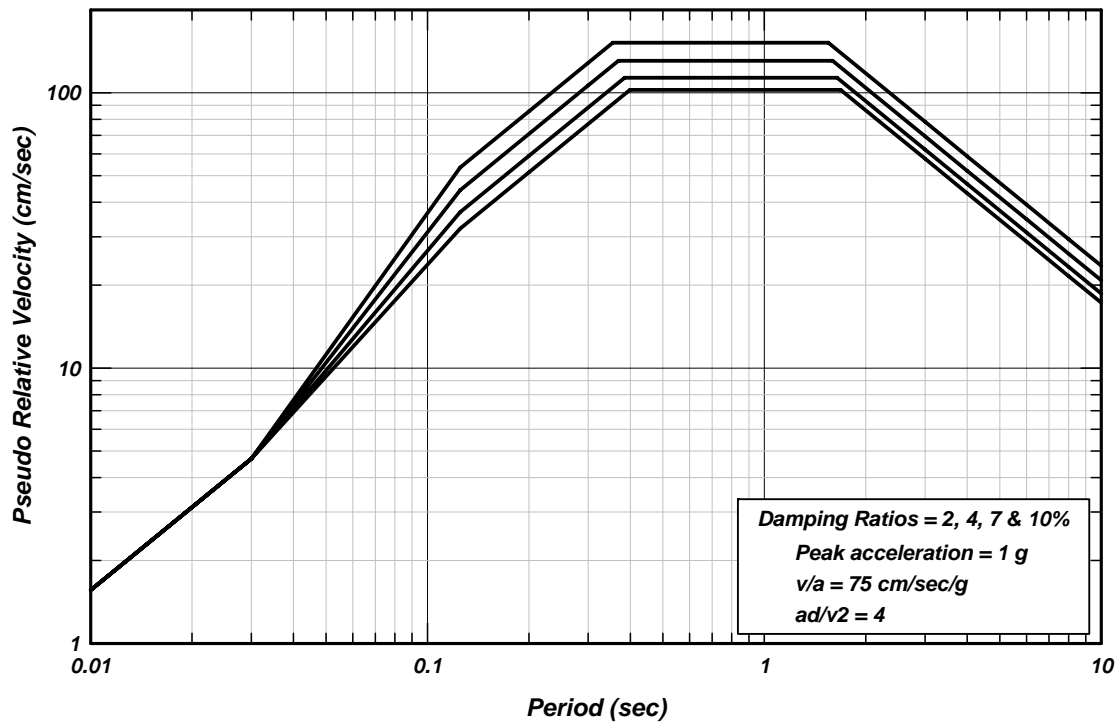
Fig. H-1 Spectral Shapes Using Relationships Proposed by
Newmark & Hall (1981)

The figure shows a log-log plot with "Pseudo Relative Velocity (cm/sec)" on the vertical axis and "Period (sec)" on the horizontal axis. A legend box contains:

Damping Ratios = 2, 4, 7 & 10%
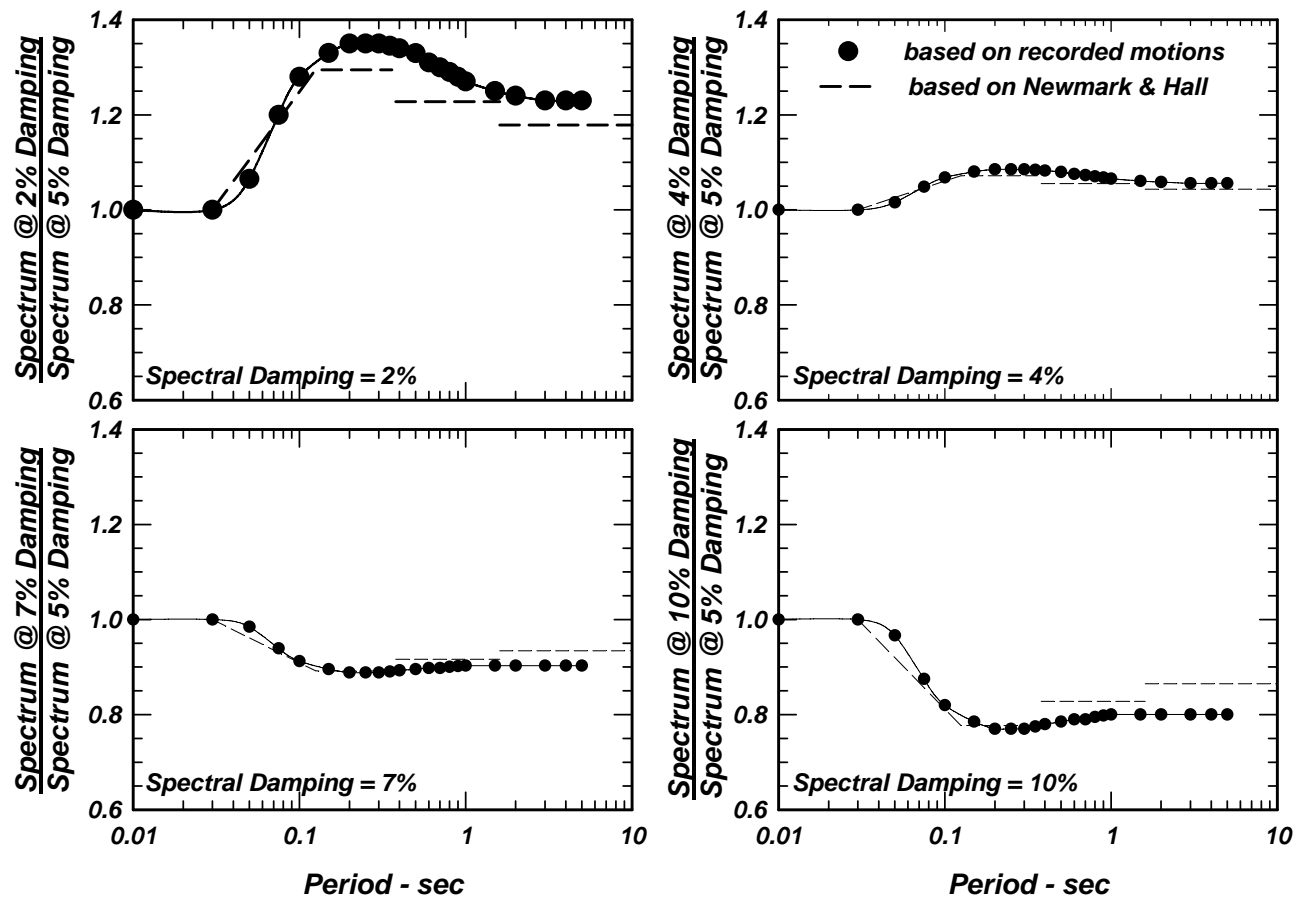*Peak acceleration = 1 g*
v/a = 75 cm/sec/g
ad/v2 = 4

Fig. H-2 Variations of Spectral Ordinates with Spectral Damping Ratio

APPENDIX I
ANALYTICAL SIMULATIONS TO GENERATE ACCELEROGRAMS
AT A ROCK SITE

I.1 INTRODUCTION

Different approaches can be used to simulate ground motion from an earthquake source. Some of these approaches are summarized below as examples, but not endorsement, of various methods being currently used. While the approaches can differ, they have in common certain elements and are critical in evaluation of their applicability. It is also important to note that the synthetic time histories of ground motion are computed for a rock outcrop, i.e., analytical models are computed using linear wave propagation and includes the Earth's free surface. Treatment of the local site condition is a complicated subject in its own right and is specific to the individual case.

The basic axiom of an analytical model is that an earthquake represents the release of elastic energy by slip occurring over some fault plane with finite area in the Earth. The earthquake initiates at the hypocenter, the point on the fault where the slip first occurs and from which the first elastic waves are emitted. As the rupture spreads over the fault, other points on the fault will slip and radiate elastic waves. The elastic waves propagate through a complex earth structure that can scatter and attenuate the waves. The final ground motion that is recorded is a convolution of the earthquake source and the path effects. Consequently, both the source and the path must be fully described to understand the ground motion that has been computed.

The essential components that one expects to be described for any analytical model are:

1. Geometrical description of fault and stations for which ground motion will be computed
    a. Length of fault
    b. Width of fault
    c. Dip of fault
    d. Strike of the fault (measured clockwise from North, Aki and Richards convention)
    e. Geometry of fault within the earth, e.g., depth of the shallowest part of the fault, depth of the deepest part of the fault.
    f. Hypocenter coordinates: latitude, longitude and depth.
    g. Geometry of the site relative to the geometry of the fault; any measure of distance between the fault and site must be specified if this distance measure is used for other purposes, e.g., empirical regression formulas. Latitude, longitude and elevation must be specified for each site.

2. Gross parameters of the earthquake
    a. Seismic moment (All magnitudes must be converted to moment magnitude; magnitude and seismic moment must be internally consistent. The precise formula for converting magnitude to seismic moment and vice versa must be specified, e.g., $M = 2/3 \log M_0 - 10.7$ where M_o is seismic moment in Nm (Hanks and Kanamori, 1979))
    b. Magnitude of slip specified for each point (ξ, η) on the fault where ξ is the coordinate along strike and η is the coordinate along the dip. The basis for deciding on a spatial distribution of slip, e.g., a distribution similar to a previous earthquake, and the basis for deciding on the amplitude of slip, e.g., scaled slip from previous

earthquake, must be specified. If the fault is a plane, this description should be a 2x2 matrix of slip values with each slip value given a coordinate on the fault (ξ, η).

    c. Slip direction for each point on the fault: rake angle. If the slip value is partitioned into two components: slip along strike and slip along the dip direction, the rake angle is superfluous.

    d. Slip time function for every point on the fault. The temporal behavior of the slip for each point on the fault must be specified.

    e. Rupture time. For each point on the fault, the time at which that points first begins to slip must be specified. The hypocenter has a rupture time of zero.

3. Gross parameters of the Earth structure everywhere in the body of the medium
    a. Velocity of elastic waves (P and S)
    b. Density
    c. Attenuation by use of the seismic quality factor Q; the quality factor may be frequency dependent. If so, its frequency dependence must be specified.

4. Site Characterization—Rock
    a. P- and S-wave velocity and attenuation, Q(f) at the site
    b. Linear response
    c. Spatially non uniform material properties if they exist.

5. Full description of the method of computing Green's functions must include:
    a. Method for computing the Green's functions must be described including details such as the exact time function used for the impulse source, the time step, numerical damping, low-pass and/or high-pass filters, etc.
    b. A precise description of the velocity structure must be given (see Item 3) as well as the frequency bandwidth for which the Green's functions are computed.
    c. If empirical Green's functions are used, their applicable frequency bandwidth must be specified. The location of the source must be specified. Any scaling between the original source and that used for the convolution must also be specified.

6. Full description of how the source is convolved with the Green's functions.
    a. Specify the exact locations of the slip functions on the fault, e.g., rectangular grid, non-uniformly, and how the slip functions are convolved.
    b. Explain how are each of the parameters used in the convolution is specified on the fault.
    c. Are there further refinements to slip functions and Green's functions before convolution? For example, are either the Green's functions or the slip functions or both interpolated to a finer spatial scale? Is there filtering applied?

7. Documentation that the analytical model computes ground motion consistent with ground motion from recorded earthquakes.
    a. There must be some measure of the misfit between the recorded ground motion and the computed ground motion. For example, it is customary to compute bias and standard error for different periods of the response spectrum, see Hartzell et al. (1999).
    b. In comparing recorded ground motion with that from an analytical method, there should be a minimum of five stations with maximum (360˚ ideally) azimuthal coverage of the source.

    c. If a preexisting method is being used for analytical computation of ground motion, any previous validation studies should be cited provided the method has not changed since the validation studies were originally performed.

4.3.1 Current Analytical Models—Linear Response, Rock Outcrop

There are a variety of different models that have been used to predict ground motion. The methods are continually evolving, especially those that include the finite extent of the fault and are broadband (frequencies from 0–20 Hz). Some approaches are for point sources, i.e., the site is far from the source so that any timing issues related to the physical dimensions of the source are small. ($d^2 << R\lambda_{min}$, where d is the maximum distance from the hypocenter to any point on the fault, R is the hypocentral distance to the site and λ_{min} is the minimum wavelength recorded.) Atkinson and Somerville (1994) discuss two different approaches—stochastic (Boore, 1983) and ray theory (Somerville et al., 1991)—for simulating ground motions from point sources as applied to earthquakes in the eastern US. For pseudo spectral acceleration, the standard error of the prediction for both methods is on the order of 2–2.5. Atkinson and Boore (1998) provide a more detailed analysis of different spectral models as applied to eastern US earthquakes.

This has been a typical standard error as well for analytical models that include finite faulting for broadband ground motion (e.g., Kamae et al., 1998; Hartzell et al., 1999; Pitarka et al., 2000; Mai and Beroza, 2003, Archuleta et al., 2003).

Rather than endorse any particular modeling effort, it is important to understand how the different elements of the model are computed and then combined to produce a broadband synthetic ground motion (Spudich and Archuleta, 1987). Selecting a source model, i.e., the slip rate function everywhere on the fault and the rupture time for each point depends on the investigator. Naturally there has to be justification for the source model (e.g., Andrews, 1980; Boatwright, 1988; Herrero and Bernard, 1994; Mai and Beroza, 2002; Oglesby and Day, 2002; Lavallée and Archuleta, 2003). However, with analytical models it is important to consider multiple source descriptions in order to understand the range of ground motion that may occur from a scenario earthquake (O'Connell et al., 2001; Hartzell et al., 2002; Archuleta et al., 2003; Day, 2003; Mai and Beroza, 2003).

A real difficulty in broadband synthetics is the appropriate Green's function. Computing full waveform Green's functions in 1D layered models is standard (e.g., Olson et al., 1984; Zhu and Rivera, 2001). The 1D Green's functions are easily computed to frequencies of 20 Hz including Q. With the development of finite difference and finite element codes it is possible to compute accurately Green's functions in 2D and 3D Earth models (e.g., Olsen et al., 1995; Graves, 1996; Day, 1982, 2001, 2005; Moczo et al., 2001, Ma et al., 2004). However, such computations are generally limited to computing ground motion for frequencies less than 1.0 Hz. If the numerical 2D and 3D Green's functions are to be extended to higher frequencies, the investigator has to find a way to stitch together the different passbands (e.g., Kamae et al., 1998; Hartzell et al., 1999; Pitarka et al., 2000; Mai and Beroza, 2003). Of course, the most straightforward approach is to use events recorded at the site as empirical Green's functions following the seminal paper of Hartzell (1978). This technique has been widely used, for example, Irikura, (1983), Joyner and Boore (1986), Dan et al. (1990), Wennerberg (1990), Somerville et al. (1991), Hutchings (1994), Irikura and Kamae (1994), Tumarkin and Archuleta (1994), Tumarkin et al. (1994), Ordaz et al. (1995), Jarpe and Kasameyer (1996), Archuleta et al. (2003), Miyake et al. (2003). This has the obvious limitation that the site must have recorded an earthquake from the source zone of the earthquake to be modeled.

Before applying an analytical model to the site-specific problem of the dam, the analytical model must be validated. The standard approach is to model a well-recorded earthquake. The synthetic time series is compared both in the time domain and spectral domain with the data. In many cases the spectral acceleration at different periods to determine if a bias exists and to quantify the standard error (Abrahamson et al., 1990). Examples of such comparisons can be found in Somerville et al. (1991), Hartzell et al. (1999), Archuleta et al. (2003) and Mai and Beroza (2003).

**APPENDIX J
SELECTION OF ACCELEROGRAMS FOR
SEISMIC ANALYSIS PURPOSES**

J.1 INTRODUCTION

There are several procedures that can be used to select earthquake ground motions at a rock site. These procedures include:

(a) Utilization of motions previously recorded at rock sites during similar size earthquakes and at distances comparable to those under consideration;

(b) Estimation of a target spectrum and then selection of natural time histories whose spectral ordinates are comparable to those of the target spectrum for the period range of interest;

(c) Estimation of a target spectrum and then generation of a synthetic time history whose spectral ordinates provide a reasonable envelope to those of the target spectrum; or

(d) Use of simulation techniques starting with the source and propagating the appropriate wave forms to generate a suite of time histories that can then be used to represent the earthquake ground motions at the rock site of interest.

Procedure (a) is difficult to utilize at most locations because the number of recorded motions is not extensive enough to cover a sufficiently wide range of possibilities. Procedure (d) is summarized in Appendix H. Procedures (b) and (c) are summarized below.

J.2 SELECTION OF NATURAL TIME HISTORIES

As noted above, either natural time histories or a synthetic time history can be used to represent the target spectrum. If these time histories are to be used in conjunction with a nonlinear analysis, then natural time histories would be preferable. Time histories recorded during several earthquakes are available from several web sites including COSMOS VDC (http://db.cosmos-eq.org/), USGS, ROSRINE, the California Geological Survey, thePacific Earthquake Engineering Research center (PEER).

When using natural time histories, it is suggested that at least three time histories, and possibly as many as seven, be used in the analyses. An example of this selection process is provided later in this report.

J.3 GENERATION OF SYNTHETIC TIME HISTORIES

Starting with a recorded motion, it is possible to modify the amplitudes of this motion so that its spectral ordinates are essentially equal to those of the target spectrum. There are a few computer programs that incorporate a procedure to modify the Fourier amplitudes of a given time history so that the response spectrum of the modified time history provides a reasonable estimate of the target spectrum. The program was developed by Silva and Lee (1987); details regarding the procedures used, a computer program listing and a user's guide are included in the publication by Silva and Lee (1987). An example of a time history generated using this program is provided later in this report.
J.4 EXAMPLES

APPENDIX K
INVENTORY OF SELECTED ACCELEROGRAMS

This appendix will contain 5 to 10 accelerograms in each of the following magnitude range: 5±0.5, 6±0.5, 7±0.5, and some subduction zone events. The following information will be provided for each accelerogram:

Plots of acceleration, velocity & displacement versus time

Plots of spectral ordinates (5% damping).

Husid plot (for estimating duration).

Fourier amplitudes versus frequency.